Journal of Geophysical Research

VOLUME 64 MAY 1959 NUMBER 5

THE SCIENTIFIC PUBLICATION
OF THE AMERICAN GEOPHYSICAL UNION

Journal of Geophysical Research

An International Scientific Publication

This Journal welcomes original scientific contribu tions on the physics of the earth and its environmen

Manuscripts should be transmitted to J. A. People Jr., Geology Department, University of Kansa Lawrence, Kansas. Authors' institutions, if in th United States or Canada, are requested to pay a pul lication charge of $15 per page, which, if honored, e titles them to 100 free reprints.

Subscriptions to the *Journal of Geophysical R search* and *Transactions, AGU* are included in mem bership dues.

Non-member subscriptions, *Journal of Geophysic Research*..... $16 per calendar year, $2 per cop

Non-member subscriptions, *Transactions, AGU*... ..... $4 per calendar year, $1.25 per cop

Subscriptions, renewals, and orders for back numbe should be addressed to American Geophysical Unio 1515 Massachusetts Ave., Northwest, Washington D. C. Suggestions to authors are available on reques

Advertising Representative: Howland and How land, Inc., 114 East 32nd St., New York 16, N. Y.

Beginning with the January 1959 issue (Vol. 64, No. 1) the *Journal of Geophysical Research* is publishe monthly by the American Geophysical Union, 1515 Massachusetts Ave., Northwest, Washington 5, D. C with the support of the Carnegie Institution of Washington and the National Science Foundation. Th new monthly combines the type of scientific material formerly published in the bi-monthly *Transaction American Geophysical Union*, and the quarterly *Journal of Geophysical Research*. The *Transactions, Ameri can Geophysical Union* will continue as a quarterly publication for Union business and items of intere to members of the Union.

Second-class postage paid at Richmond, Virginia

GEOPHYSICAL MONOGRAPH SERIES

AMERICAN GEOPHYSICAL UNION

1515 Massachusetts Avenue, N.W. Washington 5, D. C., U.S.A.

Antarctica in the International Geophysical Year—Geophysical Monograph No. 1 (Publication No. 462, National Academy of Sciences—National Research Council); Library of Congress Catalogue Card No. 56-60071; 133 pp. and large folded map of the Antarctic, 1956, 7″ x 10″

$6.00

Contains 16 separate papers by various American authorities on the Antarctic under the headings: General, Geographic and Meterological, Geological and Structural, Upper Atmospheric Physics, and Flora and Fauna. Map (41″ x 41″) compiled by the American Geographical Society. Introduction by L. M. Gould, President of Carleton College and internationally recognized authority on the Antarctic.

Geophysics and the IGY—Geophysical Monograph No. 2 (Publication No. 590, National Academy of Sciences—National Research Council); Library of Congress Catalogue Card No. 58-60035; 210 pp., 1958, 7″ x 10″

$8.00

Contains 30 separate papers by leading American authorities under the headings: Upper Atmospheric Physics, The Lower Atmosphere and the Earth, and The Polar Regions. Preface by Joseph Kaplan, Chairman of the U. S. National Committee for the IGY.

Atmospheric Chemistry of Chlorine and Sulfur Compounds—Geophysical Monograph No. 3 (Publication No. 652, National Academy of Sciences—National Research Council); Library of Congress Catalogue Card No. 59-60039; about 110 pp., 1959, 7″ x 10″

$5.50

Based on a symposium held jointly with the Robert A. Taft Sanitary Engineering Center of the U. S. Public Health Service in Cincinnati in November, 1957. Contains 23 papers (some as summaries) with discussion. Preface by James P. Lodge, Jr., of the Taft Sanitary Engineering Center and Chairman of AGU's Committee on Chemistry of the Atmosphere.

Prices plus postage, unless payment accompanies order. Quantity discounts: 5–19 copies, 10%; 20–49 copies, 15%; 50 or more copies, 20%.

It is anticipated that Geophysical Monographs 4 and 5 will be issued during 1959. Watch "Special Announcements" in the *Transactions* for word of these.

Purchase Order

To AMERICAN GEOPHYSICAL UNION

1515 Massachusetts Avenue, N.W., Washington 5, D. C., U.S.A.

Please enter our order for the following:

_____ copies of Geophysical Monograph No. 1, *Antarctica in the International Geophysical Year,* at $6.00* $_____

_____ copies of Geophysical Monograph No. 2, *Geophysics and the IGY,* at $8.00* $_____

_____ copies of Geophysical Monograph No. 3, *Atmospheric Chemistry of Chlorine and Sulfur Compounds,* at $5.50* $_____

☐ Payment of $_____ is enclosed.

☐ Please send invoice, adding postage charges.

☐ Enter our standing order for _____ copies of subsequent Geophysical Monographs at the special prepublication rates (e.g., prepublication rate for Monograph No. 3 for non-members was $4.00, payment in advance, or $4.75 on invoice).

* List price for quantities up to four; see advertisement above for discounts on quantity purchases. Special discounts to members.

Typed name _____ Signature _____

Address _____

_____

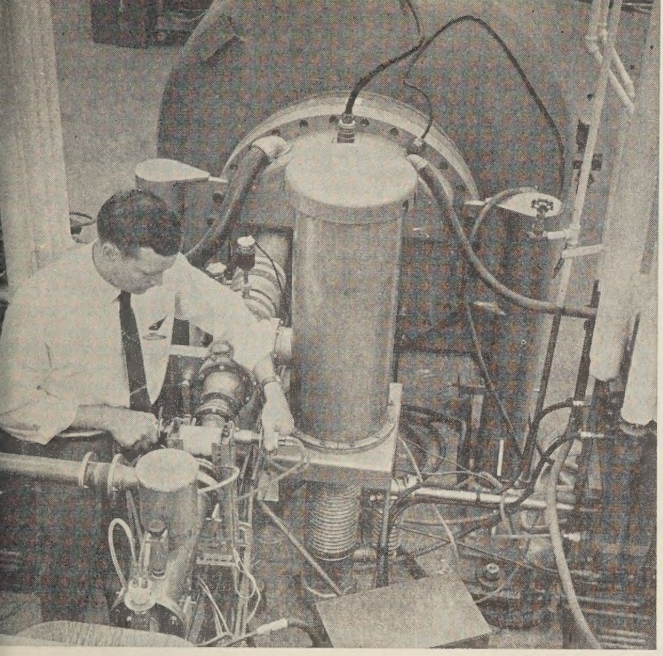

3 mev Van de Graaff accelerator—typical of advanced equipment used by Lockheed research scientists.

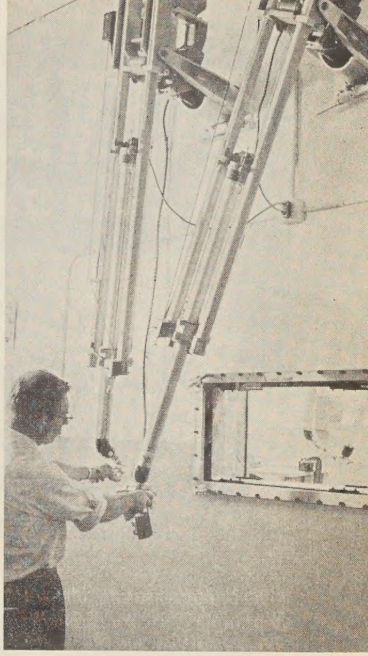

"Hot cell," for advanced radiation research in the nuclear physics laboratory.

PHYSICS / Expanding the Frontiers of Space Technology

Lockheed Missiles and Space Division is engaged in a broad, long-range program of basic scientific research at its Research and Development Laboratories in the Stanford Industrial Park at Palo Alto, California. Its modern facilities include a 3.5 mev Van de Graaff accelerator; a variety of shock tubes; extensive equipment for plasma and spectroscopic research; and one of the most modern computing centers in the nation. The Division was honored at the first National Missile Industry Conference as "the organization that contributed most during the past year to the development of the art of missiles and astronautics" and has several of the country's major programs under development.

A group of over fifty physicists is presently engaged in research and the fundamental investigation of problems in the following areas:

Nuclear Physics: Including the measurement and theory of nuclear cross sections; B-ray spectroscopy; theory of nuclear structure; reactor physics.

Weapon System Physics: The phenomenology and effects of atomic weapons, including laboratory simulation of radiation.

Space Physics: The study of the earth's upper atmosphere and beyond, including solar-terrestrial interactions.

Plasma Physics: The theoretical and experimental study of transport properties; micro-wave diagnostics; and magnetohydrodynamics.

Atomic Physics: Mass spectroscopy; theory and measurements of low energy interactions.

Members of the technical staff have every opportunity to participate in the initiation of advanced technological developments. The company encourages and sponsors individual communication with other scientists, the publication of papers and articles, and participation in symposiums and conventions.

If you have an advanced degree in physics, you are invited to join us in one of the most interesting basic scientific research programs in the nation. Write: Research and Development Staff, Dept. E-59, 962 W. El Camino Real, Sunnyvale, California. U.S. Citizenship required.

"The organization that contributed most in the past year to the advancement of the art of missiles and astronautics." NATIONAL MISSILE INDUSTRY CONFERENCE AWARD.

Lockheed / **MISSILES AND SPACE DIVISION**

Weapons Systems Manager for Navy POLARIS FBM; DISCOVERER SATELLITE; Army KINGFISHER; Air Force Q-5 and X-7.

SUNNYVALE, PALO ALTO, VAN NUYS, SANTA CRUZ, SANTA MARIA, CALIFORNIA
CAPE CANAVERAL, FLORIDA • ALAMOGORDO, NEW MEXICO • HAWAII

Journal of
GEOPHYSICAL RESEARCH

VOLUME 64 MAY, 1959 No. 5

Investigation of the Equatorial Electrojet by Rocket Magnetometer*

LAURENCE J. CAHILL, JR.

Department of Physics
State University of Iowa
Iowa City, Iowa

Abstract—A small rocket magnetometer has been developed for use in investigation of electrical currents in the ionosphere. In three flights near the magnetic equator electrical currents were detected. The equatorial electrojet was found to consist of at least two layers of electrical current, one layer near an altitude of 100 km and the other 20 to 25 km higher. A current flowing in the opposite direction to the main electrojet current was found to the north of the electrojet.

Introduction—The dynamo theory of variations in the magnetic field of the earth, first proposed by *Balfour Stewart* [1882], introduced a representation of the observed magnetic variations in terms of electrical currents flowing horizontally above the earth's surface. *Schuster* [1908], *Chapman* and *Bartels* [1940], and other workers have been successful in representing a complex and changing array of magnetic variations by a relatively simple system of currents, fixed in relation to the sun, yet, to an observer on the earth, moving always westward with the sun. In spite of the utility of the electrical current representation of the magnetic variations and the general acceptance today of the dynamo theory, there have remained several notable obstacles to a detailed understanding and substantiation of the theory.

According to the dynamo theory, charged particles in the atmosphere are moved in tidal winds across the lines of force of the earth's magnetic field. The resulting induced electromotive forces, perpendicular to the earth's magnetic field, direct the positively charged particles in the opposite direction from the negative ones and set up a system of electrical currents in the atmosphere. These currents must be principally horizontal since the horizontal layers of the ionosphere provide the necessary charged particles. The electrical current density at a given height above the earth's surface depends then on the velocity of the tidal winds producing the electromotive forces, upon the conductivity of the ionosphere at that height, and also upon the strength of the earth's magnetic field. It is the lack of detailed information about the first two of these quantities that has prevented full development of the dynamo theory.

Both the conductivity and the tidal winds appear at first to be much too low for the production of electrical currents of the magnitudes inferred from the surface magnetic variations. Various arguments have been advanced to show that the tidal winds and/or the conductivity in the ionosphere are far greater than was originally supposed. An excellent summary of this work is

* Assisted by the National Academy of Sciences and the National Science Foundation through US/IGY Project 10.1.

contained in a paper by *Baker* and *Martyn* [1952].

Generally these arguments are well founded. Radio measurements of ionospheric winds help to confirm the high tidal velocities [*Salzberg* and *Greenstone*, 1951]. Recent rocket measurements of electron densities and other particle number densities will help in more accurate conductivity determinations [*Baker* and *Martyn*, 1952]. The fact is, however, that for some time to come, knowledge of the tidal wind velocities and of the conductivity in the ionosphere will remain insufficient to allow detailed computation of the electrical currents on the basis of the dynamo theory.

With the advent of high altitude sounding rockets in 1946, *in situ* measurements of atmospheric properties became possible. *Vestine* and others [1947] first suggested direct measurement of ionospheric currents with rocket-borne magnetometers. A comprehensive summary of the ionospheric current measurements to be made through rocket flights and the relative importance of the various measurements has been given by *Chapman* [1954].

The first investigation of ionospheric currents by direct measurement was done by a group of scientists from the Applied Physics Laboratory and the Naval Ordnance Laboratory [*Maple* and others, 1950; *Singer* and others, 1951]. A total field magnetometer of the flux gate type was used. One flight was made near the magnetic equator at about the time of the daily maximum in the large magnetic variation found there [*Chapman* and *Bartels*, 1940]. The large variation has been attributed to an intense ribbon of current flowing along the magnetic equator—the equatorial "electrojet" [*Chapman*, 1951]. On this flight the rocket apparently entered but did not completely penetrate the electrojet; the total measured change in magnetic field attributed to the electrojet was 400 $\pm 50\gamma$. This pioneering attempt to detect and measure the equatorial current system was successful, but the flux gate magnetometer used was not completely satisfactory. The flight measurements had to be corrected for a drift error and an error due to the orientation of the rocket. The uncertainty in these corrections contributed to the $\pm 100\gamma$ maximum error of the measurements [*Singer* and others, 1951].

In 1953 the nuclear induction principle was extended to the measurement of weak magnetic fields, in particular to that of the earth, with the invention by *Packard* and *Varian* [1953] of the proton precession magnetometer. *Van Allen* [1954] originally suggested the use of this magnetometer for high altitude magnetic measurements. The principle of the magnetometer and the advantages of using this instrument for rocket measurements have been adequately covered in several papers [*Cahill* and *Van Allen*, 1956; *Heppner* and others, 1958; *Waters* and *Francis*, 1958].

Development of a small, rugged magnetometer for high altitude use was commenced by the State University of Iowa (SUI) laboratory in 1955. In the first test flight the magnetometer was carried to an altitude of 30 km by a plastic balloon [*Cahill* and *Van Allen*, 1956]. Measurements were received for over two hours by FM telemeter. This flight was followed by further development in 'miniaturizing' the magnetometer for use with small sounding rockets during the International Geophysical Year (IGY).

An extensive program of investigation of ionospheric currents was planned by the SUI laboratory. Flights in the northern and southern polar regions, as well as a series of flights near the magnetic equator, were made. The purposes of this report are to describe the rocket magnetometer, the equatorial flights, and the results of these flights. The polar flights will be discussed in a later paper.

Design and construction of the rocket magnetometer—The rockoon launching scheme developed by this laboratory was well suited to the program for several reasons: (1) Rockoon launching of small, sounding rockets allowed a free choice of geographical locations. The launchings were not confined to existing launching sites but could be done from shipboard at almost any desired geomagnetic latitude. (2) With the rockoon technique a light-weight magnetometer could be carried to the ionosphere at a relatively small expense per flight. (3) The apparatus needed for rockoon launchings is less complex than that used in other methods of launching rockets. The launchings could be done with the assistance of a small number of supporting personnel.

Choice of the small rocket and balloon combination as a vehicle made stringent design

equirements on the rocket magnetometer. A tudy of the peak altitudes that might be reached by the Loki II rocket with different firing altiudes and payloads was undertaken. For a payoad of 4 kg and a firing altitude of 23 km, the computed trajectory indicated that a peak altitude of 125 km would be attained. According o the computed trajectories, an increase in the payload of $\frac{1}{2}$ kg would mean a loss in peak altitude of 10 km; therefore the rocket magnetometer could not weigh much more than 4 kg f the E region of the ionosphere were to be reached.

Other restrictions on the magnetometer design were: (1) The high initial acceleration (approximately 100 g) of the fast-burning Loki II rocket motor meant that all components and supporting structure would have to be of very sturdy construction. (2) The initial phase of the flight during which the rocket would be carried to a firing altitude near 23 km would last at least 70 minutes. The batteries supplying the magnetometer and the radio transmitter should be adequate not only for the brief rocket flight but for two to three hours of pre-firing operation and testing. (3) The small diameter, 7.5 cm, of the Loki II led to some difficulty in mounting components; in particular, it limited the size of the sample bottle and its surrounding coil.

In the final flight version, the total weight of the magnetometer package ready to be attached to the front end of the rocket motor was 4.3 kg. The electronic components and batteries were mounted on aluminum decks and were supported by nonmagnetic stainless-steel rods. The outer covering of fiberglass impregnated with 91 L D resin supported the sample bottle and coil. Figure 1 is a photograph of the rocket magnetometer, Figure 2 a cross-sectional view showing placement of components, and Figure 3 a block diagram of the circuitry.

The sensing element of the magnetometer, the sample bottle of kerosene and the coil surrounding it, contributed approximately one kilogram to the total weight. Five hundred turns of teflon-insulated, no. 16 copper wire were wound on a plastic coil form which served as a container for the sample. Kerosene was chosen for its short thermal relaxation time (approximately 0.7 sec). Rapid and frequent measurements were wanted during the rocket flight since the rocket would travel several thousand feet in one second and the ambient magnetic field would be changing rapidly.

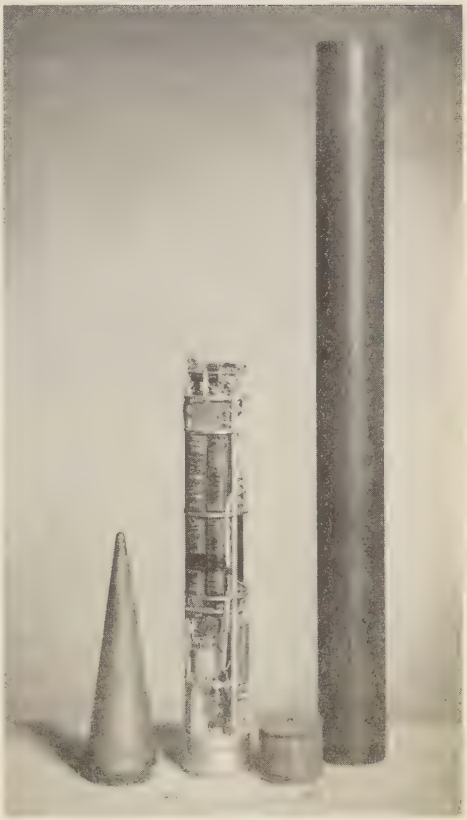

FIG. 1—Photograph of rocket magnetometer

The coil was mounted coaxially with the longitudinal axis of the rocket. This mounting avoided correction of the observed precession signal for rocket spin. For example, if the coil axis is perpendicular to the magnetic field and is rotating about the magnetic field vector, then the rotation frequency must be added to, or subtracted from, the observed signal frequency to obtain the true precession frequency. At angles other than 90° the correction is somewhat different, but if the rotation is rapid the average correction is still very nearly a direct addition or subtraction of the spin frequency.

The fiberglass covering was adopted since the

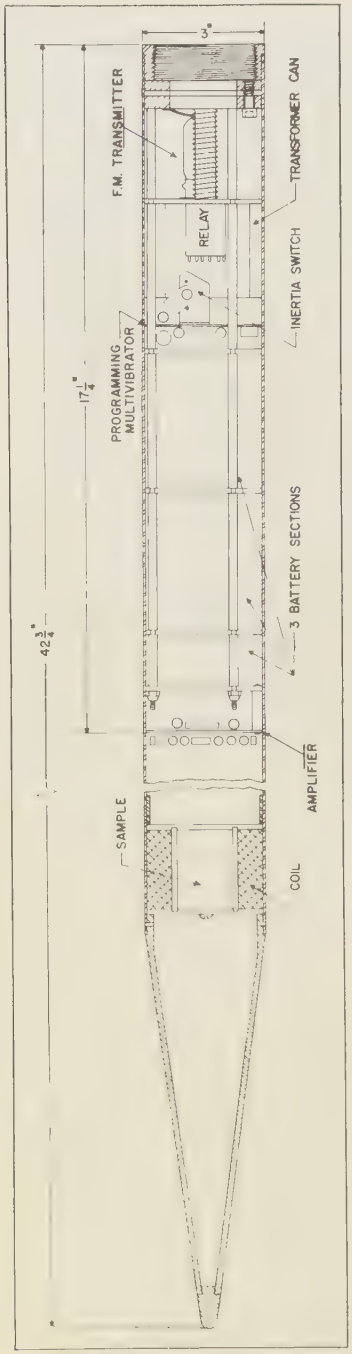

FIG. 2—General construction of magnetometer

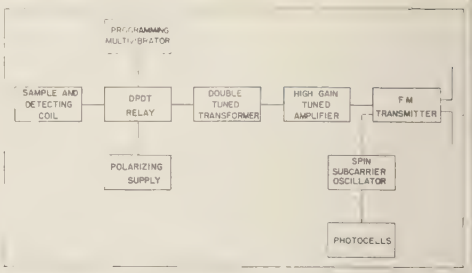

FIG. 3—Block diagram of magnetometer circuitry

presence of a closed electrical loop about the sample would cause a very rapid damping of the signal. Throughout the rocket, nonmagnetic materials were used to avoid distortion of the ambient magnetic field to be measured. The rocket motor was of aluminum, and nonmagnetic fastening pins were used. The only magnetic materials were in a relay and a toroidal coil with a permalloy core; these were mounted as far from the coil as possible. In addition all wires carrying direct current were either coaxial or twisted to prevent stray magnetic fields.

A shielded pair of wires connected the coil to a small relay. This relay was used to connect the coil first to polarizing batteries and then to the high-gain amplifier. A multivibrator operated the relay. The time between measurements was approximately two seconds. Of this time 1.2 sec were taken to align the protons in the sample.

During the balloon phase of the flight the measurement repetition rate was reduced to conserve polarizing batteries. The polarizing time was 1.2 sec but the interval between polarizations was approximately 20 sec. This still provided a measurement every 0.1 km during the balloon ascent since the rate of rise was nominally 0.3 km/min.

The transition between the balloon and rocket repetition rates upon firing the rocket was accomplished by the operation of a small rotary switch. A weighted-arm switch reacted to the firing acceleration and shorted out a high resistance that determined the 20-sec interval between measurements.

Polarizing current, 4.0 amp, was supplied by three Yardney type HR-1 batteries.

A tuned transformer between the relay and the amplifier provided a pass band from 200 to

300 cps, adequate to accommodate the anticipated changes in precession frequency, yet narrow enough to considerably limit the thermal noise from the sensing circuitry. The construction and tuning of this transformer has been discussed in an earlier paper [*Cahill* and *Van Allen*, 1956].

Subminiature double triodes (type 6112) were used in the amplifier, and additional tuning was provided by a Twin T resistance-capacitance network in a negative feedback loop [*Valley* and *Wallman*, 1940].

The transmitter was one developed for balloon flight telemetry and modified to fit into the confines of the present instrument. When coupled to the rocket motor and to the payload framework as the two ends of a dipole, the transmitter would, under optimum conditions, provide between $\frac{1}{2}$ and 1 watt of radiated radio-frequency power. Schematic diagrams of all circuits are included in the author's doctoral dissertation [*Cahill*, 1959].

A recurrent problem with the rocket magnetometer was a tendency for the amplifier-transmitter combination to oscillate at the tuned frequency of the amplifier. Conventional methods of shielding and putting radio-frequency chokes or wave traps on all leads proved not completely effective. Finally some success was had in individually adjusting each unit in frequency, in amplifier gain, and in deviation sensitivity of the FM transmitter to lessen the tendency toward oscillation.

The usual environmental tests were performed on components and on completed subassemblies before the final assembly. After assembly, the complete rocket magnetometer was tested. Since the units were tuned with a frequency pass band, corresponding to the expected magnetic field at the firing location, this magnetic field had to be reproduced quite accurately to allow testing. For example, the magnitude of the earth's magnetic field at the Line Islands on the equator is only 34,000γ, whereas the value at Iowa City is 56,000γ. A large square coil was built according to *Rubens* [1945]. The coil axis was placed along the earth's magnetic field vector. The ambient magnetic field could then be changed at will by adjusting the current through the coil. The magnetometer was placed at the center of the coil where the field was sufficiently uniform to allow measurements. This test constituted the final complete pre-flight check of the apparatus, since the large magnetic gradients caused by the steel structure of the ship prevented any observation of the proton signal prior to launching.

Recording and measurement of precession signals—Figure 4 is a block diagram of the receiving and recording equipment. Reception of the rf signal on the ship was through a Yagi antenna mounted to receive vertically-polarized radiation and free to rotate in tracking the rocket during balloon ascent and after firing. The antenna was mounted in a clear space on the deck; a coaxial cable led to a Clarke telemetering receiver in the laboratory space. The magnetometer signals and a crystal-derived 20-kc standard frequency were recorded directly on magnetic tape. A secondary method of recording the signals was employed during the rocket flight only. The beat frequency between the proton signal and a standard oscillator of nearly the same frequency was displayed on an oscilloscope face and the trace was recorded photographically [*Cahill* and *Van Allen*, 1956; *Waters*, 1955].

Frequency measurement of the precession signals was done in the SUI laboratory some time after the flights. Reading of the beat frequency auxiliary record has been discussed previously [*Cahill* and *Van Allen*, 1956]. The frequencies of the signals on magnetic tape were measured electronically. A direct count of the signal frequency during a known time interval would have resulted in an uncertainty of ± 1 cps (equivalent to $\pm 23.5\gamma$) in the measurement.

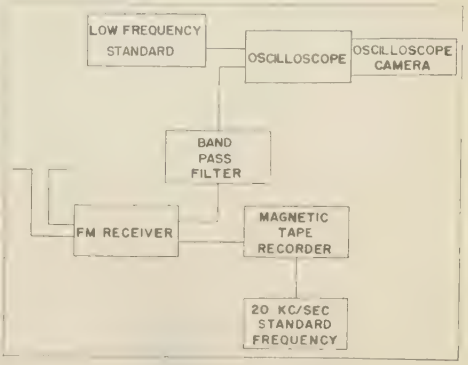

FIG. 4—Block diagram of receiving station

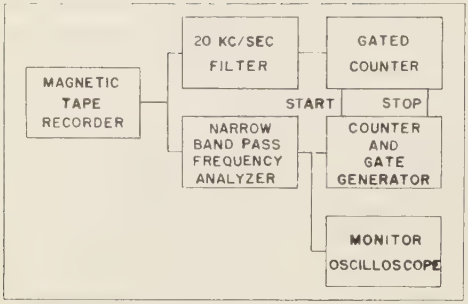

FIG. 5—Block diagram of frequency measuring apparatus

An arrangement employing two electronic counters and utilizing the recorded 20-kc standard frequency was developed. A block diagram (Fig. 5) shows the arrangement of equipment. The frequency measurement was accomplished by counting the number of cycles of the 20-kc standard frequency within a pre-set number of cycles of the precession signal. The accuracy of an individual measurement was determined by the number of cycles of the signal available for measurement and by the signal to noise ratio.

The altitude record for each flight had to be obtained indirectly. The firing altitude was known within $\pm\frac{1}{2}$km from measurement in the laboratory of the operating pressure of each of the barometric firing switches. A computed trajectory was obtained for each rocket flight in the following manner. It was assumed that magnetic field measurements on the downward leg of the flight would be approximately equal, at equal altitudes, to those on the upward leg of the flight. On this assumption, at the time midway between the times of two equal flight measurements, the rocket should be at its peak altitude. The observed time from the known firing altitude to peak was used in selecting a matching trajectory from a number of appropriately computed trajectories. The selected trajectory was then used to translate the recorded times of measurements to altitudes.

The trajectories were computed at first by hand and then with the aid of an electronic computer. For each of several firing altitudes a number of trajectories was computed using the thrust as a parameter. A vertical trajectory was assumed. Atmospheric density and temperature were taken from *Rocket Panel* [1952] data. The drag coefficient of the rocket was taken from information supplied by the Jet Propulsion Laboratory. Considerable confidence in these computed trajectories resulted from the high firing altitude and consequent small drag.

Two factors qualified the assumption made in determining the peak time. Time variations in the earth's magnetic field during the course of the rocket flight could cause a difference between the measured values of the magnitude of the magnetic field intensity **F** on the upward and downward legs. Such variations should also be observable on the ground variometer records from nearby observatories. If no significant time variation, during period of the rocket flight, were present on the ground records, then a significant variation in the rocket results would not be likely. The possibility of a local variation encountered by the rocket but not observed on the ground cannot be ruled out, however.

A more likely cause of significant variation between upward and downward measurements would be the horizontal movement of the rocket in its trajectory. Fired at an angle to the vertical of some 5 to 10 degrees, the rocket could travel 50 km or more horizontally during a normal trajectory. If the horizontal gradient of **F** were, for example, 10γ/km, a difference of 500γ between measurements at the same altitude would be expected at the bottom of the trajectory. This type of variation would be small near peak and would grow progressively larger at lower altitudes.

In obtaining peak times for the various rocket flights through the assumed symmetry of the flight measurements about the peak time, variations of the second type were often apparent. When the peak time was obtained by matching values near the top of the trajectory, a progressively larger difference between flight measurements at equal altitudes appeared in the lower parts of the flight. No detailed information about the horizontal track of the rocket was available. In some cases, however, a very rough indication of azimuthal direction of the trajectory was had from estimates of the azimuth of the receiving antenna, which tracked the rocket during flight. In these cases the observed discrepancies at low altitudes did agree with the estimated horizontal track of the rocket and the

horizontal gradient of the earth's magnetic field. The maximum error in the determination of peak time for a normal trajectory is believed to be not more than ±2 sec. The corresponding maximum error in peak altitude is ±3 km; the error is less at lower altitudes on the upward leg of the flight and greater at lower altitudes on the downward leg (as great as ±5 km at the bottom).

The equatorial flights—Magnetometer flights at the equator were made possible through arranging to accompany the USS *Glacier*, a Navy ice-breaker, on a cruise from Boston to the Antarctic at the start of Operation Deepfreeze III. Permission was obtained through Task Force 43, the Navy group directing Operation Deepfreeze III, for the *Glacier* to deviate from the normal course from the Panama Canal to the Antarctic. The deviation allowed launching of the equatorial flights near the Line Islands in the mid-Pacific (Fig. 6). The Line Islands are near the intersection of the geomagnetic and geographic equators, and three magnetic observatories, operated during the IGY by the Scripps Institution of Oceanography, were located there. The

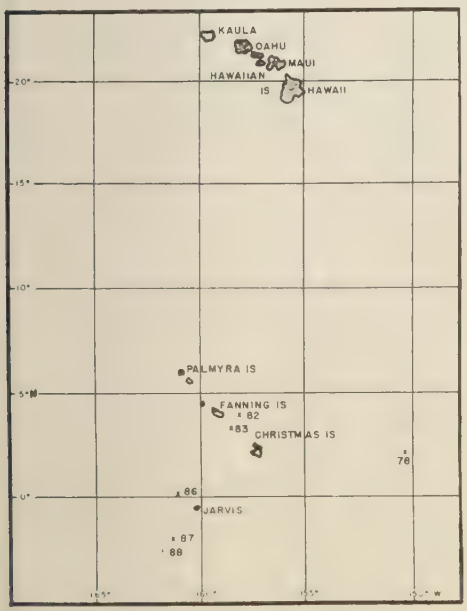

FIG. 6—Map of Line Islands

observatories were established with the intent of obtaining, through simultaneous ground observations at separated locations, new information about the equatorial electrojet.

Surface magnetic observatories near flight locations supplied necessary information about the degree of magnetic disturbance. A further unique advantage was gained in that the flights intended to detect and measure the equatorial electrojet were made in conjunction with an extensive ground level investigation of the same electrojet. The two types of measurement were complementary. The records from the ground observatories revealed the changes in the current during the day (the diurnal variation), the changes in intensity of the current in periods of magnetic storm and magnetic calm, the approximate geographical location and altitude of the center of the current, and the movement of this center north or south from day to day or during the course of the year. The rocket measurements provided several brief, but much more detailed studies of the electrojet, its extent in latitude and in altitude, and its detailed structure—a profile of current density versus altitude. In conjunction with simultaneous surface measurements, direct measurement of the overhead currents gave experimental evidence of the actual division of the observed magnetic variation at ground level into the contribution from overhead currents and the contribution from currents flowing below the surface which were induced by the overhead currents.

Locations of the flights are indicated in Figure 6, and in Table 1. Launchings were accomplished by a two-man scientific party from the State University of Iowa assisted by the crew of the USS *Glacier* (AGB 4).

On three of the flights in Table 1 an approximate inverse-cube decrease of the magnetic field was observed with no evidence of current layers. The other three flights (83, 86, and 87) apparently penetrated current layers. The results of these flights will now be discussed.

Flight 83 provided accurate and reasonably complete magnetic measurements up to 125 km, well into the ionosphere. The flight location was in the region of the equatorial electrojet. Preliminary information from the magnetic observatories at Jarvis, Fanning, and Palmyra Islands revealed that the electrojet must be closer to

TABLE 1—*Summary of flight information*

Flight	Date	Time (165th MT)[a]		Location		Peak altitude (km)
		Balloon launching	Rocket firing	Lat.	Long.	
	1957					
78	Oct. 14	1216	1331	2°16′N	150°23′W	113
82	17	1101	1216	3°56′N	158°07′W	51
83	17	1244	1359	3°23′N	158°41′W	127
86	18	1243	1356	0°02′N	160°52′W	122
87	19	0750	0907	2°05′S	161°05′W	129
88	19	1406	1519	2°31′S	161°26′W	104

[a] 165th Meridian Time = UT − 11 hr.

the Jarvis observatory than to the others (private communication from Dr. R. G. Mason, Scripps Institution of Oceanography, and radio communication during the firings with Dr. Martin Vitousek, Field Director for the observatories.) The range in the daily variation at Jarvis was twice that at Fanning and four times that at Palmyra.

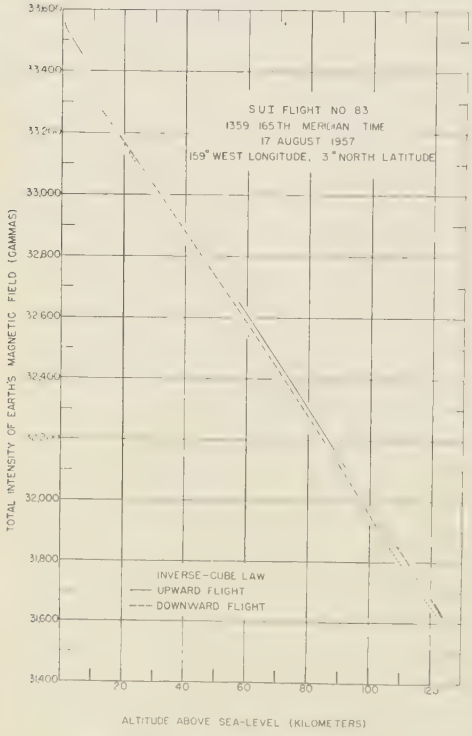

FIG. 7—Flight 83; magnetic field intensity versus altitude

An abrupt change of slope at 104 km on the upward flight record (Fig. 7) indicates penetration of a current sheet. A decrease in slope is noted, however; the contribution to **F** from the current sheet tends to decrease **F** below the sheet and to increase **F** above it. Since the main field vector **F** is horizontal and pointing northward at the equator, the current producing the observed changes must be flowing from east to west, directly opposite to the predicted direction of the equatorial electrojet.

The current sheet is thin; the flight curve at 108 km resumes its original slope. There is a gap in the upward record from 110 km to 120 km where the slope is still approximately that of the lower portion of the flight. The portion of the record above 90 km is reproduced in detail in Figure 8. Plotted here are departures of the flight measurements from an inverse-cube extrapolation of the measurements at 100 km. The extrapolation is corrected to agree with the measured rate of decrease below 100 km. Two slight increases in slope are noted at 123 km and again at 116 km. These could be due to currents from west to east. There are no upward measurements, however, to substantiate these increases in slope. The decrease in slope between 102 km and 108 km on the upward record is also evident on the downward record. The maximum relative error between the measured values of **F** plotted in Figure 8 is $\pm 5\gamma$. The validity of the east-to-

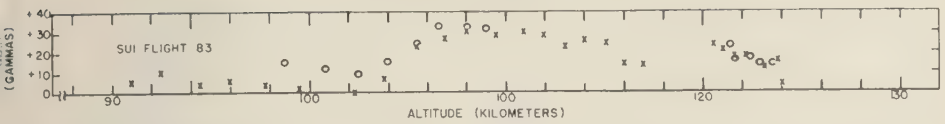

FIG. 8—Flight 83; departure from inverse cube (circles indicate upward flight, crosses downward flight)

est current is supported by the approximate greement between the upward and downward easurements and by the obvious displacement the flight record above 106 km as shown in igures 7 and 8. The slope remains approximately ne same as in the lower part of the flight, but ne upward displacement of the record by 30γ an only be attributed to a sheet current with n east-to-west component; any north-south omponent of reasonable magnitude would not e detected because of the small contribution o **F**.

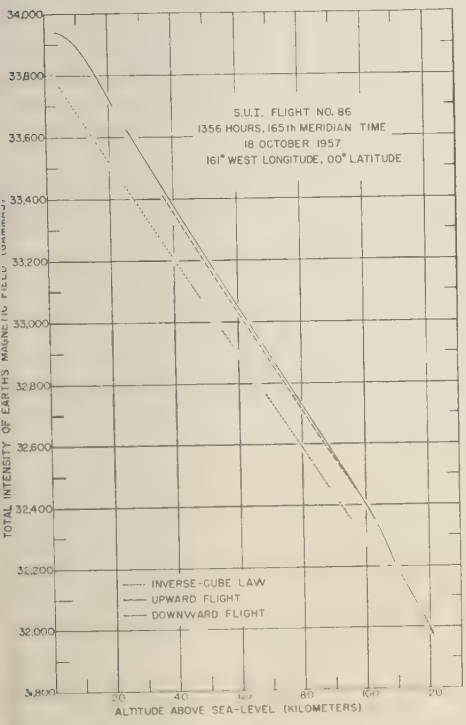

FIG. 9—Flight 86; magnetic field intensity versus altitude

SUI Flight 86 was launched just 30 miles northwest of the Jarvis observatory. The firing location (near the observatory recording the largest diurnal variation in **H**) and the time of firing (1356 local time) made penetration of the electrojet very probable. An increase in slope of the Flight 86 record (Fig. 9) at 97 km indicates entry of the rocket into the lower boundary of the electrojet. Approximate resumption of the earlier slope at 110 km indicates that the electrojet has been penetrated. The entry altitude agrees with that found in the earlier equatorial electrojet penetration in 1949.

Examination of a detailed plot of the measurements above 90 km in Figure 10 reveals, however, that the slope above 110 km does not completely return to that of the lower flight and that the slope again increases near 117 km. Two distinct layers of electrical current are indicated with a layer of lower current density between them. At the peak of the trajectory the slope of the flight record has not resumed the lower altitude slope, so the upper layer of current has not been completely penetrated at 122 km.

The maximum relative error between the measurements plotted in Figure 10 is $\pm 5\gamma$. The measurements of the lower portions of the flight lie within $\pm 10\gamma$ of the lines shown in Figure 9. The rocket traveled horizontally eastward during the flight toward lower magnetic field strengths; therefore the downward flight measurements lie below those of the upward flight.

The intensity of the current encountered during Flight 87 was much greater than that found in the previous flight. As indicated in Figure 11, two layers of current were observed—the lower at approximately the same altitude as before, the upper slightly higher. There is some evidence (Fig. 12) that the upper current layer may have been completely penetrated. Near the top of the trajectory the measurements indicate a return to the original slope. This evidence is weakened, however, by the presence of a spike

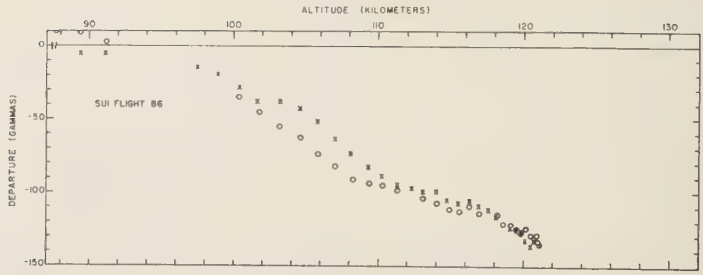

FIG. 10—Flight 86; departure from inverse cube

in the record of magnetic measurements near the peak of the upward flight. Time variation in the current intensity could account for the spike, but it could also cause the apparent return to the original slope. The upward and downward plots of the flight measurements are not so well matched as those of Flight 86. This is also attributed to time variation and to horizontal motion of the rocket. The maximum relative error between the measurements plotted in Figure 12 is $\pm 10\gamma$. Moderate magnetic disturbance was present on October 19 as is evidenced by the spike near the peak altitude and also by a large temporary increase in **F** occurring during the balloon phase of the flight. This increase may be seen on the balloon record (Fig. 11) at 11 km (1930 UT) and on the Jarvis Island variograph record (Fig. 15) at 0930 150th Meridian Time (1930 UT).

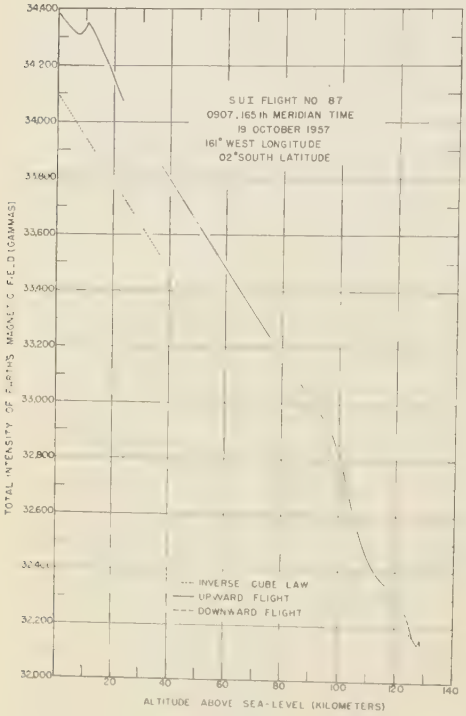

FIG. 11—Flight 87; magnetic field intensity versus altitude

The structure of the equatorial electrojet—The results of Flights 83, 86, and 87, together with records from the Line Islands magnetic observatories, may be used to sketch the intensity and the structure of the electrojet.

The magnetic records from the Jarvis Observatory from October 17, 18, and 19 are reproduced in Figures 13, 14, and 15. The difference in **H** at Jarvis between the nighttime minimum and the value at the time of Flight 86 is $90 \pm 6\gamma$. Only two-thirds of this value is thought to be due to the overhead current system; therefore $60 \pm 4\gamma$ is to be compared to the change in **F** due to the current sheet which was measured during Flight 86. The departure from the inverse cube decrease at the peak of Flight 86 is $138 \pm 10\gamma$. The uncertainty in this value is due to the error in the individual measurements, as well as to uncertainty in selecting the starting point and the slope of the approximate inverse-cube extrapolation. Only one half of the total change in **F** measured, or $69 \pm 5\gamma$, contributed to the main field below the current sheet in producing the magnetic variation. This contribution to the main field would be greater directly below the current sheet than at sea level since the current sheet is not infinite in lateral extent. The decrease at sea level is estimated, from examina-

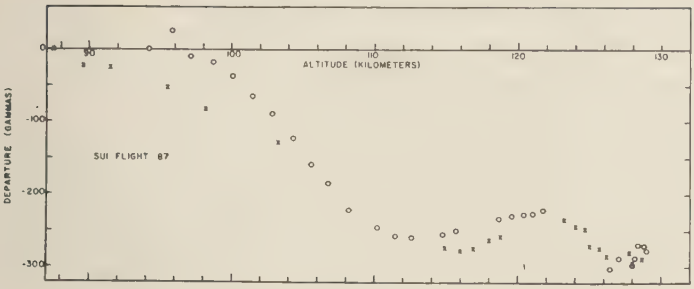

FIG. 12—Flight 87; departure from inverse cube

ion of the flight record and from calculation of he field of a simplified model of the electrojet, to e less than 15 per cent of the contribution irectly below the current sheet. The final stimate of the contribution of the measured urrent sheet to the sea-level diurnal variation s 59 ± 4γ. The agreement with the ground neasurement is excellent but surprising, since he top current layer was not completely pene-rated. Either the current density goes rapidly o zero above 122 km, or the contribution to the iurnal variation from the overhead currents is reater than two-thirds.

The total departure at the peak altitude for Flight 87 is 300 ± 20γ, slightly more than twice hat of Flight 86. The positive slope of the depar-ure curve for Flight 87 in Figure 12, both before ntering and after leaving the current layers, ndicates, as mentioned earlier, that the electrojet s not an infinite current sheet. The expected nagnetic field of the current sheet at the surface of the earth is 127 ± 9γ. The magnitude of the iurnal variation in **H** at Jarvis at the time of Flight 87 was 206 ± 6γ. Two-thirds of this is 137 ± 4γ, so the agreement between direct measurement and indirect measurement of the electrojet is not so good as in the previous flight. The reason for this may be that the overhead currents are more intense at Jarvis Island than at the flight location 120 miles farther south. The **Z** variograph records from Palmyra and Jarvis (the Fanning **Z** trace is missing) indicate the existence of local regions of more intense current embedded in the electrojet. The main diurnal **Z** variation is similar at Palmyra and Jarvis, but small temporary fluctuations are often opposite in phase. This indicates that the source of these minor fluctuations is between Palmyra and Jarvis Islands, although the center of the electrojet appears to be south of Jarvis.

The change in **F** due to the current sheet detected in Flight 83 is 30γ. One half of this is much less than either the variation of 110γ in **H** at flight time at Jarvis Observatory of the variation of 62γ at Fanning. Apparently the change in **H** at Fanning caused by the electrojet, approximately 300 km to the south, was still much larger than that due to a small overhead current. There is also some evidence that the current encountered during Flight 83 was quite limited laterally and would produce very small ground level effects even in the absence of the electrojet.

Although the currents measured up to 129 km

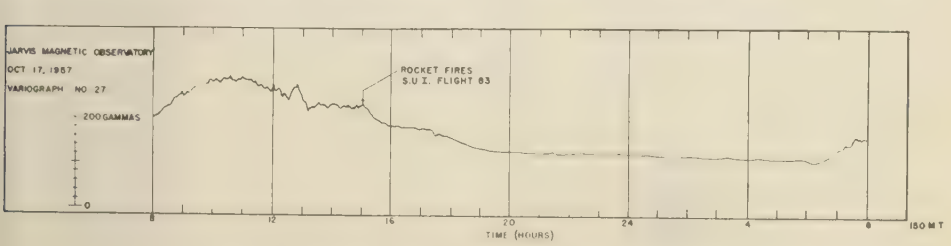

FIG. 13—Magnetic record, October 17, 1957, Jarvis Island

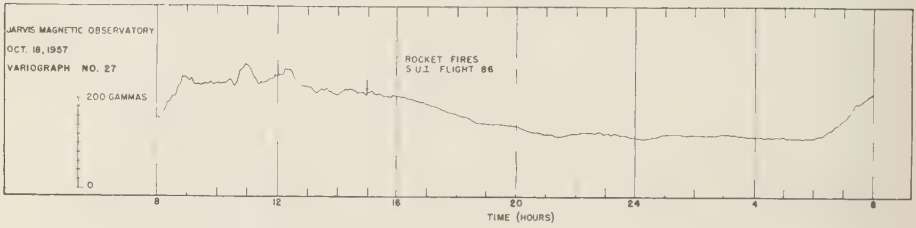

FIG. 14—Magnetic record, October 18, 1957, Jarvis Island

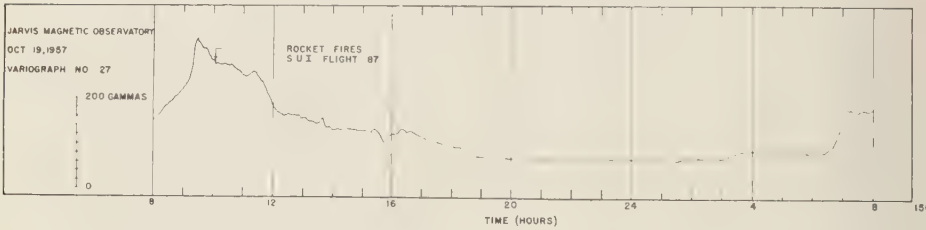

FIG. 15—Magnetic record, October 19, 1957, Jarvis Island

appear to be sufficient in magnitude to account for all of the diurnal variation measured on the ground, there may still be current layers above the peak altitudes reached by the magnetometer flights described here. These currents could be too weak to produce noticeable ground-level variation or could be in opposing pairs, if there were a reversal of tidal wind velocity at higher altitudes.

The departures of magnetic field measurements from the inverse cube decrease may be directly translated into approximate current densities. For this purpose, the electrojet is assumed to be infinite in lateral extent. The change in magnetic field strength in gammas observed in passing through an infinite current layer one kilometer thick is $0.4\pi j$, where j is the average current density of the layer in amp/km². The flight measurements shown in Figure 8 were used to compute the approximate current density as a function of altitude for the layer detected during Flight 83 (Fig. 16). Similar graphs for the currents detected in Flights 86 and 87 are presented in Figures 17 and 18. In making the current density graphs, only the major features of the departure curves were accounted for; the small deviations that could be attributed to time variations or to error in the measurements were disregarded.

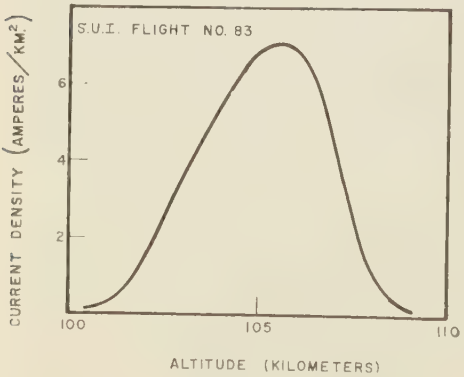

FIG. 16—Current density, Flight 83

A vertical cross-sectional view of the equatorial electrojet based on the available data was constructed. This view (Fig. 19), although based on experimental data, is an extrapolation of these data. It is intended only as a graphic means of displaying the data already presented and not as an accurate or reliable chart of the electrojet. The northern boundary of the electrojet must be between the locations of Flights 83 and 86. The observed decrease in the magnetic field of the current layers of Flight 87 with increasing distance from these layers was used to obtain a very crude estimate of the lateral extent of the

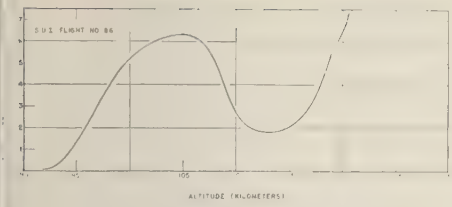

FIG. 17—Current density, Flight 86

ayers. The width is estimated to be greater han 300 km; this is in agreement with the findngs of a ground level latitude survey of the electrojet by C. A. Onwumechilli (unpublished thesis, University of Nigeria, 1957) and with the electrojet conductivity calculations by Martyn [*Baker* and *Martyn*, 1952].

The bottom of the lower layer is fixed at approximately 97 km by Flights 86 and 87 and also by the measurements by *Singer* and others [1951]. The lines drawn within the layers are contours of current density. The actual current densities vary greatly during the day and from one day to the next, and irregular regions of higher current density may be embedded in the current layers shown.

The top boundary of the lower layer is approximately 110 km. The thickness of the interval between layers, as well as the current density in this interval, is apparently variable, as are the

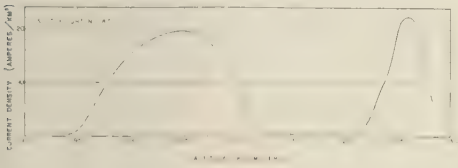

FIG. 18—Current density, Flight 87

altitude and thickness of the upper layer. This upper structure may vary in intensity and height with the degree of magnetic disturbance or with several other parameters (the season, the time of day, or the phase of the moon). The flights described took place both on disturbed and on quiet days, the flights were launched shortly after the autumnal equinox, and the moon was in the last quarter.

Again it should be emphasized that Figure 19 is a very crude attempt to depict the complete structure of the electrojet; it applies only to the specific period in which the flights were made and to the Line Islands region. The movements of the electrojet north and south with the seasons and the changes in the diurnal variation with magnetic disturbance and with the phases of the moon all must be determined by detailed study of the records from the Line Islands observatories.

Implications with regard to ionospheric conductivity and electron density—The measured current densities in the various flights agree with calculated ionospheric conductivities. Martyn, Cowling, Bates, Massey, and others have studied the ionospheric conductivity, and the major results have been summarized by *Baker* and *Martyn* [1952].

A special conductivity σ_3 is thought to be effective at the magnetic equator. This conductivity applies to currents flowing parallel to the electric field and transverse to the magnetic field in the special case where Hall current is prevented from flowing. Near the magnetic equator **F** is horizontal and the Hall current does not have a horizontal component. A polarization is built up between the top and bottom surfaces of a conducting layer, and this prevents further flow of Hall current and effectively cancels the

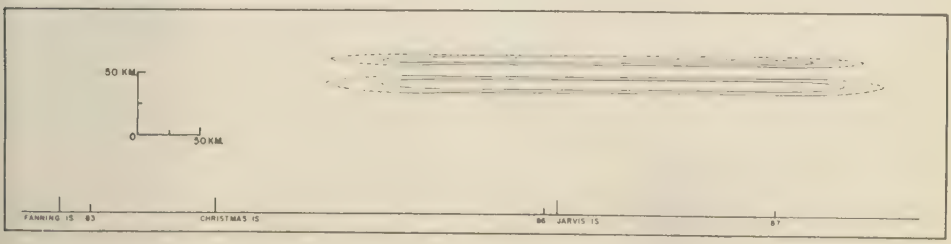

FIG. 19—Cross-sectional view of electrojet

retarding effect of the magnetic field. The resulting conductivity is very high. The specific conductivities (conductivities per ion-electron pair) must be multiplied by the electron density to obtain the appropriate conductivities governing current flow. Only the relative changes with altitude of the product of electron density and specific conductivity may be deduced from the current density profiles.

At the equator the presence of two layers of current rather than the single predicted one must be explained. The effective conductivity σ_3 has only a single narrow maximum near 100 km as indicated by *Martyn* [1952]. A possible explanation of the two layers is that a layer of high electron density is located above or below the altitude of the σ_3 peak. An intense sporadic E reflection has been observed near the magnetic equator and in the same location as the equatorial electrojet. This sporadic E layer might well be responsible for one of the two current layers. Which of the layers might be due to the peak in σ_3 and which to the sporadic E is not yet clear.

The current layer found in Flight 83 was not predicted in thickness, current density, or direction of current flow. Although there were thought to be weak dynamo electric fields near the equator, in an east-to-west direction, it was believed, from the evidence of magnetic observations, that the stronger electric fields in higher latitudes prevailed and forced the electrical currents into a counter clockwise pattern (Northern Hemisphere). As mentioned earlier the current observed in Flight 83 appears to be small in lateral extent as well as in magnitude, so that its observation at sea level would be difficult even without the masking effect of the nearby electrojet. The small vertical dimension of the current is surprising since none of the computed conductivities have such a small half-width in altitude. The thinness of the layer can be accounted for by assuming that it is caused by a thin sporadic E layer embedded in a thicker conductivity peak. The equatorial sporadic E has been observed at Christmas Island and, less intensely, at Palmyra, so it may extend beyond the edges of the electrojet [*Smith*, 1957].

Acknowledgments—The author wishes to acknowledge, first of all, the contributions of James A. Van Allen who initially proposed the use of the free precession magnetometer as an instrument for upper-atmosphere magnetic exploration and who offered encouragement throughout the development of the rocket magnetometer as well as assistance in the actual rocket launchings.

Many individuals assisted in the construction of the magnetometers, in the rocket launchings, and in the data reduction. Particular note is made of the assistance of Harold Andrews, Edward Kupka, Gary Strine, and Donald Simanek, all of the State University of Iowa, The Cooper Development Corporation of Monrovia, California, not only constructed the mechanical components of the magnetometers and portions of the electronic circuitry but offered suggestions for improving the mechanical design.

The support of various organizations of the United States Navy was essential in carrying out the rockoon launchings. Assistance in arranging for this support was provided by CDR O. E. Hearn and LCDR D. P. Wencker of the IGY Interservice Task Group. Captain B. J. Lauff of the *Glacier* and his crew were most cooperative in assisting with the rockoon launchings. LTJG S. O. Wilson was particularly helpful in supervising the balloon launchings and in arranging for assistance from the various departments of the ship.

The importance of the records of the surface magnetic observatories in confirming the rocket results and aiding in their interpretation is gratefully acknowledged. The cooperation of the U. S. Coast and Geodetic Survey and the Scripps Institution of Oceanography in providing reproductions of the variograph records is appreciated.

References

Baker, W. G., and D. F. Martyn, Conductivity of the ionosphere, *Nature*, **170**, 1090–1092, 1952.

Cahill, L. J., Jr., Magnetic exploration of the upper atmosphere, unpublished dissertation, State Univ. Iowa, 148 pp., 1959 (copies available upon request).

Cahill, L. J., Jr., and J. A. Van Allen, High altitude measurements of the earth's magnetic field with a proton precession magnetometer, *J. Geophys. Research*, **61**, 547–558, 1956.

Chapman, S., *Arch Meteorol. Geophys. u. Bioklimatol.*, **4**, 368–374, 1951.

Chapman, S., Rockets and the magnetic exploration of the ionosphere, *Rocket exploration of the upper atmosphere*, R. L. Boyd and M. J. Seaton (editors), Pergamon Press, London, 292–305, 1954.

Chapman, S., and J. Bartels, *Geomagnetism*, Oxford University Press, 2 vol., 1049 pp., 1940.

Heppner, J. P., J. D. Stolarik, and L. H. Meredith, The earth's magnetic field above WSPG, New Mexico, from rocket measurements, *J. Geophys. Research*, **63**, 277–288, 1958.

Maple, E., W. A. Bowen, and S. F. Singer, Measurement of the earth's magnetic field at high altitudes at White Sands, N. M., *J. Geophys. Research*, **55**, 115–126, 1950.

Packard, M., and R. Varian, Free nuclear induc-

tion in the earth's magnetic field, *Phys. Rev.*, **93**, p. 941, 1953.

UBENS, S. M., Cube surface coil for producing a uniform magnetic field, *Rev. Sci. Instr.*, **16**, 243–245, 1945.

ALZBERG, C. D., AND R. GREENSTONE, Systematic ionospheric winds, *J. Geophys, Research*, **56**, 521–533, 1951.

CHUSTER, A., The diurnal variation of terrestrial magnetism, *Phil. Trans. Roy. Soc., A*, **208**, 163–204, 1908.

INGER, S. F., E. MAPLE, AND W. A. BOWEN, Evidence for ionospheric currents from rocket experiments near the geomagnetic equator, *J. Geophys. Research*, **56**, 265–281, 1951.

MITH, E. K., World wide occurrence of sporadic E, *Natl. Bur. Standards Circular 582*, 278 pp., 1957.

TEWART, BALFOUR, Terrestrial magnetism, *Encyclopedia Britannica*, 9th ed., 36 pp., 1882.

THE ROCKET PANEL, Pressures, densities and temperatures in the upper atmosphere, *Phys. Rev.*, *88*, 1027–1031, 1952.

VALLEY, G. E., AND H. WALLMAN, Low frequency feed back amplifiers, *Vacuum tube amplifiers*, McGraw-Hill, New York, 384–408, 1940.

VAN ALLEN, J. A., *Upper atmosphere rocket research panel*, (Panel Rept. no. 37), Feb. 4, 1954 (unpublished).

VESTINE, E. H., L. LAPORTE, I. LANGE, AND W. E. SCOTT, *Carnegie Inst. Wash. Publ. 580*, p. 363, 1947.

WATERS, G. S., A measurement of the earth's magnetic field by nuclear induction, *Nature*, **176**, p. 691, 1955.

WATERS, G. S., AND P. D. FRANCIS, A nuclear magnetometer, *J. Sci. Instr.*, **35**, 88–93, 1958.

(Manuscript received February 4, 1959.)

Solar Activity and Transient Decreases in Cosmic-Ray Intensity *

D. VENKATESAN**

Division of Pure Physics
National Research Council
Ottawa, Canada

Abstract—The world-wide character of the intensity changes in meson and nucleon components is shown by a study of data from Ottawa, Churchill, and Resolute during the period October 1956 to December 1957. Further discussion is essentially restricted to the mean nucleonic component derived from the three stations. The investigation reveals an association between transient decreases in cosmic-ray intensity and the central meridian passage of active solar regions. On an average, the greater the activity rating of the regions, the larger is the cosmic-ray decrease. It is not possible, however, to discuss the relation specifically in terms of the characteristics of the regions, such as flares, sunspots, and the like. Further support for the relation comes from observation of geomagnetic data. Attention is drawn to the similarity between small as well as large transient decreases in intensity with regard to presence or absence of recurrence tendency. The study supports the view that both the 27-day variation and the Forbush events differ only in degree and could therefore be attributed to the same mechanism. It is possible to attribute the cosmic-ray decreases to beams of ionized rarified gas emitted from the sun and differing considerably in their characteristics.

Introduction—The interplanetary electromagetic state appears to be a vital link in many henomena observed at the earth. It is reasonable o suppose that it would be influenced to a arge extent, if not completely governed, by olar activity. A study of cosmic-ray intensity ariation with time is expected to throw some ght on this.

The close connection between solar activity nd cosmic-ray intensity variations is well nown. The inverse correlation between the ong-term changes in cosmic-ray intensity and he eleven-year change in solar activity was rst pointed out by *Forbush* [1954] from a study f the meson component. This has been further onfirmed by *Fenton* and others [1958] and *ockwood* [1958] who also used the nucleonic omponent. Fenton and his co-workers have urther pointed out that the long-term change s not the result of cumulative effects of shorterm or transient decreases but a superposition f two different types of variation. The long-term hange has been discussed by *Alfvén* [1954], *Davis* [1955], *Morrison* [1956], and *Parker* [1956] in terms of their modulation theories. Only the transient decreases are considered here.

Phenomenologically these could be grouped into the quasi-periodic 27-day variation and Forbush events. The latter are sudden decreases and are often associated with geomagnetic disturbances [*Forbush*, 1938]. It has often been questioned whether the two are caused by the same mechanism, differing only in degree. *Meyer* and *Simpson* [1954] consider the quasi-periodic 27-day variation to be masked by the nonperiodic Forbush events. The studies of *Venkatesan* [1958], *Singer* [1956, 1958], *Galli* (private communication, 1956), and *Fenton* and others [1958], on the other hand, would favor the same mechanism for both. In fact the study of Fenton and others seems to indicate that the 27-day variation could be closely identified with the Forbush decreases, since a considerable number of such small ones spread irregularly over several days gives the appearance of almost sinusoidal intensity changes. If both the slow and sudden types of transient decreases could be attributed to the same mechanism, one would expect to observe a recurrence in Forbush events, at least on some occasions. It would therefore be valuable to investigate the intensity

* Issued as N.R.C. No. 5154
** Postdoctorate Fellow

changes during an epoch of high solar activity when there are a number of Forbush events.

Attempts have been made in the past to relate the changes in cosmic-ray intensity with specific areas of solar activity. (We are not referring here to the five cases of solar flare increases.) For example, *Simpson* and others [1955] have pointed out a case of an intensity increase associated with repeated central meridian passages of the so-called UM regions, but it is not certain that the relation between the two is unique, nor is it definite that the 27-day variation is an increase. *Van Heerden* and *Thambyahpillai* [1955] and *Brown* [1956], among others, consider the 27-day variation to be a decrease, and that is the view taken here. Hence a study of transient changes in intensity and their relation to specific active regions on the sun is of importance.

Alfvén [1954], *Brunberg* and *Dattner* [1954], and *Venkatesan* [1956, 1957ab] have attempted to explain the 27-day variation in terms of beams of ionized rarified gas emitted from the sun. These beams have a magnetic field frozen in them and an electric field due to polarization effects. With an increase in solar activity, it is reasonable to expect a greater number of beams which persist for a longer time. On the other hand, in view of the increase in number of beams, independent ones (and hence independent cycles of 27-day variation) separated by a few days might interfere with each other. This would complicate any detailed analysis of the recurrence tendencies of decreases and their association with active solar regions. Nevertheless, a careful examination of the decreases, both individually as well as together, would be worth while, since such a study might help to distinguish between the relative merits of Alfvén's beam theory of cosmic-ray variation and Parker's diffusion theory of modulation. Alfvén pictures a beam which in the idealized case would have a fairly definite boundary, whereas Parker pictures a sweeping by an outward flow of solar gas which becomes turbulent and has boundaries which need not be so definite. At present nothing definite is known about either the region of production or the mechanism governing the emission of the beams. If these originate in a specific part of the active solar region, such as the center of gravity of the region, we might get a clear correlation with the central meridian passage (CMP) of the same. In the case of Parker's ideas, it appears that such a clear connection with CMP may not be necessary.

World-wide variation and the central meridian passage of areas of solar activity—The period of study, October 1956 to December 1957, was one of extremely high solar activity which revealed a number of Forbush events. Figures 1 and 2 show the changes in the daily mean intensity (the mean hourly intensity over a 24-hour period from 00 to 24 hours GMT) of the meson and nucleonic components registered at Ottawa, Churchill, and Resolute. The data have been suitably corrected for barometric pressure. The figures refer to the periods July to September 1957 and October to December 1957. The figures reveal the general agreement between the two components at any one station or at the different stations, and this is particularly marked in the case of the nucleonic component. These data have been corrected for pressure only; and, because of the well-known temperature effect on the meson component, one should not expect it to show the same detailed correlation either with the nucleonic component at the same station or with the same component at different stations. This problem is discussed in some detail by *Fenton* and others [1958] and *Mathews* [1959]. Some improvement is apparent when we consider the average of the data from the three stations, Ottawa, Churchill, and Resolute. The stations are separated far enough so that their meteorological changes would not be closely correlated, although the primary intensity changes would be expected to affect the measurements at the three stations similarly.

Figures 3 to 7 show the mean nucleonic component for each day for every three-month period, the CMP dates of active areas on the sun* [*High Altitude Observatory Quarterly Reports*], and the K_p sum for each day. The standard deviation (S.D.) shown on the figures refers to the square root of the average number of counts per day for all the three stations together and is included merely to show the accuracy of the experimental observations.

Table 1 represents a way of recording the relation between the CMP of areas of solar activity and decreases in the cosmic intensity.

*The nomenclature of the active solar regions is the same as that adopted by the High Altitude Observatory, Boulder, Colorado.

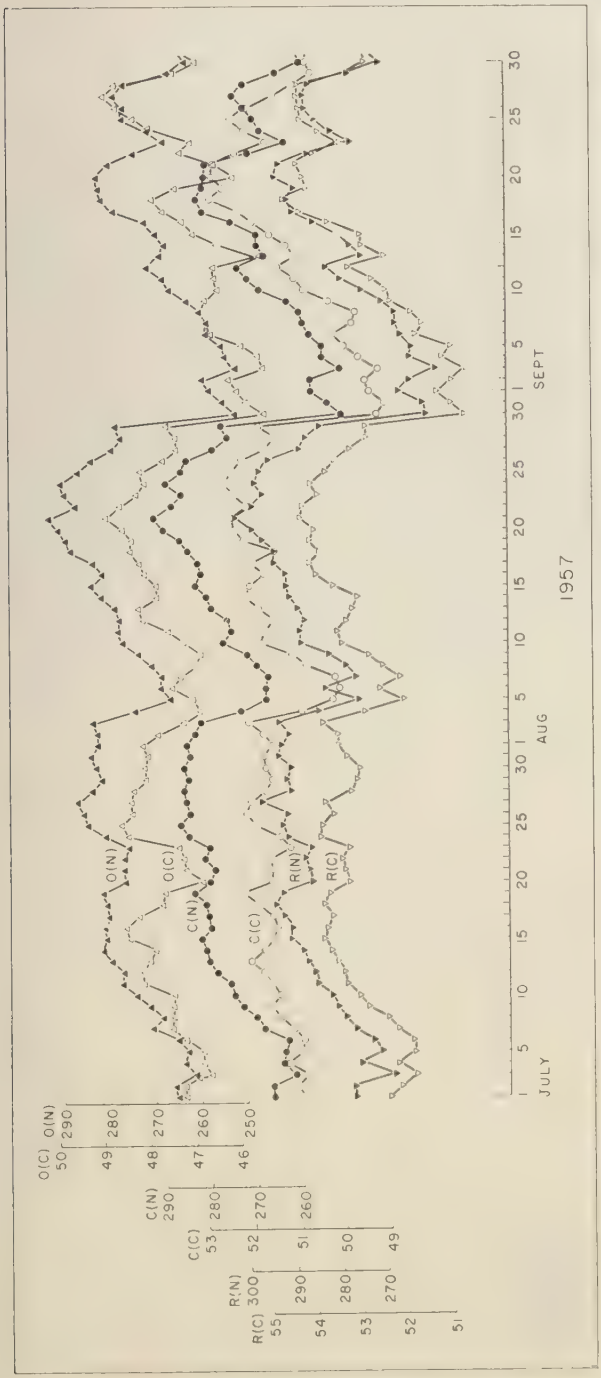

FIG. 1. Time variation of the daily mean intensity, July to September, 1957; O(C), C(C), and R(C) refer respectively to the international cubical meson telescope at Ottawa, Churchill, and Resolute, and O(N), C(N), and R(N) to the nucleonic component at the three stations. Scaling factor for meson telescope is 1024 and for the neutron 64 (see text for details)

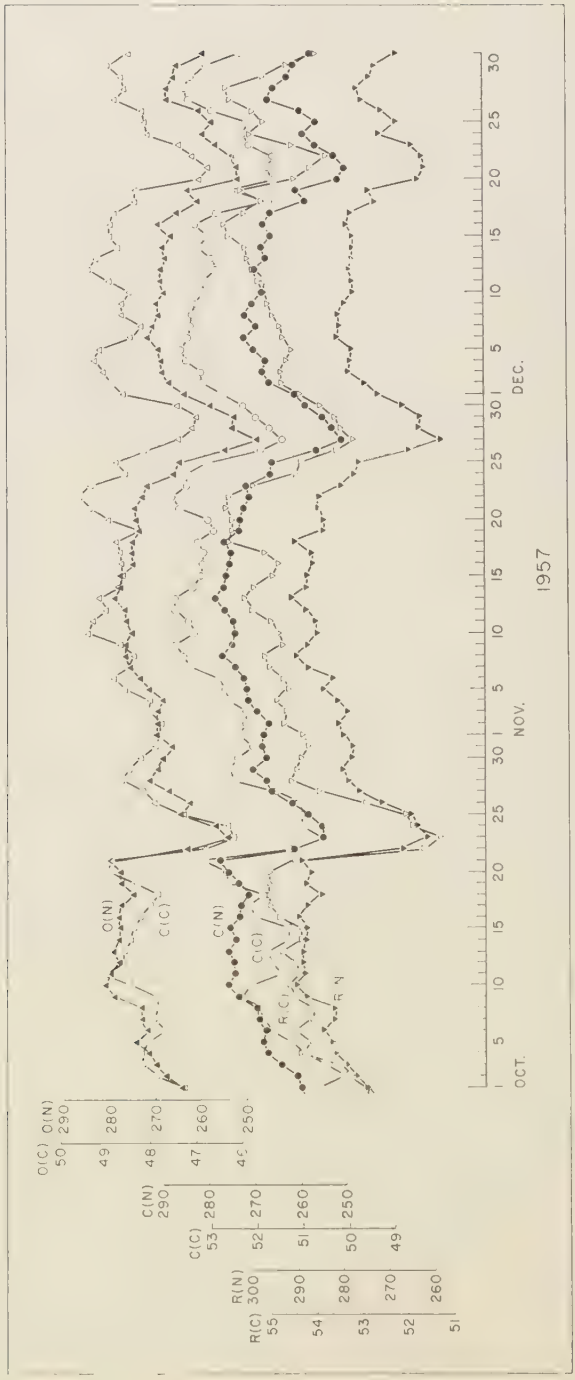

FIG. 2—Time variation of the daily mean intensity, October to December, 1957 (see text for details).

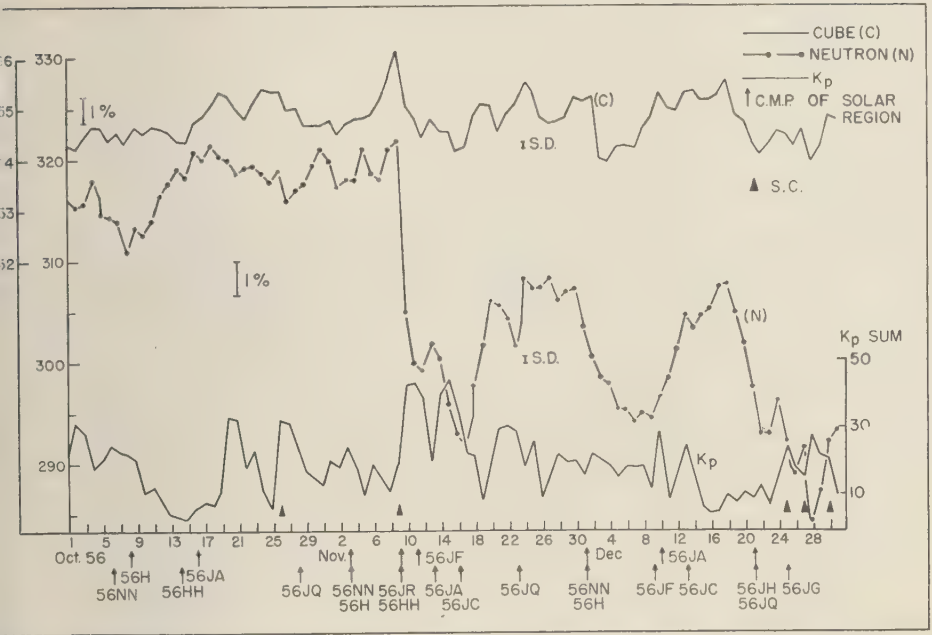

IG. 3—Time variation of the mean nucleonic component (N) and mean meson component (C), October December, 1956. *S.C.* (▲) refers to sudden commencement and *S.I.* (Δ) to sudden impulse (see text for details)

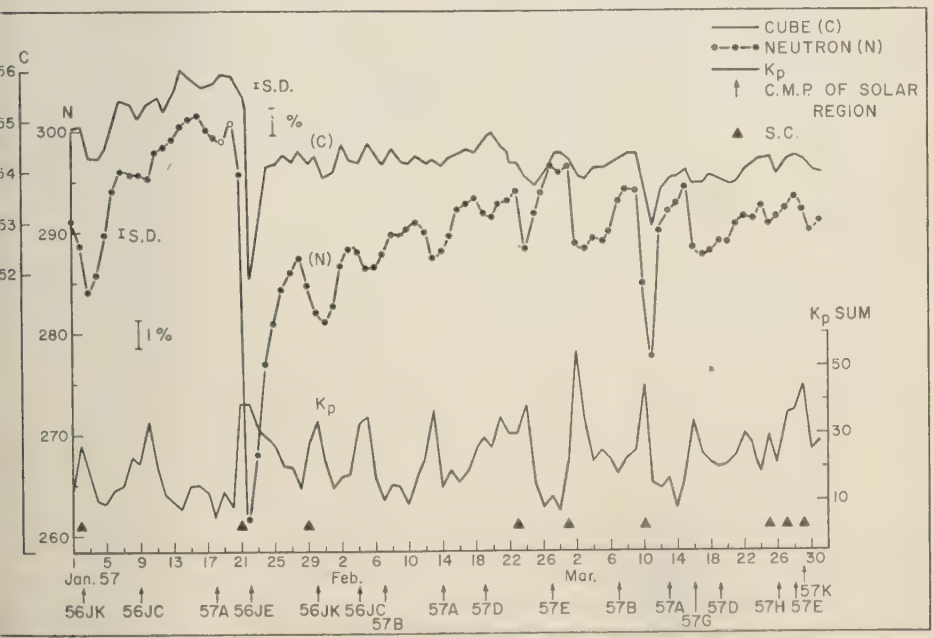

IG. 4—Time variation of the mean nucleonic component (N) and mean meson component (C), January to March, 1957 (see text for details)

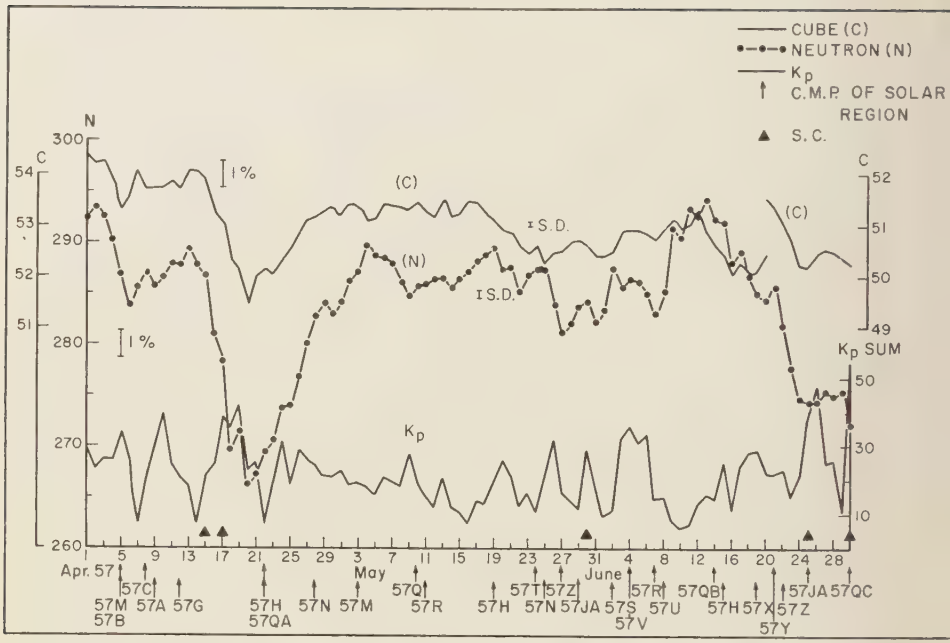

FIG. 5 -Time variation of the mean nucleonic component (N) and mean meson component (C), April to June, 1957 (see text for details)

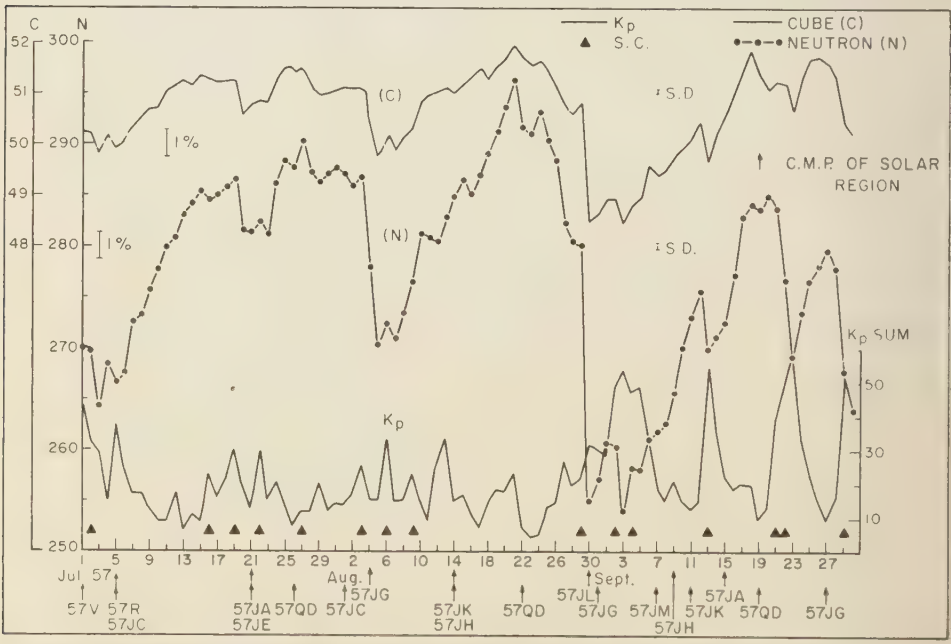

FIG. 6 -Time variation of the mean nucleonic component (N) and mean meson component (C), July to September, 1957 (see text for details)

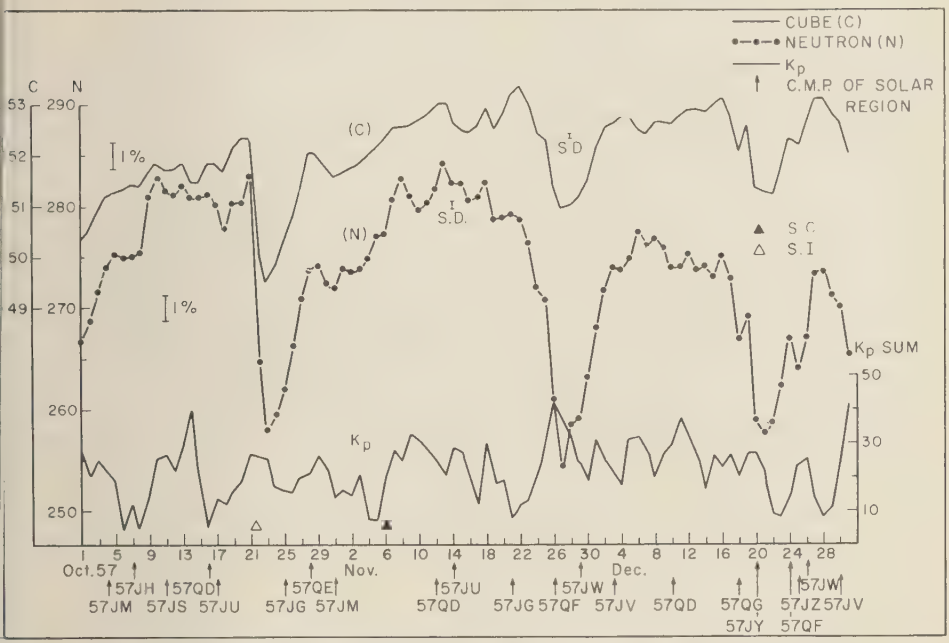

FIG. 7—Time variation of the mean nucleonic component (N) and mean meson component (C), October to December, 1957 (see text for details)

Though the period studied covers fifteen months, only six months are shown for the sake of brevity; namely, January 1 to June 30, 1957. The whole period is included in Figures 3 to 7. During this period 52 prominent, active solar regions were listed. In 44 cases of these, a reasonably clear connection with cosmic-ray decreases could be seen. In seven of the remaining cases the correlation is not so definite, and in one case the situation was too complicated for analysis. All cosmic-ray decreases were considered where the magnitude of the decrease was equal to or greater than the standard error of 0.1 per cent which is due to the counting rate. (The nucleonic component was considered here.)

When there are two decreases near each other it is hard to pinpoint the exact recurrence. There are cases where a smaller decrease occurs while recovery from an earlier heavy decrease is taking place. In such cases, little or no decrease might be observed. One might at best observe a somewhat steady value for the intensity in the midst of a recovery. There are also examples of two active regions on or about the same longitude, one in each hemisphere. One could only attribute the same observed decrease to both regions, since both would cross the central meridian on the same day or within a day.

About a hundred decreases could be said to be associated with the prominent active areas on the sun discussed so far. There are, however, 13 minor decreases which could not be associated with these prominent regions. Of these, seven are less than twice the standard error, and four are between three and four times the standard error due to the counting rate (0.1 per cent).

The true relations between the cosmic-ray decrease and the CMP are not always the same and will be discussed in a later paragraph. The repetition of decreases (in relation to solar revolutions) and the impossibility of connecting decreases with individual flares or sunspots will be discussed. But before generalizing, let us consider one or two cases in detail. The first appreciable decrease in January 1957 corresponds to the dates 7 to 10. This is a small decrease and is probably a recurrence of the decrease of

TABLE 1—*Relation between CMP of active solar regions, decreases in cosmic-ray intensity, and geomagnetic disturbances*

Case No.	Initial cosmic-ray decrease	Fall (%)	Recurrence	Date of recurrence	Fall (%)	Period	First CMP	Solar region	Activity rating	Recurrence	Date of recurrence	Activity rating	Period	Date* of K_p peak	Date* of recurrence	Period	S.C.
1	Dec. 31, 56-Jan. 3, 57	3.14	yes	Jan. 28-Jan. 31, 57	2.13	28	Jan. 2, 57	56 JK	a	yes	Jan. 30, 57	d	28	Jan. 2, 57 [27-]	Jan. 30, 57 [34⁰]	28	Dec. 30, 56 Jan. 2, 57-Jan. 29
2	Mar. 1-Mar. 2	2.55	yes	Mar. 28-Mar. 30 (1)	1.14	27½	Feb. 27	57 E	c	yes	Mar. 28	d	29	Mar. 2 [55-]	Mar. 29 [44⁰]	27	Mar. 1-Mar. 29
3	Mar. 28-Mar. 30 (2)	1.14	no				Mar. 29	57 K	b	no				Mar. 29 [44⁰]			Mar. 29
4	Jan. 16-Jan. 19	0.79	yes	Feb. 11-Feb. 13	1.20	25½	Jan. 18	57 A	b	yes	Feb. 14	e	27	Jan. 15-Jan. 17 [14+]	Feb. 13 [37−]	28	
			yes	Mar. 9-Mar. 11	5.54	26				yes	Mar. 13	c	27		Mar. 10 [45−]	25	Mar. 9-Mar. 10
			?	?	?					yes	Apr. 9	e	27		?		
5	Jan. 20-Jan. 22	13.02	yes	Feb. 18-Feb. 20 (3)	0.62	29	Jan. 22	56 JE	b	? minor activity				Jan. 21-Jan. 22 [39⁰, 39+]	Feb. 19 [29⁰]	28½	Jan. 21
6	Feb 18-Feb. 20 (4)	0.62	?	Mar. 19-Mar. 20	0.03 ?	28½	Feb. 19	57 D	c	yes	Mar. 18	c	27	Feb. 19 [29⁰]	Steady Level Mar. 18-Mar. 21 [21]		
7	Mar. 15-Mar. 17	2.25	yes	Apr. 13-Apr. 15	0.93	29	Mar. 16	57 G	c	yes	Apr. 12	b	27	Mar. 16 [34⁰]	No peak		
8	Mar. 24-Mar. 25, 57	0.55	yes	Apr. 19-Apr. 20, 57 (5)	1.90	26	Mar. 26, 57	57 H	b	yes	Apr. 22, 57	b	27	Mar. 25, 57 [29+]	Apr. 19, 57 [42⁰]	25	Mar. 24-Mar. 25, 57
			yes	May 19-May 20	0.75	30*				yes	May 19	c	27		May 20 [26−]	31*	
			yes	June 13-June 16 (6)	2.09	27				yes	June 15	d	27		June 15 [25+]	26	
9	Apr. 3-Apr. 6	2.99	yes	May 4-May 5	0.29	30	Apr. 5	57 M	c	yes	May 3	d	28	Apr. 5 [34+]	May 3 [19+]	28	
															May 6 [21−]	31	
10	Apr. 8-Apr. 9	0.40	no				Apr. 8	57 C	c	no				Apr. 10 ?[40−]			
11	Apr. 29-Apr. 30	0.41	yes	May 25-May 27 (7)	2.10	28	Apr. 28	57 N	c	yes	May 25	d	27	Apr. 29-May 1 [22−]	May 26 [32⁰]	25	

TABLE 1—*Relations between CMP of active solar regions, decreases in cosmic-ray intensity and geomagnetic disturbances*-(concluded)

Case No.	Initial cosmic-ray decrease	Fall (%)	Recurrence	Date of recurrence	Fall (%)	Period	First CMP	Solar region	Activity rating	Recurrence	Date of recurrence	Activity rating	Period	Date* of K_p peak	Date* of recurrence	Period	S.C.
12	May 25-May 27 (8)	2.10	no				May 24	57 T	c	no				May 26 [32⁹]			
13	May 25-May 27 (9)	2.10	yes	June 21-June 24 (10)	3.90	27½	May 27	57 Z	c	yes	June 22	a	26	May 26 [32⁹]	June 22 [23−]	26	
14	June 21-June 24 (11)	3.90	no				June 21	57 Y	b	no				June 22 [23−]			
15	June 2-June 3, 57	0.68	no				June 2, 57	57 S	b	no				June 4, 57 [36−]			
16	June 5-June 7	1.08	yes	July 2, 57-July 3	2.02	27	June 4	57 V	c	yes	July 1, 57	c	27	June 6 [34−]	?		July 2, 57
17	June 9-June 10	0.30	no				June 8	57 U	c	no				June 8 small peak in midst of fall (15⁹)			
18	June 13-June 16 (12)	2.09	no				June 14	57 QB	c	no				June 15 [25+]			
19	May 21-May 22	0.85	yes	June 17-June 20	1.60	28	June 19	57 X	b	no				May 23 [16+]	June 18, 57 June 19 [29−]		
20	June 29-July 1	1.94	.?	July 24-July 26	0.63	25½	June 30	57 QC	a	?	(57 QD rising very near			June 30 [55−]			June 30

* K_p sums in brackets.

* *See text for this change in periodicity.*

1. *See also 57 K (Case 5).* 2. *See also 57 E (Case 2).* (3) *See also 57 D (Case 6).* (4) *See also 56 JE (Case 5).* (5) *Part of general decrease Apr. 18-Apr. 21. Discussed in detail in the text.* 6. *Also connected with 57 OB (Case 17).* (7) *See also 57 T (Case 12) and 57 Z (Case 13).* (8) *See also 57 N (Case 11) and 57 Z (Case 13).* (9) *See also 57 T (Case 12) and 57 N (Case 11).* (10) *See also 57 Y (Case 14).* (11) *See also 57 Z (Case 13).* (12) *See also 57 H (Case 8).*

December 13 to 14, 1956, which in turn is probably a recurrence of the decrease of November 13 to 17, 1956. The decrease during February 3 to 5 may also be a later recurrence of the same formation. These are associated with the active region 56 JC whose CMP dates are November 16 and December 13, 1956, January 9 and February 4, 1957.

A larger event is typified by Region 57 E and the decrease of March 1 and 2. A possible repetition of this is the decrease of March 28 to 30 which could also be partly due to Region 57 K. The very large decrease of January 21 (the largest of the period) shows no evidence of a recurrence; this phenomenon will be discussed later. The decrease of May 6 to 9 is one of the seven decreases where association with a particular active region is uncertain. Here two active areas were very close together; namely, 57 Q and 57 R. There is a small decrease, June 5 to 7, which could be a recurrence of this formation. The case which gave no suggestion of a clear resolution is that of 57 QA whose CMP was April 22, 1957. This is apparently connected with some part of the general decrease extending from April 13 to 20.

There may be an element of uncertainty in the exact association of decreases in cosmic-ray intensity with the CMP of active regions if considered only from an inspection of the curves in Figures 3 to 7. This is due to the simultaneous presence of a number of active areas, not too greatly separated. However, there are other points which make the conclusion appear more objective. If the data are classified in relation to the times between the CMP and the period during which the decrease lasts, the result in Table 2 is obtained. The unit of time is one day, since daily averages are used, and the table represents the number of events with different time differences between the decrease and associated CMP of the active region. Out of the 97 cases of decreases and recurrences observed during the period, 44 correspond to decreases lasting one day, 34 to those lasting two days, and the remaining 19 to those lasting three or more days. Cases corresponding to those lasting more than three days could generally be shown to be a superposition of two independent decreases or more. None of the decreases lasting for one day could be put in column 4 of Table 2, which corresponds to cases of CMP of active solar regions coinciding with the middle of the cosmic-ray decrease. If, for example, there is a cosmic-ray decrease from January 9 to 10, and the CMP of active region is on January 8, 9, 10 or 11, these could be put in columns 2, 3, 5, or 6 of Table 2 but not in column 4. For a finer study one needs to look into hourly values. Such a study, which should include the onset time of the Forbush events, would be highly useful in a discussion of the relative merits of the different theories concerning the decreases.

TABLE 2—*Relation between CMP date of solar regions and days during which the decrease in cosmic-ray intensity lasts*

Event	No. of cases
CMP precedes the beginning of cosmic-ray decrease by 2 days	11
CMP precedes the beginning of cosmic-ray decrease by 1 day	18
CMP coincides with day of beginning of cosmic-ray decrease	18
CMP coincides with middle of cosmic-ray decrease	30
CMP coincides with day of minimum cosmic-ray intensity	9
CMP follows day of minimum intensity by 1 day	6
CMP follows day of minimum intensity by 2 days	5

Another way of presenting these data is to examine the average of cosmic-ray intensity changes over a short period of time before, during, and after the CMP date of an area of solar activity. Figure 8 shows an analysis of this, following the well-known Chree technique. The day of each CMP is labeled zero, the days before, -1, -2, etc., and the days after, $+1$ $+2$, etc. The cosmic-ray intensity for each day similarly labeled is added and the sum plotted as ordinate. The same procedure is applied to the K_p magnetic indices. The relative decrease ΔI in cosmic-ray intensity per day is also plotted. ΔI follows K_p; this agrees with the earlier results of *Venkatesan* [1956, 1957ab] and is expected from Alfvén's beam theory.

In Table 2, every decrease has equal value whereas in Figure 8 the large decrease will be

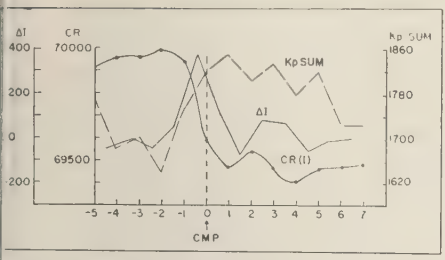

FIG. 8—Chree analysis from −5 days to +7 days. The zero days correspond to the dates of CMP of active solar regions. I refers to the mean nucleonic intensity, K_p for K_p sum, and ΔI for the relative increase in intensity per day.

dominant in fixing the shape of the curve. The distribution in time of the cosmic-ray decreases in relation to the CMP of active solar regions could be due to one of two factors. (1) We may have made a wrong association of some of the decreases with the CMP of solar regions. (2) The effect on the terrestrial cosmic-ray intensity is caused by a beam (or cloud of particles) whose origin is not in the center of gravity of the region to which the CMP refers (D. E. Trotter, private communication, 1958). There is a sufficient number of clear-cut cases to make it most likely that the distribution in time is not due to wrong association of cosmic-ray decreases and CMP's. The distribution in time of the cosmic-ray decreases in relation to CMP of active solar regions and the differences observed from one decrease to another would support the view that the beams (or cloud of particles) from the sun to which the cosmic-ray decreases are attributed, would have considerable differences in characteristics, such as place of origin on the sun, frozen-in magnetic field, velocity of particles, width, and perhaps the direction of emission of the beams in relation to the solar meridional plane. The depression in cosmic-ray intensity should last as long as the earth is in the region of outward flow of gases and is usually followed by a rise in intensity which can be due to the earth moving out of the stream or the stream decreasing in intensity.

There is a definite and significant peaking in the number of events, as can be seen from Table 2. This, coupled with our knowledge of the transit time involved, could give us some information about the place of origin of the beams to which the decreases are attributed. A rough estimate would indicate that beams having their origin within ±15° of longitude from the center of gravity of active solar region (to which the CMP refers) could account for nearly 50 per cent of the cases cited in Table 2. If we consider the origin of the beams to be within ±30° of longitude, we could account for 75 per cent of the cases. The remaining cases would correspond to the origin of the beams outside the ±30° boundary. In this case it is relevant to point out that flares and sunspots are observed beyond 30° of longitude from the center of gravity of the active region, and it is possible that some of the beams are tied up with these flares and sunspots.

One could estimate the extension of the beams in the equatorial plane from the time of duration of geomagnetic disturbances and the cosmic-ray decreases. But nothing definite is known regarding the extension of the beams in the meridional plane. When there are two regions at the same longitude, and hence two beams, one from each hemisphere, it is possible that the two are equivalent to a single one of very large dimensions in the longitudinal plane.

Excepting one at 40° of latitude, all the other active regions occur within the heliographic latitude belt 30° to 10° in both hemispheres (30° in the south and 22° in the north). From this we could infer that the beams are emitted from within this belt.

This region of production of the beams is of importance since it is coupled with the problem of whether the frozen-in magnetic field is governed by the general field of the sun or the local field of the region of production.

Recurrence tendencies in transient decreases—The study clearly reveals that recurrence tendencies are very apparent (see Table 1 for part of the period). The examples listed in Table 3 reveal that the amplitude of the recurrent decrease is very variable, being sometimes smaller (cases 1 to 4), equal (cases 5 to 6), and larger (cases 7 to 9) than the first observed decrease. Very large decreases, such as the two largest, 13 per cent and 9 per cent (cases 10 and 11, Table 3) show no evidence of recurrence. This is understandable since, with reasonable

assumptions regarding the possible frozen-in magnetic field and the velocity of beams such as are suggested by Alfvén, *Venkatesan* [1957ab] has shown that the magnetic flux of the sun would be emptied very quickly unless replenished in some way. The amount of energy involved in maintaining the flow for several months would be very large.

Again, absence of recurrence is not limited to large cosmic-ray decreases of 2 to 4 per cent (see cases 12 to 14, Table 3) but also to small decreases of about 0.3 per cent (see cases 15 to 16, Table 3).

Solar flares and sunspots—The connection between the CMP of active solar regions and the cosmic-ray intensity decreases has been pointed out. The next step would be to make a more detailed study to see whether any definite relationship could be established between the cosmic-ray decreases and special features of the active regions. The occurrence of magnetic storms with a lag of the order of a day after some intense solar flares, and the correlation often observed between cosmic-ray decreases and magnetic storms would indicate a connection between the modulating solar beam and the flare. This is particularly so since the few cases of sudden increases in cosmic-ray intensity associated with flares suggest that the flare action is the source of particles with energies up to a few Bev. From a consideration of the transit time for particles from the sun, one could attribute the decrease associated with the region, and hence the beam, to a particular flare. But the lack of observable effects from the other flares in the region raises the question of whether all flares of the same magnitude do not eject beams or whether such beams do not hit the earth. Let us consider, for example, the cosmic-ray decrease of September 20 or 21 to 23, 1957. This has been attributed to solar Region 57 QD whose CMP is on September 19. There are 28 flares of magnitude 2 to 3+ connected with this region, and these occur during the period September 14 to 23. Some of these are associated with radio fade-outs. There are no other decreases or CMP of other regions at this time to complicate the study. Even if we consider only the largest flares (although there is no justification for this procedure, since regions not having flares of magnitude 3 also produce terrestrial effects) there are four of magnitude 3 (two on Sept. 18, one on Sep 19, and one on Sept. 21) and one of magnitu 3+ on September 18. Even if the flare on Se tember 21 is disregarded in view of the trans time involved, it is not possible to say which the other four should be associated with t decrease. This difficulty becomes greater there are two or more regions near each oth and a number of flares associated with eac It could be summarized that, in general, a regions associated with the larger cosmic-ra decreases were found to have produced flares magnitude 3 or 3+. But not all regions havi flares of this magnitude are always associate with larger cosmic-ray decreases. The decrease in general, started within a day or two of suc flares. *Hartz* [1958] has pointed out that n all flares, even of magnitude 3, produce reco nizable terrestrial effects.

A few cases such as 57 QB (CMP June 1 1957), 57 N (CMP May 25, 1957), 57 V (CM June 4 and July 1, 1957), and 57 JA (CM May 29, 1957), have no flares of magnitud greater than 1 before CMP. Again it is har to see how flares occurring two to seven da after CMP could be connected with decrease attributed to the regions in question, sinc the chances that beams arising from thes flares will hit the earth are rather slende

The same problem arises when one tries t associate the cosmic-ray decreases with sun spots. From an examination of the sunspo structure of active solar areas, it can only b said that no obvious correlation exists. Ther is no evidence for supposing that sunspots ar necessary prerequisites for emission of beam to which the decreases in cosmic-ray intensit are attributed. One cannot rule out the fac that the high magnetic fields observed in sun spots may form all or some part of the sourc of the magnetic fields responsible for the modu lating effect on cosmic rays, when the conductin beams or clouds carrying a magnetic field reac the neighborhood of the earth. It is relevan to recall that *Kiepenheuer* [1953] has pointed ou that sunspots themselves are not known to b sources of corpuscules causing geomagneti disturbances, but that their extensive magneti fields must have a decisive effect on them

Almost all of the active solar regions liste have sunspot groups near the center, whil cases like 57 QD (CMP September 19, 1957)

Case No.	Initial cosmic-ray decrease	Fall (%)	Recurrence	Date of recurrence	Fall (%)	Period	First CMP	Solar region	Activity rating	Recurrence	Date of recurrence	Activity rating	Period	Date* of K_p peak	Date* of recurrence	Period	S.C.
1	Dec. 31,56-Jan. 3, 57	3.14	yes	Jan. 28,57-Jan. 31	2.13	28	Jan. 2, 57	56 JK	a	yes	Jan. 30, 57	d	28	Jan. 2, 57 [27 −]	Jan. 30, 57 [34⁹]	28	Dec. 30, 56 Jan. 2, 57 Jan. 29
2	Mar. 1-Mar. 2	2.55	yes	Mar. 28-Mar. 30	1.14	27½	Feb. 27	57 E	c	yes	Mar. 28	d	29	Mar. 2 [55 −]	Mar. 29 [44⁹]	27	Mar. 1-Mar. 29
3	Mar. 15-Mar. 17	2.55	yes	Apr. 13-Apr. 15	0.93	29	Mar. 16	57 G	c	yes	Apr. 12	b	27	Mar. 16 [34⁹]	No peak		
4	Apr. 3-Apr. 6	2.99	yes	May 4-May 5	0.29	30	Apr. 5	57 M	c	yes	May 3	d	28	Apr. 5 [34 +]	May 3 [19 +]	28	
															May 6 [21 −]	31	
5	Oct. 4, 56-Oct. 5	1.07	yes	Oct. 31, 56-Nov. 2	1.16	27½	Oct. 6, 56	57 NN	b	yes	Nov. 3, 56	c	28	Oct. 6, 56 [24 +]	Nov. 1, 56 [21 −]	26	
	Oct. 7-Oct. 8	0.96	yes ?	Nov. 3-Nov. 4	Steady in midst of recovery	27									Nov. 3 [25 +]	27	
6	Oct.16, 57 Oct. 18	1.22	yes	Nov. 13, 57 Nov. 16	1.29	28½	Oct. 17, 57	57 JU	a	yes	Nov. 14, 57	c	28	Oct. 17, 57 [14⁹]	Nov. 14, 57 [29] −	28	
7	Jan. 16-Jan. 19	0.79	yes	Feb. 11-Feb. 13	1.20	25½	Jan. 18	57 A	b	yes	Feb. 14	e	27	Jan. 15-Jan. 17 [14 +]	Feb. 13 [37 −]	28	
			yes	Mar. 9-	5.54	26				yes	Mar. 13	c	27		Mar. 10 [45 −]	25	Mar. 9-Mar. 10
8	May 25-May 27	2.10	yes	June 21-June 24	3.90	27½	May 27	57 Z	c	yes	June 22	a	26	May 26 [32⁹]	June 22 [23 −]	26	
9	June 5-June 7	1.08	yes	July 2-July 3	2.02	27	June 4	57 V	c	yes	July 1	c	27	June 6 [34 −]	?		July 2
10	Jan. 20, 57-Jan. 22	13.02	no				Jan. 22, 57	56 JE	b	no				Jan. 21-Jan. 22, 57 [39⁰]			Jan. 21, 57
11	Aug. 29-Aug. 30	8.99	no				Aug. 30	57 SL	a	no				Aug. 30 [32 −]			Aug. 29
12	May 25-May 27	2.10	no				May 24	57 T	c	no				May 26 [32⁰]			
13	June 21-June 24	3.90	no				June 21	57 Y	b	no				June 22 [23 −]			
14	June 13-June 16	2.09	no				June 14	57 QB	c	no				June 15 [25 +]			
15	Apr. 8-Apr. 9	0.40	no				Apr. 8	57 C	c	no				Apr. 10? [40 −]			
16	June 9-June 10	0.30	no				June 8	57 U	c	no				June 8 (small peak in midst of fall)			

* K_p *sums in brackets.*

57 H (CMP April 22, 1957), etc., have two or more distinct groups. 57 JE (CMP July 21, 1957) had spot groups extending continuously over 60° of longitude and is difficult to associate with any particular group. In the regions 56 JQ and 56 JH, both of which cross the meridian on December 21, 1956, and to both of which the decrease on December 18 to 22, 1956, could be attributed, there are no sunspots before December 20 to 21. Any possible terrestrial effect due to spots seen crossing the meridian on December 21 or later would normally produce a terrestrial effect after December 22. Nor could spots due to any other regions be associated with the decrease mentioned, since the other two regions, 56 JA (CMP December 10) and 56 JC (CMP December 13), and their associated spots crossed the meridian by December 13. Here, then, is an example of a decrease (and consequently a beam) which has no association with sunspots. Again, there are regions with hardly any spots before CMP which develop spots afterwards. Normally it is difficult to imagine how these could produce any terrestrial effects, unless one makes a further assumption that the beams are ejected considerably inclined to the solar surface.

Discussion of results—There are a few further details of this analysis worth discussing. It seems impossible from these data to connect the modulating forces on cosmic rays with any more detailed features of solar activity except to say that the decrease is associated with the active region. However, there is an apparent relation between the strength or activity rating [*High Altitude Observatory Quarterly Reports*] of the solar regions and the cosmic-ray decreases (Table 4). Each group is associated with an average cosmic-ray decrease which has been obtained by combining all decreases attributed to regions of that activity rating. A clear relationship between the decrease and activity rating can be seen.

TABLE 4—*Relation between intensity of solar region and cosmic-ray intensity decrease (mean nucleonic component) during the year* 1957

No.	Intensity rating of active solar region	Cosmic-ray decrease (%)
1	a	3.67
2	b	2.62
3	c	1.49
4	d	1.43
5	e	1.20

The question of increases occurring in the cosmic-ray intensity was prominent a few years ago [*Simpson* and others, 1955]. When intensity changes occur with the periodicity of solar rotation, it would be difficult to say whether these are increases or decreases. The evidence that the Forbush decreases and slower, irregular decreases, which sometimes are repetitive, are the same phenomena (from this analysis and from that of *Fenton* and others [1958]), suggests strongly that increases do not occur except as the recovery from decreases of this type. A more detailed study of similar variations during the coming phase of decline in the eleven-year cycle of solar activity (and hence increase in cosmic-ray intensity) might throw more light on this.

The question of the nature of the variation of the cosmic-ray flux is still important, and continued observations of these decreases over more than one solar cycle is desirable. In Alfvén's beam picture for the variation the general field of the sun is considered to be responsible, and this is in a direction which will always produce a decrease when the earth moves into a beam. *Alfvén* [1958] and *Dorman* [1958] consider that the cosmic-ray intensity variations could be explained in terms of beams with a frozen-in magnetic field. They further have pointed out that turbulence in beams cannot be of any great importance, a view which is not held by *Parker* [1956]. If turbulence is dominant in the beams it would be difficult to account for diurnal variation.

In connection with diurnal variation, *Sarabhai* and others [1956] have considered the local field to be frozen in. *Dorman* [1958] has discussed two types of beams, one from the high heliographic latitudes and supposed normally to have the general field frozen in, and the other from the middle and equatorial heliographic latitudes with the comparatively stronger sunspot fields frozen in.

The sunspot fields, ranging from 100 gauss in the smallest measurable spots to as much as 4000 gauss in the large ones, decrease from the center of the spot to less than 50 gauss at the outer edge of the penumbra [*Kiepenheuer*, 1953].

; is an open question how far out this field is ffective. The general solar field, although very uch weaker than the limited regional sunspot elds, extends over a much larger dimension. n view of the fact that nothing definite was nown about the exact region of production f the beams, the Alfvén group have assumed at the general field would be the predominant nfluence in determining the nature of the agnetic field frozen in the beams.

If the sunspot field ultimately determines ne magnetic field frozen in the beams, then ne direction of the field would be expected o vary from time to time and might even everse with the known reversal of sunspot olarity in alternate solar cycles. In this case, ncreases rather than decreases might be observed.

There have been occasional indications of a eversed field in beams [*Venkatesan*, 1957ab]. A tudy of transient changes during two successive olar cycles would be of great importance in hrowing some light on this problem.

The dependence of the amplitude of the verage cosmic-ray decrease on the activity ating of the solar region, as seen from Table 4, ould mean that with a higher activity of the egion there is more energy available and hence higher velocity, **V**, in the beams. This would esult in a stronger electric field, **E**, and a onsequently larger cosmic-ray decrease, since $\mathbf{E} = 1/C\ \mathbf{V} \times \mathbf{H}$, where **H** is the frozen-in nagnetic field. It is also equally possible that greater energy in the solar region might esult in the ejection of a greater number of articles, altering the density in the beams. gain, if instead of the general solar field, the unspot field is frozen in the beams, **H** also aries from beam to beam. There could, therefore, be considerable differences in the haracteristics of the different beams and, ence, considerable differences in the cosmic-ray ecreases and geomagnetic disturbances and heir interrelation. A superposed second-order urbulence in the beams, if it exists, could omplicate the issues further.

In some of the decreases studied there is a uggestion of structure or variability in the nodulating stream. In some cases (not included in Table 1), for instance that of December 24 and 26, 1956, two decreases have been attributed to the same active region. These could well represent structure in the modulating stream of particles or two independent sources from different points on the active area. It is relevant to point out that in some cases the High Altitude Observatory reports show the existence of two main growths in two different parts of the active region. There are also instances where the old center at the western end of the active region dies and a new one appears at the eastern end. This leads to an apparent break or shift in the periodicity of the recurrence formation connected with the region.

Conclusion—An analysis of the time of the decreases in cosmic-ray intensity has shown a relationship with the CMP of areas of solar activity. For a period of 15 months (October 1956 to December 1957) all important areas of solar activity have been considered and also all decreases in the mean daily cosmic-ray intensity where the magnitude of the decrease is equal to or greater than the standard error of the counting rate. It is relevant to recall that the mean cosmic-ray intensity is derived by averaging the neutron data from Ottawa, Churchill, and Resolute, which are all above the latitude knee. One hundred and twenty-three cases showing a clear decrease or a definite suggestion of a decrease have been considered. Out of these, 110 could be associated with the CMP of 54 active solar regions. The remaining 13 cases are small for the most part, and are not connected with any prominent solar region.

Assuming that the effect is a variation of the cosmic-ray flux probably taking place relatively near to the earth (at a distance much smaller than the distance between the earth and the sun), one can say that the area of solar activity appears to be the source of the modulating beam or cloud. On the other hand, there is insufficient clear evidence to connect the source of the modulating effect with any detailed structure in the active solar regions such as sunspots or flares.

The data and this analysis are insufficient to allow us to distinguish clearly between a simple polarized beam theory, such as that of Alfvén, or a turbulence theory, such as that of Parker. From the differences in the time coordination between CMP's and cosmic-ray decreases, and from the differences in the individual decreases, one is led to conclude that the modulating solar beams have considerable

differences in their characteristics. Recurrences are observed which have close correlation with the rotation of active regions, as long as the region remains active. Instances of recurrence, as well as nonrecurrence, are exhibited by both large and small cosmic-ray intensity decreases. This indicates that the large and small decreases differ only in degree, and hence the same mechanism could be invoked to explain both. The largest decreases show no tendency to recur.

A study of the relation between the time of onset, or time of duration, of the decreases and CMP reveals a distribution of a random nature. There is, however, a peak. In relation to the CMP of active solar areas, 70 per cent of the decreases are included in situations where the CMP occurs one day before the cosmic-ray decrease starts, or the CMP occurs on the same day the decrease starts, or the CMP corresponds to one day after the decrease starts (the CMP occurs in the middle of the decrease). This gives some indication of the region from which the beam originates.

There is an apparent relation between the activity of solar areas and the magnitude of the associated cosmic-ray decrease.

Acknowledgments—The author wishes to thank the National Research Council for the award of a Postdoctorate Fellowship and D. C. Rose and J. Katzman for useful discussions. The author is also grateful to D. E. Trotter for providing solar data before publication and for her comments on the same. The analyses were made possible by the tireless efforts of all the people in the Cosmic-Ray Group of the National Research Council who maintained the equipment at the various stations, and of those in the computation section who have tabulated and averaged the data. It is a pleasure to express my thanks to all of them.

References

Alfvén, H., On the origin of cosmic radiation, *Tellus*, **6**, 232–259, 1954.

Alfvén, H., On the theory of magnetic storms and aurorae, *Tellus*, **10**, 104–116, 1958.

Brown, R. R., Time variations of cosmic ray intensity, *J. Geophys. Research*, **61**, 639–646, 1956.

Brunberg, E. Å., and Dattner, A., (a) On the interpretation of the diurnal variation of cosmic rays, *Tellus*, **6**, 73–83, 1954; (b) Variations of the cosmic ray intensity during magnetic storms, *Tellus*, **6**, 254–259, 1954.

Davis, L., Interplanetary magnetic fields and cosmic rays, *Phys. Rev.*, **100**, 1440–1444, 1955.

Dorman, L. I., *Cosmic rays variations* (translation), Tech. Doc. Liaison Office, Wright-Patterson Air Force Base, 1958.

Fenton, A. G., K. B. Fenton, and D. C. Rose, The variation of sea level cosmic ray intensity between 1954 and 1957, *Can. J. Phys.*, **36**, 824–839, 1958.

Forbush, S. E., Cosmic ray effects associated with magnetic storms, *Terrestrial Magnetism and Atmospheric Elec.*, **43**, 203–218, 1938.

Forbush, S. E., World wide cosmic ray variations 1937–1952, *J. Geophys. Research*, **59**, 525–542, 1954.

Hartz, T. R., Defense Research Telecommunications Establishment, *Radio Phys. Lab. Rep., No.* 23-2-3, 1958.

High Altitude Observatory Quarterly Reports, no. 36, 15 July 1957; no. 38, 15 November 1957; no. 39, 20 March 1958; and no. 40, 16 June 1958.

Kiepenheuer, K. O., *The sun*, G. P. Kuiper, ed., Univ. Chicago Press, ch. 6, 1953.

Lockwood, J. A., Variations in the cosmic ray neutron intensity from 1954-57, *Bull. Am. Phys. Soc.*, series 2, vol. 3, no. 3, 1958.

Mathews, P. M., Atmospheric effects on cosmic ray intensity at sea level, in press, *Can. J. Phys.*, 1959.

Meyer, P., and J. A. Simpson, Changes in amplitude of the cosmic ray 27-day intensity variation with solar activity, *Phys. Rev.*, **96**, 1085–1088, 1954.

Morrison, P., Solar origin of cosmic ray time variations, *Phys. Rev.*, **101**, 1395–1404, 1956.

Parker, E. N., Modulation of primary cosmic ray intensity, *Phys. Rev.*, **103**, 1518–1533, 1956.

Sarabhai, V. A., S. P. Duggal, H. L. Razdan, and T. S. G. Shastry, Electromagnetic phenomena in cosmical physics, *Proc. Intern. Astron. Union Conf.*, Stockholm, 1956.

Simpson, J. A., H. W. Babcock, and H. D. Babcock, Association of a "Unipolar" magnetic region on the sun with changes of primary cosmic ray intensity, *Phys. Rev.*, **98**, 1402–1406, 1955.

Singer, F., *Maryland Univ. Phys. Dept. Tech. Rept.* 40, 1956.

Singer, F., *Progress in elementary particles and cosmic ray physics*, vol. 4, North Holland Publishing Co., Amsterdam, 1958.

Van Heerdan, I. J., and T. Thambyahpillai, The 27-day recurrence tendency of cosmic ray intensity, *Phil. Mag.*, **46**, 1238–1251, 1955.

Venkatesan, D., Electromagnetic phenomena in cosmical physics, *Proc. Intern. Astron. Union Conf.*, Stockholm, 1956.

Venkatesan, D., *Tellus*, **9**, 209, 1957.

Venkatesan, D., Proc. Intern. Union Pure and Appl. Phys. Cosmic Ray Conf., Varenna, 1957.

Venkatesan, D., *Tellus*, **10**, 117, 1958.

(Manuscript received September 5, 1958; revised January 5, 1959.)

Daily and Annual Courses of Natural Atmospheric Radioactivity

Marvin H. Wilkening

New Mexico Institute of Mining and Technology
Socorro, New Mexico

Abstract—Measurements of the radon-decay products in the atmosphere over a 6-year period have been made with a monitor which precipitates fine airborne particulate matter onto a moving metallic tape. A calibration of the apparatus showed that the mean value for radon content at Socorro, New Mexico, is 2.4×10^{-13} curie/liter, with an average diurnal fluctuation of a factor of 3.1 between maximum and minimum values. The diurnal variation is attributed to the amount of vertical mixing due to eddy diffusion in the lower atmosphere. The gustiness in air motion near the ground is taken as a measure of the mixing that occurs, and it is measured with a hot-wire anemometer. An annual variation in the atmospheric radioactivity is found which gives values during the fall months that are about twice those during the spring. This variation can also be explained in terms of the mixing that occurs at low levels as judged from mean wind-speed data. Values for the coefficient of vertical diffusion are calculated from measurements of the exhalation rate of radon from the ground and the concentration of radon near ground level as determined from the monitor data. The mean value of the height-independent diffusion coefficient is 6.7×10^4 cm²/sec. Maximum values of as high as 55×10^4 cm²/sec are found in the late afternoon of the month of April. Minimum values of the order of 2.0×10^4 cm²/sec are found in the early morning hours in the fall months.

Introduction—The daily fluctuation in the radon content of the air near the earth's surface was first reported by *Becker* [1934]. A need has been expressed by *Israel* [1951] for long-term measurements using automatic equipment in order that a more detailed understanding of the phenomenon may be obtained.

The present study, begun in the latter part of 1951, includes results obtained at intervals since that time with a continuously recording instrument which electrostatically precipitates particulate matter from the atmosphere onto a moving aluminum tape [*Wilkening*, 1952]. The alpha activity of the material deposited on the tape is detected by means of a scintillation counter. Since under normal conditions the decay products of radon are found in equilibrium amounts on the very fine particulate matter in the atmosphere, the monitor gives a reliable measure of the radon content. The fact that the apparatus proved to be trouble-free in operation and that it could be checked easily with standards made it particularly useful for recording data pertinent to the study of long-term variations. Although the monitor was usually operated so that it was sensitive to alpha emitters only and so that the radon daughters would be favored over nuclides of longer half-life, data were discarded from those periods during which the presence of atmospheric contaminants such as those from the test of nuclear weapons was suspected and verified.

The monitor was calibrated by comparing its output in alpha counts per minute with the atmospheric radon concentration as measured directly with a radon-condensing apparatus. Radon from a known quantity of air was condensed in a copper coil maintained at the temperature of liquid oxygen. At the end of a one-hour collection period the radon was flushed into an ion chamber. The efficiency of collection, transfer, and detection of the radon within the apparatus was determined by using radon from a standard radium solution obtained from the National Bureau of Standards. The mean of seven runs taken at different activity levels gave $(2.9 \pm 0.2) \times 10^{-13}$ curie per liter per 100 alpha counts per minute.

The daily course—The mean daily course of activity for each month is shown in Table 1. The data represent the operation of the monitor from November 1951 through June 1957 (692 days).

TABLE 1—Mean daily course of natural radioactivity by month in alpha counts per minute

Local Time	Jan	Feb	Mar	Apr	May	June	July	Aug	Sept	Oct	Nov	Dec
1	105	82	70	53	80	92	83	88	77	138	136	90
2	112	89	70	57	89	96	93	90	84	151	137	93
3	121	90	81	62	92	104	103	102	89	156	150	98
4	122	97	83	67	99	111	110	112	97	163	161	94
5	117	103	88	73	109	116	126	114	102	175	161	96
6	123	104	89	71	115	123	141	124	103	178	160	94
7	122	106	98	78	119	132	149	132	113	202	163	101
8	127	116	104	77	110	104	120	105	109	207	172	108
9	137	125	98	69	88	74	78	73	82	180	163	128
10	129	113	74	58	82	62	72	54	63	136	128	117
11	110	95	68	52	77	54	63	54	54	110	108	110
12	87	81	59	49	67	49	61	49	48	101	92	92
13	79	77	53	42	60	51	56	44	45	87	80	82
14	68	67	54	35	41	48	47	42	42	74	69	76
15	59	56	53	32	31	41	39	39	40	65	62	70
16	53	52	48	32	30	39	36	38	40	62	59	63
17	48	47	42	28	34	38	37	38	39	67	58	56
18	51	46	41	28	36	40	39	38	39	61	63	56
19	56	48	40	31	41	48	42	41	41	74	72	60
20	68	56	44	34	49	55	46	46	48	96	85	67
21	81	65	50	39	58	67	55	54	57	83	94	74
22	86	70	55	43	65	77	63	64	59	121	110	79
23	95	72	58	47	69	83	69	75	64	123	118	85
24	102	74	65	48	75	88	75	79	78	128	125	87
Mean counts/min	94	81	66	50	72	75	80	71	67	122	114	86
Ratio: max/min	2.8	2.7	2.6	2.8	4.0	3.3	4.1	3.5	2.8	3.3	3.0	2.3
No. of days	50	57	54	47	34	101	80	73	34	35	77	50
Years	'52 '54	'52 '54 '56	'52 '54 '55	'52 '55 '56	'53 '55	'52 '53 '55 '56 '57	'52 '53 '55	'52 '53 '55	'53 '55	'52 '55	'51 '52 '53 '55	'51 '52 '53 '55

Horizontal bars give approximate time of sunrise and sunset.

The well-known early-morning 'high' follows sunrise on the average of 70 minutes. The level of activity falls rapidly during midmorning and reaches a minimum in the late afternoon. A slow recovery toward the maximum is observed during the night hours. The mean activity for each month and the ratio of the maximum to the minimum are given at the bottom of Table 1. The over-all average activity is 81 counts/min or, on the basis of the calibration figure, 2.4 ×

0^{-13} curie of radon per liter. The mean ratio of maximum to minimum activity each day is 3.1. An idea of the statistical fluctuation of monthly averages for a given hour from year to year is suggested by a mean standard deviation of 21 counts/min for the 1200 (noon) readings. The number of days used in the hourly averages and the years in which these data were taken are also given.

The data of Table 1 also show a pronounced seasonal effect, the spring months showing mean activities of only about half those of the fall months of October and November.

Explanation of the diurnal effect—Previous investigators [*Israel*, 1951; *Burke* and *Nolan*, 1950; *Blifford* and others, 1956] have considered temperature, change in barometric pressure, humidity, and air movements, particularly vertical exchange by eddy diffusion, as contributing factors to the diurnal change. The lack of any marked deviation from equilibrium between radon and its decay products measured at different hours of the day, and the sharp drop in activity accompanying the passage of a cold front or the sudden break-up of an inversion, seemed to indicate that large-scale mixing in the atmosphere is much more important than factors such as temperature and changes in barometric pressure which affect the rate of transport of radon gas across the earth-air interface. Accordingly, it was desired to make some measurement which would reflect as directly as possible the amount of vertical mixing occurring in the air near the surface of the earth.

Sutton [1953] emphasized that the main effect of turbulence in the atmosphere is to cause large-scale mixing. Since the most direct and easily recognized evidence of turbulence is the fluctuating record of an anemometer capable of indicating instantaneous values of wind speed [*Sutton*, 1949], a hot-wire-thermopile type of air-velocity meter and a recording potentiometer were used to give a continuous plot of wind speed versus time. The half-width of the recorder trace averaged over 15-minute intervals was defined as the "gust amplitude," which is taken as a measure of the local turbulence. The hot-wire thermopile was kept at a height of one meter above the ground in a space free of trees and buildings. Figure 1 gives a comparison between recorder traces for the count-rate meter and the hot-wire anemometer on two successive nights. The activity record for the overnight run of July 27–28 is typical of conditions yielding high early-morning peaks. The peak activity at 0630 on July 28 represents 300 alpha counts/min or 8.4×10^{-13} curie/liter.

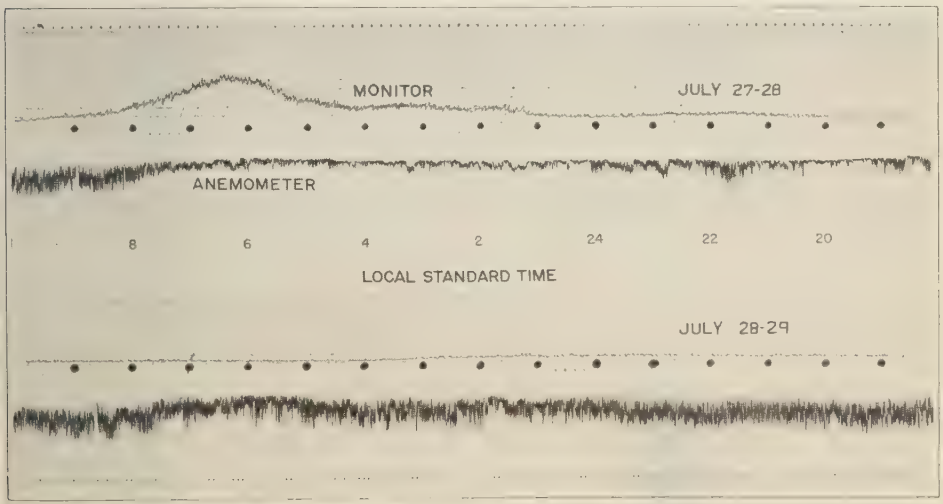

FIG. 1.—Radioactivity monitor and hot-wire anemometer traces for two successive nights

Except for some gustiness, as indicated by the anemometer record from about 2030 to midnight, the night hours were calm, and the radioactivity increased markedly after midnight until about 0630 on the morning of July 28. At that time turbulence near the ground began the mixing process, which in turn reduced the activity level to about 30 counts/min by 0945. The next night presented a marked contrast. Gustiness was at a high level and continuous through the night. The corresponding activity remained low throughout the period.

The day-by-day correspondence between the natural radioactivity and gust amplitude is shown in Figure 2 for the period of August 4 to

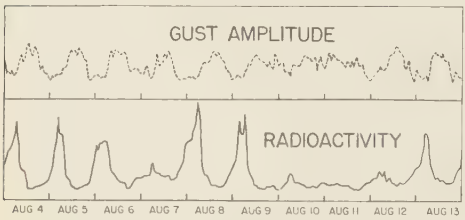

FIG. 2—Comparison of daily gust-amplitude and natural-radioactivity records

13 inclusive. Typical radioactivity is seen for the days of August 4, 5, 6, 8, 9, and 13. These days were characterized by clear, calm early mornings without exception, even though some of the afternoons were partly cloudy, with some gusty winds. The days of August 7, 10, 11, and 12, which were marked by relatively high gust amplitude, included cloudy, unsettled weather, with some light precipitation. These same days showed very low natural radioactivity.

The mean daily course of gust amplitude and radioactivity for August 1955 is given in Figure 3. The agreement between the two curves, particularly with respect to the onset of turbulence as measured by the gust amplitude and the sharp drop in activity at the same time, gives convincing evidence that the mixing hypothesis as an explanation for the diurnal change in natural radioactivity is correct.

The annual course—Considering the nature of the cause of the diurnal variation, it is not surprising that a seasonal effect was observed in the data of Table 1. Mean values for all months

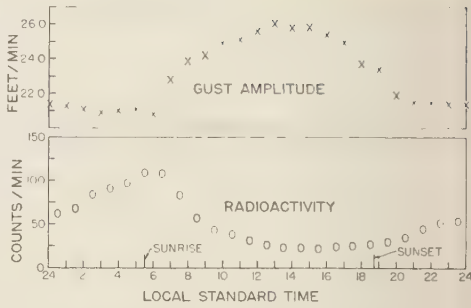

FIG. 3—Mean gust amplitude and natural radioactivity for the month of August, 1955

for which data were available in the period of November 1951 to December 1955 are shown in Figure 4. Mean wind speeds recorded at the nearby U. S. Weather Bureau station are plotted for comparison, since gust amplitude data were not available. A limited correlation between natural radioactivity and mean wind speed can be expected since gustiness is proportional to the mean wind only under certain conditions [*Sutton*, 1949]. The spring and early summer months, with high average wind speeds, show the lowest mean values for natural radioactive content; and the calm, clear months in late fall show predominantly high values of radioactivity. The mean values of natural radioactivity for the months of July, August, and September would undoubtedly be higher if it were not for the summer thunderstorm activity, with the accompanying additional mixing, that occurs during these months in New Mexico.

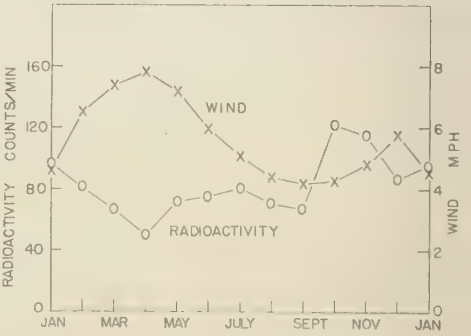

Fig. 4—Annual course of natural radioactivity and mean wind speed

The recent work of *Reiter* [1957] suggests that a different pattern of annual variation exists in the northern Alps.

Vertical diffusion—The data obtained with the monitor can be used to calculate values of the coefficient of vertical diffusion in the atmosphere. The earth can be considered an infinite plane source for supplying atmospheric radon. Since the rate at which radon is supplied at the earth-air interface per unit area must equal the rate of radioactive decay of the radon contained in a vertical column of the same unit area, one can write

$$E = \int_0^\infty \lambda N \, dZ$$

where E is the exhalation of radon from the ground, λ the decay constant of radon, N the concentration of radon atoms per unit volume, and Z the distance above the surface. The dependence of N on Z is obtained from a solution of the diffusion equation

$$K \frac{\partial^2 N}{\partial Z^2} = \lambda N$$

where K is the coefficient of vertical diffusion due to eddy motion in the atmosphere. If K is assumed to be independent of the height Z, a solution of the diffusion equation is

$$N = N_0 e^{-(\lambda/K)^{\frac{1}{2}} Z}$$

where $N = N_0$ at $Z = 0$, and $N = 0$ at $Z = \infty$. Substitution of N in the exhalation equation above gives, on integration,

$$E = N_0(\lambda/K)^{\frac{1}{2}}$$

Although K is known to vary with altitude, it is of interest to use the exhalation equation to calculate representative values of a height independent K. Measurements by *Hand* [1958] in this Laboratory give a value for E of 90×10^{-18} curie per cm² and sec. His results further show that E is essentially independent of the time of day. The mean value of N_0 obtained from all the monitor data is 2.4×10^{-13} curie/liter. The monitor actually sampled air 0.8 meter above the ground, but negligible error is made by using this value of N_0 for the concentration at $Z = 0$. It is further assumed that N_0 is not appreciably affected by horizontal airmass movements. This assumption is supported by a comparison of radioactivity level with wind direction at six-hour intervals over 233 days of operation of the monitor. No significant correlation was found in at least 80 per cent of the cases. Also, negative-wire collection made during low-level plane flights over varied types of terrain under fair-weather lapse conditions during the summer of 1952 showed remarkably uniform radon-product content. Collections were made at five points over a 150-mile course between Socorro and Roswell, New Mexico.

From the values of E and N_0 given and the known value of λ for radon, the mean value of K is 6.7×10^4 cm²/sec.

TABLE 2—*Diurnal variations of the mean radon content and of the mean coefficient of the vertical component of eddy diffusion in the atmosphere*

Local Time (hour)	April		November	
	N_0 curie/liter ($\times 10^{-13}$)	K cm²/sec ($\times 10^4$)	N_0 curie/liter ($\times 10^{-13}$)	K cm²/sec ($\times 10^4$)
2	1.6	14	4.1	2.3
4	1.9	10	4.6	1.8
6	2.1	8.6	4.7	1.8
8	2.2	8.1	4.9	1.6
10	1.7	13	3.8	2.6
12	1.4	20	2.7	5.3
14	1.0	35	2.0	9.4
16	0.9	48	1.7	13
18	0.8	55	1.9	11
20	1.0	39	2.4	6.5
22	1.2	25	3.1	4.0
24	1.4	19	3.7	2.9

The data from Table 1 for the months of April and November, which represent extremes in the annual cycle, are used in Table 2 to show the diurnal variation of K for these same months. It is observed that K varies from 1.7 to 55 ($\times 10^4$ cm^2/sec), with maximum values occurring in the late afternoon on the diurnal cycle and in the spring months (April) on the annual cycle. Conversely, minimum values of K are found in the early morning hours and during the fall months. Representative values of K which were obtained fall within the upper limits of the range given in *Lettau's* summary [1951] of values for the vertical coefficient of eddy diffusion in the height range 0 to 1 km and within the lower limits of the 1- to 10-km range for ordinary turbulence. *Kawano* [1957] obtained values for a height independent K from atmospheric electricity data that are consistently lower than those given in Table 2.

Conclusion—The gust amplitude data here presented give sound evidence that the diurnal course of natural radioactivity can be explained in terms of the corresponding diurnal changes in vertical mixing by eddy diffusion in the lower levels of the atmosphere.

The spring minimum and fall maximum in the annual course are related in an inverse fashion to the mean wind speeds at these seasons. Since an increase in mean wind speed is accompanied in general by an increase in gust amplitude, and hence also in turbulent mixing, one can assume that the spring minimum in activity results from excessive mixing in the lower atmosphere, whereas the relatively calm days of the fall months contribute to less vertical mixing, with resulting higher levels of natural radioactivity.

The diurnal variation of the mean coefficient of the vertical component of eddy diffusion in the atmosphere has been determined. The monitor data were used to determine ground-level concentrations of radon, and separately measured values were used for the exhalation rate of radon from the soil into the atmosphere.

References

Becker, F., Measurement of the emanation content of air at the Meteorological Institute at Frankfurt on the Main, *Gerlands Beitr. Geophys.*, **42**, 365–384, 1934.

Blifford, I. H., Jr., H. Friedman, L. B. Lockhart, Jr., and R. A. Bans, Geographical and time distribution of radioactivity in the air, *J. Atmospheric and Terrestrial Phys.*, **9**, 1–17, 1956.

Burke, Thomas, and J. J. Nolan, Observations on the radium A content of the atmosphere, *Proc. Roy. Irish Acad., A*, **53**, p. 145, 1950.

Hand, John, Radon flux at the earth-air interface, Master's thesis (to be published), New Mexico Institute of Mining and Technology, 1958.

Israel, H., Radioactivity of the atmosphere, *Compendium Meterol.*, Am. Meteorol. Soc., pp. 155–161, 1951.

Kawano, M., Coefficient of eddy diffusivity estimated by the method of atmospheric electricity, *J. Meteorol. Soc. Japan*, **35**, 29–32, 1957.

Lettau, Heinz, Diffusion in the upper atmosphere, *Compendium Meteorol.*, Am. Meteorol. Soc., pp. 320–333, 1951.

Reiter, Reinhold, Schwankungen der Konzentration und des Verhältnisses der Radon- und Thoronabkömmlinge in der Luft nach Messungen in den Nordalpen, *Z. Naturforsch.*, **12a**, 720–731, 1957.

Sutton, O. G., *Micrometeorology*, McGraw-Hill Book Co., New York, p. 68, 1953.

Sutton, O. G., *Atmospheric turbulence*, Methuen and Co., Ltd., London, pp. 14–16, 1949.

Wilkening, M. H., Monitor for natural radioactivity in the atmosphere, *Nucleonics*, **10**, p. 36, 1952.

(Manuscript received August 11, 1958; revised February 13, 1959.)

Green Coronal Line Intensity and Geomagnetism

C. Warwick

National Bureau of Standards
Boulder, Colorado

Abstract—Climax Observatory spectograms of the green coronal line, λ5303, for the period 1942-1944 near solar activity minimum have recently been remeasured. Analysis of these revised intensities indicates that the most consistent feature in the relation of green line intensity to geomagnetism is a minimum in geomagnetic activity following central meridian passage (CMP) of regions of high green line intensity. This effect may be interpreted as a result of the tendency of solar activity regions to coincide with regions of high green line intensity and to avoid M regions. In the period October 1953 to October 1954, at sunspot minimum, no relation appeared between green line intensity and geomagnetic activity.

Introduction—A number of authors have concluded from various statistical studies that systematic changes in geomagnetic activity are associated with intensity of the green coronal emission line. [See *Bell* and *Glazer*, 1957, for a summary of this work; also *Sinno*, 1957.] Two fairly consistent results appear from most of these studies, *for the period near sunspot minimum*:

1. A minimum in geomagnetic activity follows two or three days after central meridian passage (CMP) of a region of strong green corona [*Shapley* and *Roberts*, 1946; *Kiepenheuer*, 1947; *Bell* and *Glazer*, 1954, 1956, 1957]. In the period 1942–1944 this minimum was preceded by a maximum in geomagnetic activity about three days before CMP of the region [*Shapley* and *Roberts*, 1946; *Kiepenheuer*, 1947], but in the 1951–1953 period this maximum was not pronounced [*Bell* and *Glazer*, 1954, 1956, 1957].

2. A maximum in geomagnetic activity follows two or three days after CMP of regions of exceptionally low green coronal intensity [*Bell* and *Glazer*, 1954, 1956, 1957; *Sinno* 1957].

Results from one period to another, however, have not been consistent, and even within short time periods marked differences often appear from year to year [*Kiepenheuer*, 1947; *Bell* and *Glazer*, 1954, 1956, 1957]. In the present study we propose to re-examine the question of the relation between geomagnetic disturbance and the solar corona in the light of revised coronal intensity measures for the period 1942–1944.

Observations—Original Climax coronal spectrograms for the period April 27, 1942 to May 24, 1944 have recently been remeasured [*Billings*, 1957]. The new measures are based on densitometer tracings, rather than on visual estimates, and have been corrected for the threshold effect. Intensity measures of west limb observations which were missing from the original publications have been added. On the basis of these revised data zero days were selected for a superposed epoch analysis of the geomagnetic character figure A_p. For each day and for each quadrant of the solar limb the highest value of intensity of λ5303 was selected. When both east limb and west limb coronal observations were available for a given solar longitude, we used the mean of the two measures. During the period studied, 61 per cent of the CMP dates had coronal observations for at least one limb. From the maximum daily values, the dates of the six highest and the six or more lowest (we include all days when the maximum intensity was ≤ 1) were selected for periods equalling one-eighth of a year, so that 48 high values and 48 or more low values were selected for each hemisphere for each year. We have used this simple index of coronal intensity because *Bell* and *Glazer*'s results [1957] indicate that its relation to geomagnetic activity is similar to that of the mean of the five highest intensities.

Analysis—Figures 1 and 2 show the results of superposed epoch analysis of A_p around CMP dates of regions of high and low green line intensity. In each case, the lower curve shows

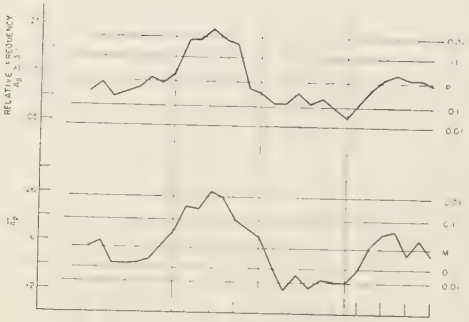

FIG. 1—CMP of regions of high intensity of green coronal line, 1942–1944; 203 cases

the mean value of A_p, and the upper curve shows the frequency of values of $A_p \geq 30$ for each day. The horizontal lines indicate the probability that a point for some one day should fall outside the line. These probabilities were computed from Student's distribution; the effect of autocorrelation of A_p for days 0, 1, 2, 26, 27, and 28 was taken into account.

In Figure 1, the maximum in geomagnetic index three or four days after east limb passage of regions of high green line intensity is consistent with that found by *Shapley* and *Roberts* [1946] for the same period. A maximum in geomagnetic activity (Figure 2) follows CMP of regions of low green line intensity by five days; whereas *Bell* and *Glazer* [1957] found, for the period 1951–1953, a maximum at CMP + 2 days. Only the pre-CMP maximum for regions of high green line intensity falls beyond the 1 per cent level of significance for both mean A_p and frequency of high A_p values.

Because both coronal intensity and geomagnetic activity tend to show a 27-day periodic variation, it is possible for a strong statistical relation between the two quantities to appear even in the absence of any physical relation. We have found that the data from a limited period, autumn of 1943, when an intense geomagnetic disturbance recurred several times, tend to dominate the results of the whole analysis. *Shapley* and *Roberts* [1946] and *Bell* and *Glazer* [1957] have also noted the strong effect of this single recurrent region. In Figures 3 and 4 are plotted the superposed epoch results of A_p and of frequency of $A_p \geq 30$ for CMP dates occurring in the fall of 1943, compared with the results for all other selected dates. We see that, indeed, when data from this period are eliminated, the relation between coronal intensity and geomagnetic activity becomes very much weaker. The maximum following CMP of regions of low coronal intensity is practically lost,

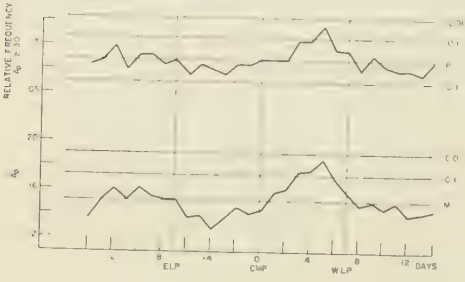

FIG. 2—CMP of regions of low intensity of green coronal line, 1942–1944; 216 cases

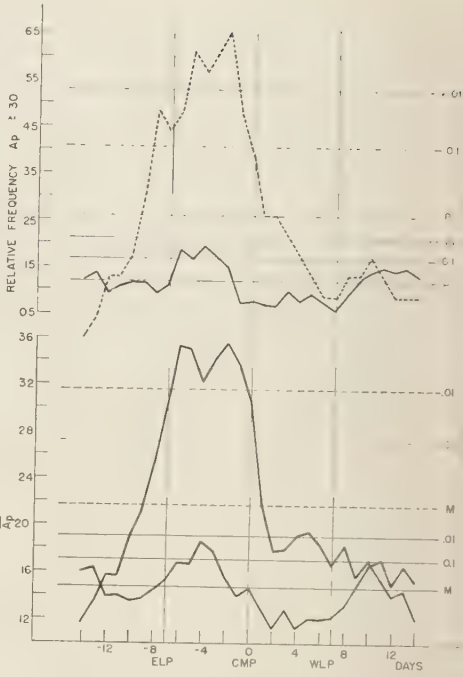

FIG. 3—CMP of regions of high intensity of green coronal line; upper curve: regions occurring in the northern hemisphere in the autumn of 1943; 23 cases; lower curve: all other regions, 1942–1944; 129 cases

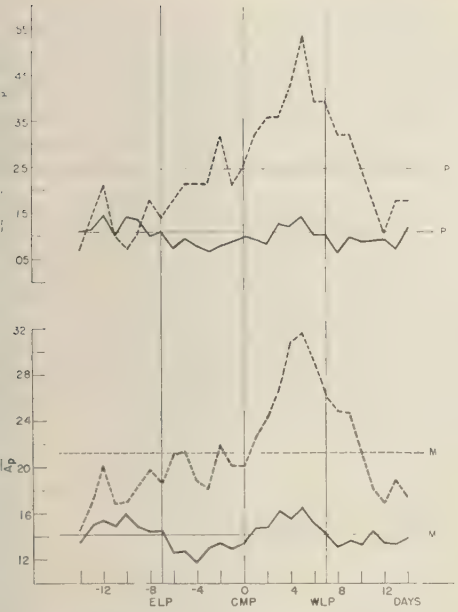

FIG. 4—CMP of regions of low intensity of green coronal line; upper curve: regions occurring in the southern hemisphere in the autumn of 1943; 28 cases; lower curve: all other regions, 1942–1944; 188 cases

and the maxima and minimum of the curve for regions of high coronal intensity fall within the 1 per cent level of significance, although they still appear as the most striking features of the curve.

We next ask to what extent the coronal intensity–geomagnetic relation is dependent on the association of each phenomenon with solar active regions. It has been shown [*Allen*, 1944; *Sinno*, 1956] that M-region storms, which dominate

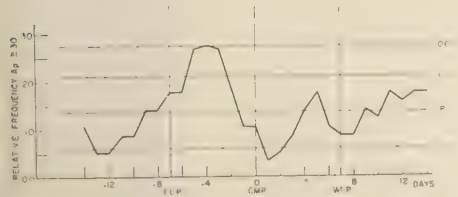

FIG. 5—CMP of regions of high intensity of green coronal line associated with active regions, 1942–1944; 56 cases; autumn of 1943 omitted

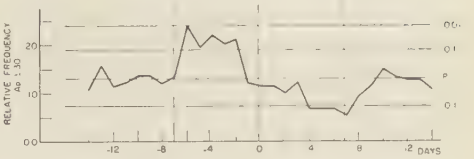

FIG. 6—CMP of regions of high intensity of green coronal line not associated with active regions, 1942–1944; 147 cases; autumn of 1943 omitted

geomagnetic activity near sunspot minimum, are negatively correlated with active regions, as characterized by large sunspots, high flux of solar radio noise, and high intensity of green coronal line. If there is a close relation between high coronal intensity and active regions, we would expect that the strongest coronal-geomagnetic relation, near sunspot minimum, would be a depression of geomagnetic activity associated with regions of strong coronal intensity. The coronal data of 1942–1944 indicate that this is so. This interpretation is strengthened by the results of Figures 5 and 6, which show that the minimum in frequency of high A_p values following CMP of regions of high coronal intensity associated with active regions (as listed in the *IAU Quarterly Bulletin of Solar Activity*) is somewhat more pronounced than for regions of high coronal intensity not associated with active regions. Superposed epoch curves around the CMP date of active regions, near the time of sunspot minimum, show essentially the same characteristics as the high coronal intensity curves (Fig. 7).

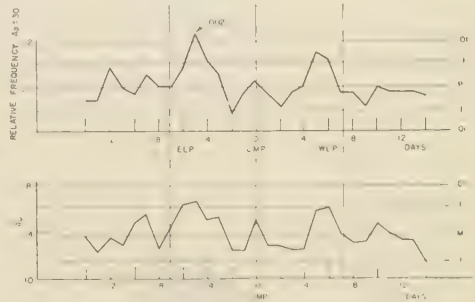

FIG. 7—CMP of active regions with high Meudon activity index; years of low solar activity 1942–1945, 1952–1955; 71 cases

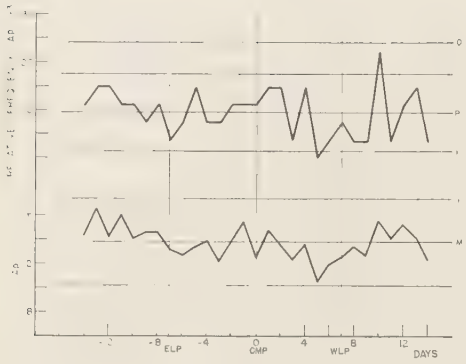

FIG. 8—CMP of regions of high intensity of green coronal line, 1953–1954; 27 cases

Bell and Glazer's study extended to October 1953, some months before sunspot minimum. We have extended the analysis to the year October 1953 to October 1954, which includes minimum of the sunspot cycle and corresponds most nearly to 1944 (Figs. 8 and 9). The most striking feature of these plots is the absence of any large deviations from the mean. Analysis of the frequencies of $A_p \geq 30$ for the single year 1944 (at the previous sunspot minimum) indicates that the coronal-geomagnetic relations were as strong in 1944 as in 1943. A glance at the *IAU Quarterly Bulletins* for 1944 and 1954 shows that the number of active regions and frequency of flares were considerably higher in 1944 than in 1954. *C. Pecker* and *Trotter* [1954] have pointed out that mean green line intensity remained at a very low level for several months in 1953 and 1954. This again suggests that the coronal-geomagnetic relation is highly dependent on active regions.

Conclusion—The most consistent relation found in this study of a period of low solar activity is a minimum in A_p following CMP of a region of high coronal intensity. The curves for regions of high coronal intensity are remarkably similar to those presented by *Allen* [1944], showing the frequency of M-type disturbance around the date of CMP of large sunspots. This suggests that our regions of high coronal intensity are the regions of coronal condensations over active regions, rather than regions associated with coronal streamers. The green line data for 1942–1944 lead us to conclude that the relation between coronal intensity and geomagnetic activity can be explained as the tendency of bright green line emission to appear with active regions and the tendency of M-regions to avoid these regions. The maxima in A_p that tend to appear at CMP − 4 and CMP + 10 days, and the intervening minimum, suggest the "cone of avoidance" proposed by *Roberts* and *J. C. Pecker* [1955].

Thanks are due to Jerry Josties, who carried out the selection of zero-days, and to the many colleagues at the Bureau of Standards and at High Altitude Observatory who made valuable comments and suggestions.

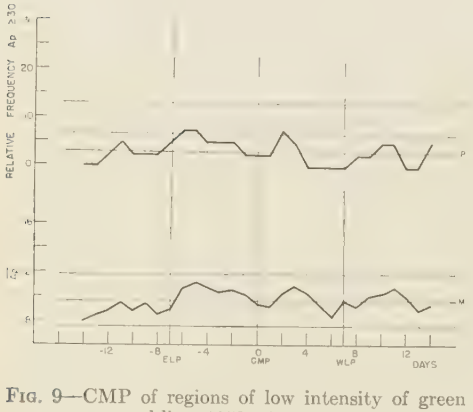

FIG. 9—CMP of regions of low intensity of green coronal line, 1953–1954; 41 cases

REFERENCES

ALLEN, C. W., Relation between magnetic storms and solar activity, *Monthly Notices Roy. Astron. Soc.*, **104**, 13–21, 1944.

BELL, B., AND H. GLAZER, Geomagnetism and the emission-line corona, *J. Geophys. Research*, **59**, 551–553, 1954.

BELL, B., AND H. GLAZER, Geomagnetism and the emission-line corona, *J. Geophys. Research*, **61**, 179–182, 1956.

BELL, B., AND H. GLAZER, Geomagnetism and the emission-line corona, 1950–1953, *Smithsonian Inst. Contrib. 2*, 51–107, 1957.

BILLINGS, D. E., Climax coronal intensities, Dec. 12, 1941 to May 21, 1944, *High Altitude Observatory Solar Activity Rept. 37*, 1–49, 1957.

Kiepenheuer, K. O., A slow corpuscular radiation from the sun, *Astrophys. J.*, **105**, 408–423, 1947.

Pecker, C., and D. E. Trotter, Phase du cycle solaire actuel, *Compt. rend.*, **239**, 633–635, 1954.

Roberts, W. O., and J. C. Pecker, Solar corpuscles responsible for geomagnetic disturbances, *J. Geophys. Research*, **60**, 33–44, 1955.

Shapley, A., and W. O. Roberts, The correlation of magnetic disturbances with intense emission regions of the solar corona, *Astrophys. J.*, **103**, 257–274, 1946.

Sinno, K., On the radio propagation disturbances, *J. Radio Research Lab.*, **3**, 155–160, 1956.

Sinno, K., On the origin of the long-lived solar corpuscular streams which appeared last solar cycle, 1950-53., *J. Radio Research Lab.*, **4**, 25–35, 1957.

(Manuscript received January 7, 1959.)

Formation of Thermal Microstructure in a Narrow Embayment during Flushing

JACK T. SHAW AND G. R. GARRISON

Applied Physics Laboratory
University of Washington
Seattle, Washington

Abstract—Thermal microstructure formations, coincident with the occurrence of flushing in a narrow Puget Sound embayment, have been observed and measured with a high-sensitivity probe. Accompanying the larger formations which extend horizontally for thousands of yards, a microstructure is shown to exist which consists of elongated layers extending hundreds of yards with temperature differences of less than 0.1°C. Two series of isothermal diagrams constructed from vertical temperature measurements taken in the area during winter and summer flushing are presented to show the manner in which such formations are developed.

INTRODUCTION

For the past five years an extensive study [*Garrison* and *Shaw*, 1958] of temperature structure has been made in the Dabob Bay–Hood Canal area of Puget Sound by members of the staff of the Applied Physics Laboratory, University of Washington. Of chief interest has been the investigation of thermal microstructure formations that occur in the area at intermediate depth during periods of seasonal flushing.

The physical size, shape, and motion of such formations are difficult to measure with a limited amount of equipment. This paper is primarily devoted to the presentation of the results of efforts to measure these properties and the flushing process that leads to their occurrence.

The waters of the Puget Sound basin, in general, are known to be seasonally flushed out by renewal processes which mainly are related to the over-all salt balance requirements of the area. This is typical of a basin system where fresh water runoff and precipitation exceed evaporation. Other investigators [*University of Washington*, 1954] have shown that this results in a circulation pattern in which diluted surface waters flowing seaward are compensated for by landward influxes at depth of water of higher salinity. It is believed that the formation of thermal microstructure at intermediate depths in Dabob Bay is related to these seasonally occurring renewal processes. More specifically, they are believed to be the direct result of the intrusions of distinct water types across the subdivision sills that separate the area from the main Puget Sound basin.

TEMPERATURE MEASUREMENTS OF THE FLUSHING PROCESS IN DABOB BAY

The flushing processes in the bay area depend in a complex way on the climatic changes which take place within the immediate and adjacent areas. Simultaneous observations of the many variables involved would be necessary for a full understanding of the mechanics of such a process. For the purpose at hand, however, the examination of the temperature variable alone has sufficed as a basis for tracing the transitory water masses to their immediate origin. This was obviously facilitated, particularly during the summer months, by the horizontal stratification of the thermal structure during the flushing periods.

There are indications from temperature observations made in the area during other years that the predominant tendency is for a renewal process to occur twice each year. In some instances only partial flushing was noted, but the presence of warm intrusions during the summer months and cold ones in winter is the cycle that apparently prevails.

Two distinct renewal processes occurred in Dabob Bay during the period between August 1956 and July 1957 which appeared to have resulted in the complete replacement of water

within the bay. The first, which was represented by a series of warm intrusions, began in midsummer and lasted until October. This was subsequently followed by a second series of cold intrusions which began in December and continued through the winter months.

During this period a series of isothermal diagrams was constructed from vertical temperature profiles taken by a thermistor probe at the midchannel stations whose locations are shown in Figure 1. Eight of these diagrams, presented in Figures 2 and 3, are discussed in detail below. The main divisionary sill, which separates the Hood Canal–Dabob Bay area from the main basin and is not shown on the isothermal diagrams, is located about four miles north of the Bangor station. The maximum depth at this location is about 150 ft. A secondary sill, separating Dabob Bay from Hood Canal proper, is located at the junction of those areas. The maximum depth at that location is approximately 410 ft.

Summer flushing—It can be seen from the August 9 diagram of Figure 2 that the previous winter's flushing was complete and that a mass of cold water (7.0° to 7.5°C) had been trapped

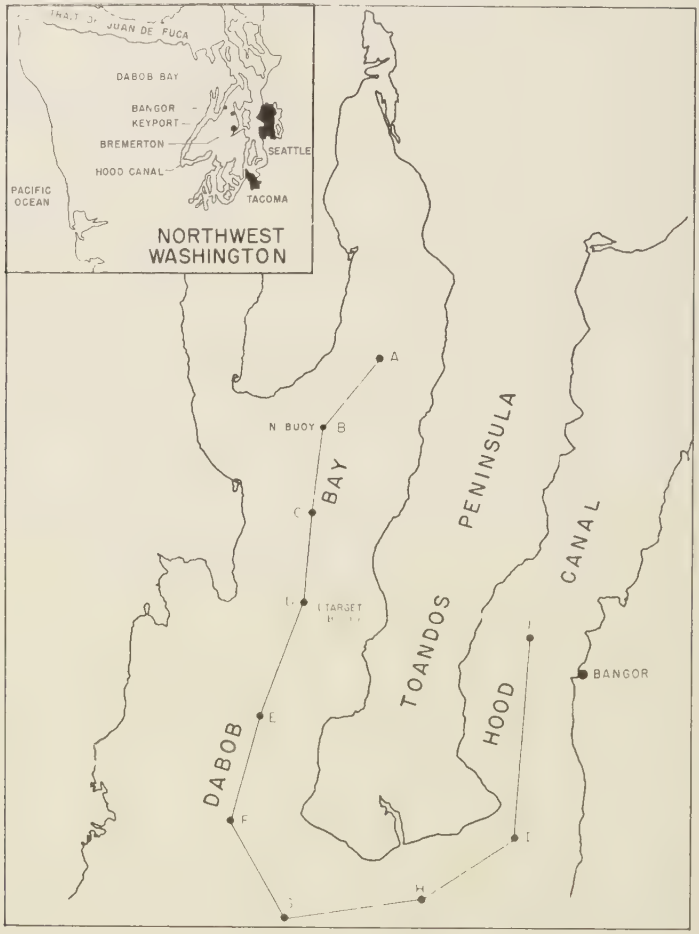

Fig. 1—Station location chart

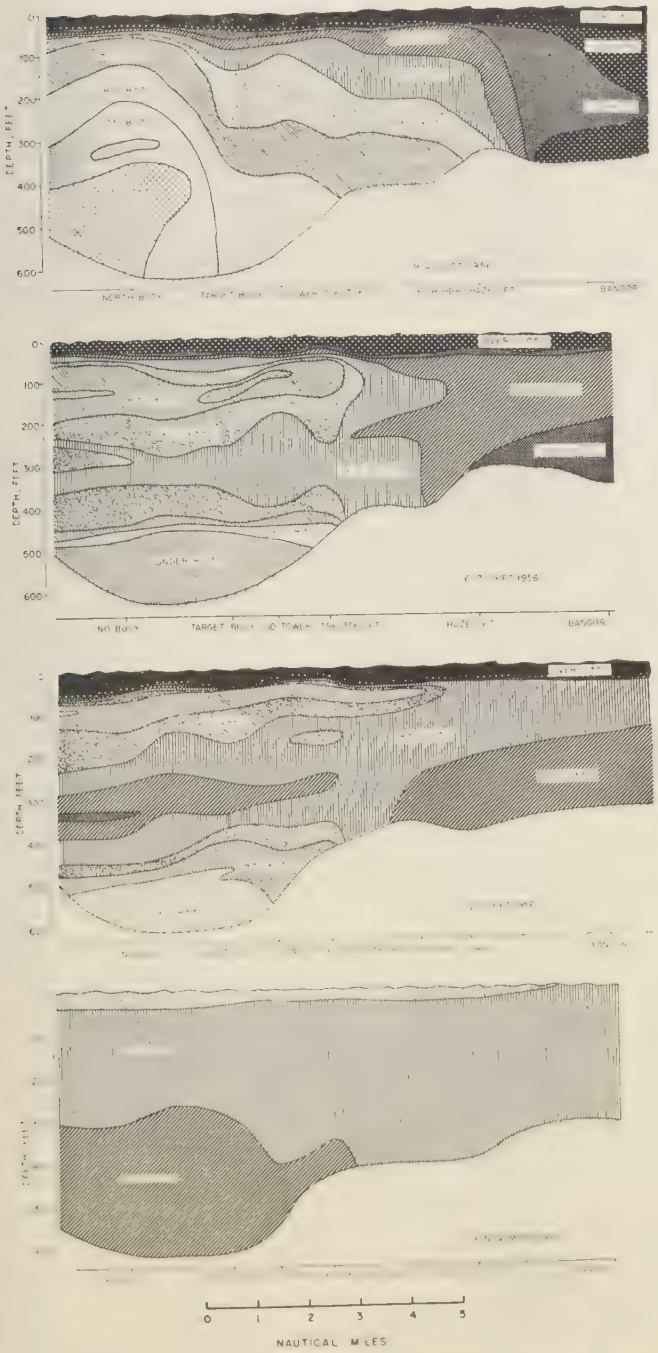

FIG. 2—Isothermal diagrams showing summer flushing process, 1956

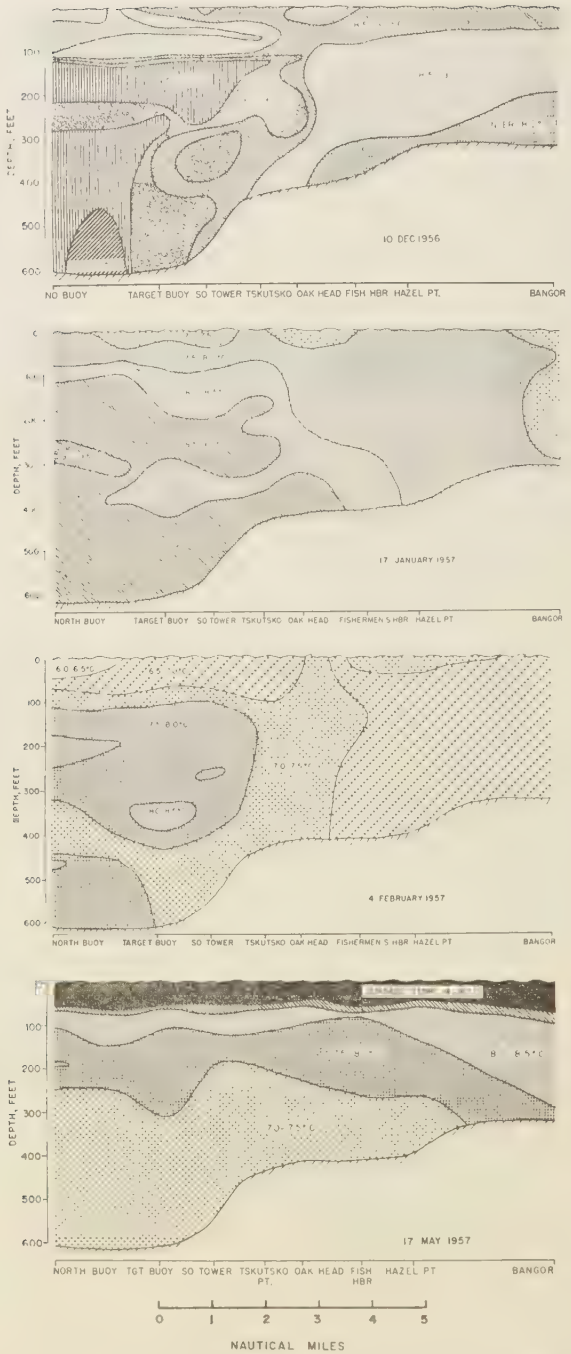

FIG. 3—Isothermal diagrams showing winter flushing process, 1956-1957

ehind the sill at the bay entrance. The tendency or an intrusion to start at this time is quite vident from the downward flexion of otherwise osely packed surface isothermals and the inward rogression of a wedge of warm water (11.0° to 1.5°C) along the bottom of the canal.

As shown in the September 6 and September 20 iagrams, the warm intruding wedge had pro-ressed into the bay and, by September 20, had ecome generally continuous throughout the ay at intermediate depths. This process is hown to have resulted in the vertical upward lisplacement of 'old winter water' and its sub-equent removal from the bay in the upper ayers. The lowering of the density of the dis-laced water through mixing with the insolated urface layer obviously aided in its removal, and t may in some degree account for the short period f time during which the summer flushing process occurred.

The thermal state within the bay at the termi-ation of the summer flushing process consisted f a gradual increase of temperature with depth rom 9.0°C at the surface to 10.5°C at the bottom (November 6 diagram of Fig. 2). The conditions for vertical stability obviously require that in this state the warmer bottom layers be of greater salinity than those above.

Winter flushing—In contrast to the uniformity shown in the thermal circulation patterns that accompanied the summer flushing, the winter ones appear somewhat less defined, and the source of the intruding water appears less definite (Fig. 3). However, there is enough significant resemblance to indicate that the 'old summer water' was replaced in much the same manner as that in which the 'old winter water' was displaced during the summer flushing process.

The pattern of the isothermals for December 10 indicates that by this time the winter renewal process had started and that a wedge of cool water had moved into the bay along the bottom and had progressed as far as the target buoy station. A penetration is also shown to have occurred at an intermediate depth level which is represented by the interleafing of the 9.0° to 9.5°C water with the warmer water (9.5° to 10.0°C) above and below.

By January 17, 1957 the entire mass of 'old summer water' trapped behind the sill at the bay entrance had been almost completely mixed with the cooler incoming intrusions that penetrated into the lower levels. Except for the cooler intruding tongue of 8.0° to 8.5°C water and a small warm lens (9.0° to 9.5°C) representing a vestige of 'old summer water' at the 300-ft level, the main mass was at a temperature of 8.5° to 9.0°C on this date. Later, as shown in the February 4 diagram of Figure 3, continued penetrations had resulted in the cooling of the main mass to a 7.5° to 8.0°C temperature. The vestiges of 'old summer water' again were represented by the lens (now 8.0° to 8.5°C) shown at intermediate depth levels.

The termination of the winter flushing process, represented by the nearly stable state shown in the May 17 diagram, is a return of the bay to a thermal state closely resembling the one at the beginning of the summer flushing of the previous year. The closely-packed surface isothermals, associated with increasing surface insolation, were now well formed and continuous throughout the bay and the adjoining mixing area above the restrictive entrance sill. One can readily see that the advent of the next warm summer intrusion over the sill could result in a pattern of isothermals similar to the one shown in the August 9 diagram of Figure 2.

Measurements of Thermal Microstructure

In light of the preceding measurements, it is quite apparent that during periods when the flushing processes are most active the main water mass is thermally non-homogeneous at the depth levels of the incoming intrusions. The result of such activity is the formation of a thermal structure with many finely detailed variations incorporated upon variations of much larger scale.

In order to observe and record the finer details of such structure, it was necessary to use a temperature probe with a short time constant of response and a very high sensitivity. For these purposes a Veco type 32A1 thermistor, which was mounted in an epoxy-resin (Scotchcast) mount and which had a response rate of less than one second in water and a sensitivity of about 0.01°C, was found to be suitable.

The problem of observing the nature of the space and time variations of the microstructure with a one-dimensional measurement system was partially resolved by: (1) making many rapid, successive measurements at one location, and

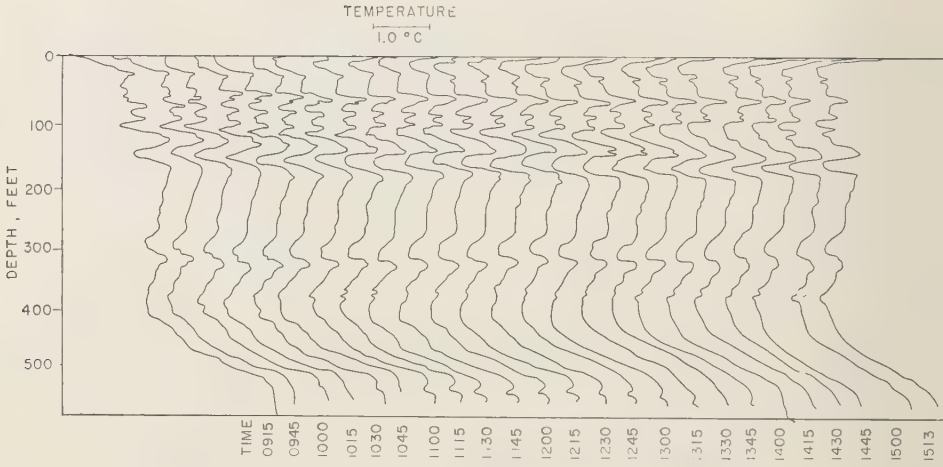

FIG. 4—Temperature profiles, Dabob Bay, March 15, 1956

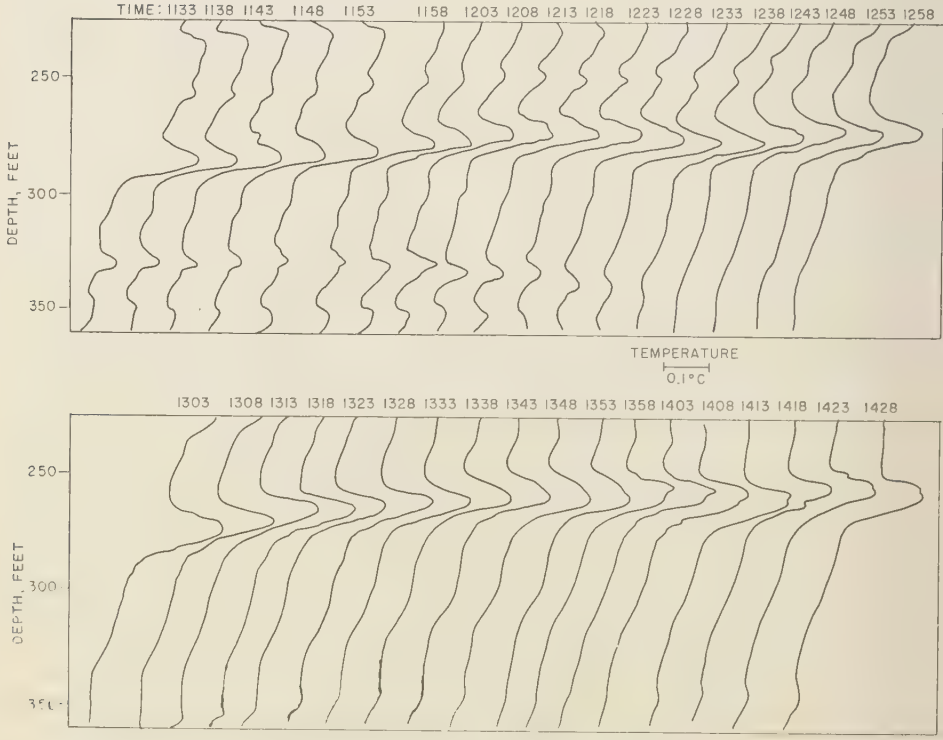

FIG. 5—Temperature profiles, Dabob Bay, August 3, 1955

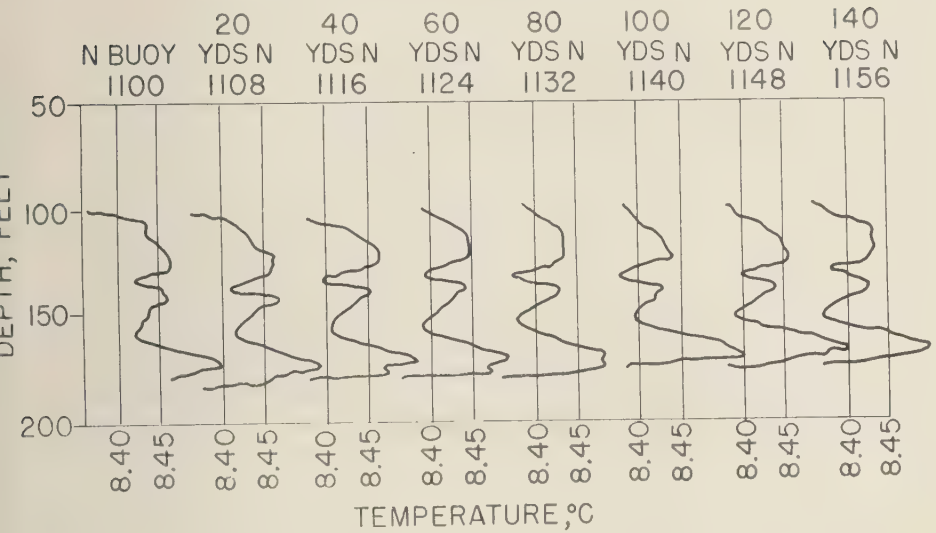

FIG. 6—Temperature profiles, Dabob Bay, March 22, 1955

2) making measurements at closely adjacent ocations as quickly as possible. Although the patial variations at one instant are not truly letermined by this approach, many pertinent eatures of the variations are nevertheless bservable and can be studied.

In Figures 4 and 5, which shows a series of measurements taken during winter flushing, it can be seen that the larger structure remained intact during the entire six-hour measurement period but that the variations of less than 0.1°C appeared to change significantly in an hour. Similarly, the successive measurements which were taken during the summer flushing of 1955 show that the larger variations were prominent for the entire three-hour measurement period, whereas the smaller variations changed completely in less than one hour.

Figure 6 shows the measured variation in the microstructure with distance. In this example, a structure with variations of a few hundredths of a degree retains its detail for over a hundred yards. The examination of many such sets of measurements indicates that large temperature variations extend farther in space than do smaller temperature variations.

SUMMARY

During the flushing process, the thermal structure which forms consists of elongated layers which have temperature differences of several tenths of a degree centigrade and extend for thousands of yards. An examination of the structure in finer detail reveals a thermal microstructure in which layers with a temperature difference of less than 0.1°C extend for several hundred yards.

Acknowledgment—This work was supported by the Bureau of Ordnance, U. S. Navy, under Contract NOrd 12937.

REFERENCES

GARRISON, G. R., AND J. T. SHAW, Oceanographic Measurements in Dabob Bay, *APL/UW/TE/56-37, Appl. Phys. Lab., Univ. Washington*, 25 pp., 1958.

UNIVERSITY OF WASHINGTON, Puget Sound and approaches, *A literature survey*, **3**, 40–66, 1954.

(Manuscript received January 19, 1959.)

Comparison of Several Methods for Rainfall Frequency Analysis

F. A. HUFF AND J. C. NEILL

Illinois State Water Survey
Urbana, Illinois

Abstract—Five frequency distributions were compared for their ability to fit maximum rainfall values in Illinois. Analyses were performed on both seasonal and annual maxima for storm periods of one to ten days. Calendar-day rainfall amounts from 39 stations for the 40-year period, 1916–1955, provided the basic data for the study. Initially, an evaluation was made of frequency relations based upon individual station data. This evaluation indicated that more reliable results would be obtained by determining average relations based upon data from several stations within an area. Consequently, the state was divided into four sections having approximate storm rainfall homogeneity. Next, average frequency relations based upon each of the five frequency distributions were determined for each section and storm period. Statistical tests indicated no marked superiority for any one of the distributions. Comparisons were made between results obtained from the methods of moments and least squares in data fitting. It was concluded that differences obtained between the two methods are insignificant.

Introduction—Considerable information on rainfall frequency for periods of 5 minutes to 24 hours has been provided by *Yarnell* [1935], *U. S. Weather Bureau* [1955], and others. However, longer periods of rainfall which are of importance in agriculture, water supply replenishment, and hydrologic design have not been analyzed in detail for Illinois. Consequently, analyses were performed to determine the recurrence interval of heavy rainfall amounts encompassing periods of one to ten days.

The basic physical processes involved in the production of precipitation have not been completely defined or evaluated at present, although considerable research is being directed toward this problem. Consequently, the investigator of the frequency of rainfall is forced to depend to a large extent upon application of statistics to rainfall observations which he hopes will be representative of future experience. Since the occurrence of rainfall is obviously dependent upon complex reactions in nature, the authors could find no basis for designating in advance one of the several frequency distributions appearing in the literature as best for analysis of the Illinois data. Therefore, the selection of a distribution was determined on the basis of how well each of several distributions represented a common and extensive set of data.

To accomplish detailed analyses of the frequency of heavy precipitation within Illinois, maximum storm rainfall values for annual and seasonal periods were analyzed from 39 stations for the 40-year period, 1916–1955. Calendar-day data were utilized in order to include U. S. Weather Bureau cooperative station records. Use of these records provided a relatively large number of stations for the study. Stations were chosen to give a sampling pattern as uniform as possible throughout the state (Fig. 1).

Illinois was divided into four sections having similar storm rainfall characteristics (Fig. 1). The sections were selected on the basis of several statistical measures, such as means and standard deviations of storm rainfall, and upon consideration of meteorologic and climatic factors. Although the selections were partially subjective, it is felt that the grouping is representative of climatic divisions of storm rainfall within Illinois. After dividing the state into four sections, average frequency relations were developed for each of these sections for rainfall periods of one to ten days.

Approach to problem—After thorough study it was decided that the most reliable frequency

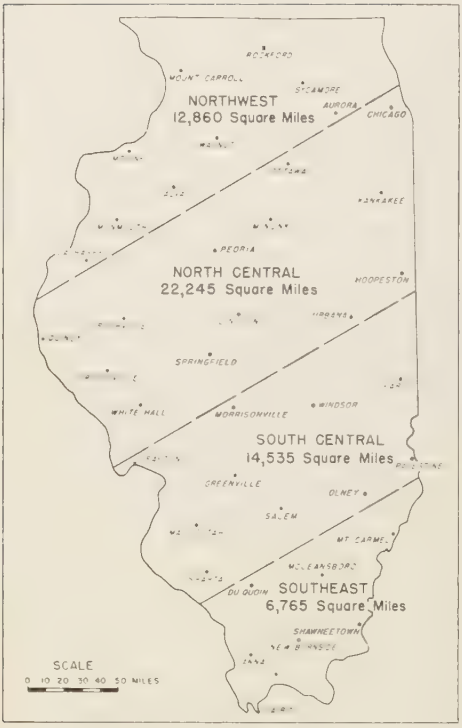

FIG. 1—Station and section locations

relations would be based on the average for an area. Although the study was devoted mainly to determining average frequency relations for areas or sections of Illinois, frequency relations based on individual stations were also investigated. Results of this phase of the study indicated that a 40-year sampling period at a single station is inadequate to define the frequency for maximum storm rainfall. The variation of rainfall frequency which results from inadequate sampling is illustrated in Figure 2 where station data for the 40-year study period have been divided into two groups by the random-start sampling technique [*Huff* and *Neill*, 1957]. Isohyetal patterns in inches are shown for a 40-year recurrence interval of one-day rainfall. These patterns were obtained by fitting the *Gumbel* distribution [1941] to each data group of individual stations. Appreciable differences in the orientation and distribution of isohyets is evident.

Another example to emphasize the variability among individual stations is presented in Table 1. In this table the range of observed maximum 40-year values of one-day rainfall among the various stations in each section is shown. Obviously, the station frequency curve is considerably affected by the magnitude of the extreme values, and the relatively large differences which may be obtained between nearby stations is apparent. For example, the Gumbel distribution fitted to Rockford and Sycamore data in the Northwest section provides computed 50-year recurrence values of 6.7 and 4.7 inches, respectively. Climatological and topographic factors indicate no cause for such a marked difference between these two stations, approximately 25 miles apart. The average 50-year recurrence value for this section, based upon the Gumbel distribution, is 5.6 inches which is intermediate between the above values.

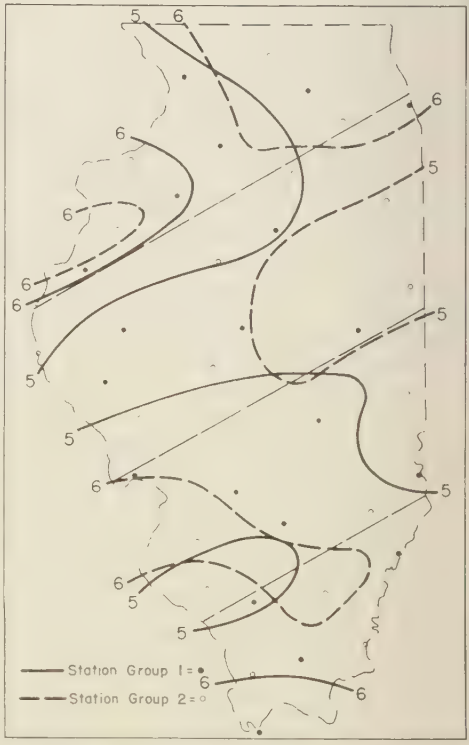

FIG. 2—Effect of sampling on rainfall frequency estimates

TABLE 1—*Range of 40-year maxima of 1-day rainfall among stations*

	North-west	North Central	South Central	South-east
ighest (in.)	10.48	6.61	8.24	6.40
owest (in.)	4.65	3.71	4.42	4.25
ifference (in.)	5.83	2.90	3.82	2.15
atio: highest/ lowest	2.25	1.78	1.86	1.51
umber of stations	9	13	10	7

Frequency distributions tested—The frequency istributions tested included the log-normal, og-skew [*Chow*, 1954], Gumbel, Frechet [*Gumbel*, 956], and *Jenkinson* [1955]. The log-normal nd Gumbel distributions, which have been ommonly used in hydrologic analyses, are haracterized by two parameters, the mean nd a measure of dispersion. The log-normal istribution assumes that the logarithms of the lata are normally distributed. The Gumbel istribution assumes a constant coefficient of kewness of 1.14 and applies the extreme value heory of *Fisher* and *Tippett* [1928]. The log-skew istribution, which assumes variable skewness, as been treated in considerable detail by *Hazen* [1930] and *Chow* [1954] but has had imited application in practice. The Jenkinson istribution assumes a variable-shape factor pplied to the Fisher and Tippett extreme value theory, in contrast to the constant skewness used by Gumbel. As with the log-skew distribution, there appears to have been only limited application of this method. The Frechet distribution is another two-parameter distribution similar to that of Gumbel, but it requires a logarithmic transformation of the data before the curve-fitting process is begun.

Results of frequency distribution comparisons—In the evaluation of the several distributions, both the method of moments and least squares were used for fitting the sectional data to the individual distributions. In recent years, *Chow* [1953] and others have suggested the use of least squares for curve fitting in frequency analysis. However, since the choice between the two methods may be controversial, the two techniques were compared in the Illinois study. Results of the comparisons indicated that the differences in rainfall obtained for a given recurrence interval with the two methods are insignificant from the standpoint of practical application. Table 2 illustrates the magnitude of the differences between the two techniques for one-day storm periods in each of the four sections. The percentages in Table 2 were obtained by subtracting the moment values from the least-squares values and dividing by the least-squares values.

Comparison of the several frequency distributions later in this paper will be restricted to least-squares fitting. The least-squares fitting process utilizes a frequency factor which depends upon the particular frequency distribution that is assumed to describe the data. *Chow* [1953]

TABLE 2—*Differences (per cent) for 1-day storms between method of moments and least squares*

Recurrence interval (years)	Gumbel				Log-normal			
	North-west	North Central	South Central	South-east	North-west	North Central	South Central	South-east
2	0	0	0	0	0	0	0	0
5	−1	−2	−2	0	+1	0	0	+2
10	−2	−1	−2	0	−1	+1	0	+3
20	−1	−1	−1	+1	−2	0	0	+3
40	−2	−2	−2	0	−2	0	0	+4
100	−2	−2	−2	0	−3	0	0	+4
Absolute average	2	2	2	0	2	0	0	3

has expressed this frequency factor as

$$K = \frac{X - \overline{X}}{s}$$

where X represents a ranked value of rainfall, $\overline{X}$ is the mean of the rainfall, and s is the standard deviation of the rainfall. A plot of X versus K is assumed to linearize the data. The least-squares process is then performed on an X versus K–coordinate system by fitting

$$X = \overline{X} + b(K - \overline{K})$$

to the data, where b is the slope of the line and $\overline{K}$ is the mean of the frequency factor, K.

Standard errors and correlation coefficients were obtained for the regression of rainfall versus recurrence interval for each rainfall period, section, and frequency distribution. Comparisons of correlation coefficients for one-day rainfall are shown in Table 3. The correlation coefficient permits a direct comparison of results by the reader, since it is a pure number which provides a measure of the goodness-of-fit. Since part of the distributions involved logarithms, the standard error is less suitable for direct comparisons in this instance. Table 3 shows only small differences among the correlation coefficients. Similar results were obtained from comparison of other rainfall periods. The analysis at this point had established no marked superiority of any one of the five distributions in fitting the rainfall observations.

In a further attempt to evaluate the several statistical distributions, a comparison of actual ranked data with the derived curves for recurrence intervals of two years or greater was made, since this is the portion of the curve most useful to the hydrologist. Results of this phase of the analysis are presented in Table 4 for one-day rainfall. In this table, differences in percentage are shown between the ranked data and the regression curve values for each section, statistical method, and for selected recurrence intervals. A positive value indicates that the curve gave higher values than the ranked data. Calculations were made for the other rainfall periods but are not shown here, as results were very similar. Again, little choice between the five frequency distributions is indicated. If all sections and recurrence intervals are considered, the Frechet curve shows a more even distribution of positive and negative deviations. However, there is less than one per cent difference in the over-all average between the several distributions. Consequently, it was still not feasible to make a preferential selection of the most applicable frequency distribution after this analysis.

TABLE 3—*Correlation coefficients associated with regression equations for annual maxima of 1-day rainfall*

Distribution	North-west	North Central	South Central	South-east
Gumbel	0.91	0.95	0.95	0.96
Log-normal	0.95	0.96	0.97	0.97
Frechet	0.96	0.96	0.97	0.96
Log-skew	0.95	0.96	0.97	0.96
Jenkinson	0.93	0.96	0.96	0.96

Although statistical tests indicated no significant differences between the several distributions, examination of calculated rainfall depths showed considerable differences in values for long recurrence intervals. Rainfall depths for selected recurrence intervals of one-day storm periods are shown in Table 5, based on data for the Northwest section (Fig. 1). This table shows values at the 40-year recurrence interval ranging from 5.1 to 6.7 inches for one-day rainfall. Similar differences were obtained for other rainfall periods and recurrence intervals which are not included here. The Frechet, log-skew, and Jenkinson distributions give larger values for long recurrence intervals. For shorter recurrence intervals the magnitude of the differences obtained with the five distributions is not large. Naturally, one cannot judge whether the relatively large values predicted for long recurrence intervals are more or less appropriate than the smaller ones. Furthermore, this portion of the frequency curve is less reliable than the central portion. Theoretically, the more complex Chow and Jenkinson methods should be superior, since they allow for greater flexibility with regard to skewness.

Since 1948 the Illinois State Water Survey has been making detailed field surveys of severe rainstorms in Illinois as part of its meteorological program [*Huff* and others, 1958]. It was decided

TABLE 4—*Difference (per cent) between ranked data and regression curve values obtained from several statistical distributions applied to 1-day rainfall*

Section	Gumbel	Frechet	Log-normal	Log-skew	Jenkinson
	40-year recurrence interval				
Northwest	−19	−6	−23	0	−9
North Central	−8	+5	−12	+3	+1
South Central	−16	−3	−19	−4	−8
Southeast	0	+12	−5	−6	+3
Absolute avg.	11	7	15	3	5
	20-year recurrence interval				
Northwest	+2	+9	−4	+10	+6
North Central	−7	0	−11	−2	−4
South Central	+1	+8	−3	+7	+4
Southeast	+8	+16	+5	+14	+10
Absolute avg.	5	8	6	8	6
	10-year recurrence interval				
Northwest	+2	+1	−2	0	0
North Central	+1	+1	−1	0	−1
South Central	+3	+3	0	+2	+1
Southeast	+5	+6	+3	+4	+3
Absolute avg.	3	3	2	2	1
	5-year recurrence interval				
Northwest	+1	−5	−1	−8	−5
North Central	+2	−1	+1	−1	−1
South Central	+2	−2	+1	−2	−2
Southeast	0	−4	−1	−2	−3
Absolute avg.	1	3	1	3	3
	2-year recurrence interval				
Northwest	+3	−3	+2	−7	−6
North Central	0	−3	+1	−4	−6
South Central	0	−4	+1	−4	−5
Southeast	+1	−4	0	−4	−5
Absolute avg.	1	4	1	5	6
Over-all avg.	4.2	5.0	5.0	4.2	4.2
Number "+"	12	9	7	6	7
Number "−"	4	10	11	11	12
Number "0"	4	1	2	3	1

TABLE 5—*Comparison of computed 1-day rainfall (inches) for various recurrence intervals in Northwest section*

Recurrence interval (years)	Distribution				
	Gumbel	Log-normal	Frechet	Log-skew	Jenkinson
2	2.5	2.4	2.3	2.2	2.2
5	3.5	3.4	3.2	3.1	3.3
10	4.1	4.0	4.1	4.1	4.0
20	4.8	4.5	5.1	5.1	4.9
40	5.4	5.1	6.3	6.7	6.1
100	6.2	5.9	8.3	9.2	7.8

to study results from analyses of these storms for indications of the magnitude, extent, and frequency of unusually heavy rainfall amounts within the state. An areal analysis of Illinois frequency relations was made using detailed isohyetal maps of severe rainstorms during 1948–57. Analysis was restricted to the area enclosed by isohyets of six inches or greater, where the rainfall distribution was most accurately defined from field surveys. As a result of this phase of the study, the Frechet distribution was selected for use with annual maxima in Illinois. The reader is referred to *Illinois Water Survey Bulletin 46* [*Huff* and *Neill*, 1959] for details of the areal isohyetal analyses which are too lengthy for description here.

Although the Frechet distribution was selected for use in the analysis of the annual maxima of rainfall, the authors do not consider it a unique tool for the frequency analysis of storm precipitation. It merely appeared to provide a slightly better yardstick for analysis within the limits of the data in this situation. In fact, when seasonal rainfall maxima were analyzed, it was concluded that the log-normal distribution was superior for use with winter, spring, and fall data; whereas the Frechet distribution was the most satisfactory for summer data. In this report seasons were obtained by dividing the year into quarters with, for example, December, January, and February representing winter. Table 6 shows a comparison between the log-normal and Frechet distributions for the frequency analysis of winter rainfall, based upon recurrence intervals of two years or longer. Interpretation is the same as for Table 4.

Results presented in Table 6 indicate that the log-normal distribution is an appreciably better yardstick than the Frechet distribution for analysis of the frequency of winter rainfall. The Frechet distribution produces overestimates that are relatively large for the longer recurrence intervals. With the summer data the Frechet distribution was found to be superior. In spring and fall differences between the distributions were small.

Considering meteorological and climatological factors, it is not surprising that the most satisfactory distribution for Illinois storm rainfall analysis varies from season to season. For example, examination of the 40 years of data for one-day storm periods in the Northwest section shows that winter maxima among the individual stations varies from 0.3 inch to 3.0 inches. In summer, the station values have varied from 0.6 inch to 9.2 inches. Nearly 50 per cent of the annual maxima were drawn from the summer maxima. The frequency and intensity of heavy rainstorms is much greater in summer than in winter in Illinois.

TABLE 6—*Difference (per cent) between ranked data and regression curve values for 1-day rainfall in winter season*

Section	Recurrence interval (years)				
	40	20	10	5	2
			Log-normal		
Northwest	−9	−5	−2	+2	0
North Central	−3	−6	−3	+4	−1
South Central	−6	−6	−5	0	−1
Southeast	+1	+1	−4	+5	−2
Absolute avg.	5	4	3	3	1
			Frechet		
Northwest	+13	+9	+1	−3	−5
North Central	+22	+8	−1	−1	−8
South Central	+18	+5	−2	−4	−6
Southeast	+31	+18	−1	−4	−9
Absolute avg.	21	10	1	3	7

When winter data were analyzed it appeared that the Frechet rainfall values increased too rapidly with increasing recurrence interval to satisfy climatological observations and meteorological theory relating to the production of rainfall. In the summer, when unusually heavy rainfall is most likely to occur over the state, the Frechet characteristics appear more appropriate for defining the rainfall frequency distribution. Since a large portion of the annual maxima were from summer storms, the Frechet distribution appeared to be as good or better than the other distributions for fitting the annual data.

Summary and conclusions—Five distributions were compared in the determination of rainfall frequency relations for storm periods of one to ten days in Illinois. Results indicated no marked superiority of any of the several methods. Instead, it appeared that the most satisfactory distribution for use with the observational

ıta varied as seasonal and annual maxima
rainfall were analyzed. This finding appears
mpatible with meteorological and climatolog-
al characteristics of Illinois storm rainfall and
dicates that normally a particular distribution
nnot be designated as best for storm rainfall
equency analysis. When doubt exists as to the
ost appropriate distribution and after both
atistical theory and meteorological factors
ave been considered, tests of several methods
re recommended.

Comparison was made of frequency relations
btained by use of the method of moments and
east squares in fitting the five distributions
o the data. Differences in rainfall obtained with
he two fitting procedures are considered in-
ignificant.

Computations using both individual station
nd sectional average data indicated that
requency relations are more reliable when based
pon a sectional analysis.

References

Chow, Ven Te, Frequency analysis of hydrologic data with special application to rainfall intensities, *Univ. Illinois Eng. Expt. Sta., Bull. 444*, 1953.

Chow Ven Te, The log-probability law and its engineering applications, *Proc. Am. Soc. Civil Engrs.*, **80**, Separate no. 536, 1954.

Fisher, R. A., and L. H. Tippett, Limiting forms of the frequency distribution of the largest and smallest member of a sample, *Proc. Cambridge Phil. Soc.*, **24**, 180-190, 1928.

Gumbel, E. J., The return period of flood flows, *Ann. Math. Statistics*, **12**, 163-190, 1941.

Gumbel, E. J., Methods graphiques pour l'analyse des debits de crue (avec une intervention de J. Bernier), *Extrait de Houille Blanche*, no. 5, 1956.

Hazen, Allen, *Flood flows, a study of frequencies and magnitudes*, John Wiley and Sons, New York, 1930.

Huff, F. A., and J. C. Neill, Rainfall relations on small areas in Illinois, *Illinois State Water Survey, Bull. 44*, pp. 43–46, 1957.

Huff, F. A., and J. C. Neill, Frequency relations for storm rainfall in Illinois, *Illinois State Water Survey, Bull. 46*, 1959.

Huff, F. A., R. G. Semonin, S. A. Changnon, and D. M. A. Jones, Hydrometeorological analysis of severe rainstorms in Illinois 1956-57 with summary of previous storms, *Illinois State Water Survey, Rept. Invest. 35*, 1958.

Jenkinson, A. F., Frequency distribution of maximum values, *Quart. J. Roy. Meteorol. Soc.*, **81**, 158–171, 1955.

U. S. Weather Bureau, Rainfall intensity-duration-frequency curves, *Tech. Paper 25*, 1955.

Yarnell, D. L., Rainfall intensity-frequency data, *U. S. Dept. Agr., Misc. Publ. 204*, 1935.

(Manuscript received September 22, 1958; revised February 16, 1959; presented at the Thirty-Ninth Annual Meeting, Washington, D. C., May 7, 1958.)

Water Table Fluctuations Induced by Intermittent Recharge

MARINUS MAASLAND

Bureau of Reclamation
McCook, Nebraska

Abstract—The problem of water table fluctuations in response to repeated recharges is considered. The effect on the water table of intermittent constant recharge (recharge applied intermittently at a constant rate) and of intermittent instantaneous recharge (recharge applied instantaneoulsy at regular intervals) is analyzed in detail. The final results are shown to consist of a combination of periodic and transient components; the transients are monotonic decreasing functions.

The theory may be applied to problems of ground-water flow through aquifers and to land drainage problems.

Introduction—The effect of intermittent recharge recurring at regular intervals is of interest in several ground-water problems. In nature, this type of recharge occurs in regions where wet and dry seasons alternate regularly. It is artificially induced in areas where frequent irrigations are applied. Recurrent rainfall in humid regions may also produce an effect similar to that of the recharge patterns assumed in this paper.

All the results of this study are stated in infinite series and are applicable to any number of successive recharges, ranging from zero to infinite. The infinite series generally converge so rapidly that in many problems only one or two terms of the series need be considered. The results should prove useful in the study of various ground-water and drainage situations. Several 'drain spacing formulas' could be devised from them to fit a variety of requirements.

Strictly speaking, the theory is applicable only to water table aquifers; that is, for unimpeded downward flow in the zone near the water table. If the aquifer is covered with a semipervious layer on which surface-applied recharge accumulates, and if the lateral hydraulic conductivity of the material above that layer is sufficiently high, a more or less uniform head will be maintained throughout on top of the confining layer and 'leaky aquifer' conditions (*Hantush* and *Jacob*, 1955] obtain. The requirement of a uniform head above the semi-impervious layer restricts the usefulness of the 'leaky aquifer' theory.

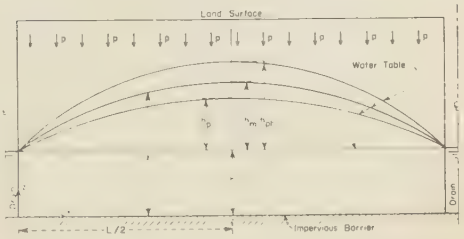

FIG. 1—Ground-water flow over a horizontal impervious barrier

In the following, the water levels in the drains are assumed to be at equal elevation (Fig. 1). This assumption is made for convenience and is not necessary. An interesting paper has recently been published by *Werner* [1957] in which, among other factors, the effect of different elevations of the water levels in the drains and of a sloping impervious barrier is taken into account. Considering the number of variables already introduced in the present paper, the author abstained from incorporating additional ones, although it is quite possible to extend the analysis to include others.

List of symbols—The major symbols are listed below.

		Dimension
x, z	horizontal and vertical coordinates	L
L	width of aquifer or spacing of drains	L

h_1	height of the water levels in the drains measured from the impermeable barrier	L
h_p	or h_{pi}; height of the water table measured from the line connecting the top of the water levels in the drains, as calculated from the periodic function	L
h_t	or h_{ti}; height of the water table measured from the line connecting the top of the water levels in the drains, as calculated from the transient functions	L
h_m	height of the water table *midway* between the drains measured from the line connecting the top of the water levels in the drains	L
h_{ph}	or h_{pih}; maximum water table level *midway* between the drains for intermittent recharge, calculated from the periodic function; h_{ph} is measured from the line connecting the top of the water levels in the drains	L
h_{pl}	or h_{pil}; minimum water table level *midway* between the drains for intermittent recharge, calculated from the periodic function; h_{pl} is measured from the line connecting the top of the water levels in the drains	L
K	lateral hydraulic conductivity	LT^{-1}
D	weighted mean depth of the profile through which the flow occurs	L
p	constant rate of surface-applied recharge per unit area of land surface	LT^{-1}
q	amount of surface-applied recharge per unit area of land surface	L
t	time since the beginning of the first recharge	T
T	duration of period	T
t_1	interval of recharge within the period T	T
k	KD/ϵ, coefficient of diffusivity	L^2T^{-1}
P_c	p/KD, recharge coefficient for $L \gg h_1 > h_m$ and $p \ll K$	L^{-1}
P_w	$2p/K$, recharge coefficient for $L \gg h_1 + h_m$ and $p \ll K$; h_1 is now small compared with h_m	—
r	number of periods considered	—
ϵ	effective porosity or specific yield	—
π	3.14159...	—
τ	time measured within the period T; $0 \leq \tau \leq T$	T
μ	$k(2n + 1)^2(\pi/L)^2$	T^{-1}

Discussion of the differential equations and steady state formulas—Using the Dupuit-Forchheimer assumptions, we find, for $L \gg h_1 \gg h_m$ and $p \ll K$ (Figure 1), the following differential equation [for example, *Jacob*, 1943]:

$$KD\frac{\partial^2 z}{\partial x^2} = \epsilon\frac{\partial z}{\partial t} - p \qquad (1$$

The symbols used are defined in the List of Symbols. In this equation, p is a constant rate of surface-applied recharge. Division of (1) by KD gives

$$\frac{\partial^2 z}{\partial x^2} = \frac{1}{k}\frac{\partial z}{\partial t} - P_c \qquad (2$$

For steady-state flow ($\partial z/\partial t = 0$), it follows from (1) or (2) that for $z = h_1$ at $x = 0$ and L the water table is given by the equation

$$z = h_1 + (P_c/2)(L - x)x \qquad (3$$

The subscript c of P_c is to indicate that these equations are particularly suited for the study of flow through semi-confined water-bearing strata. Equation (2) is valid for flow through nonconfined strata when h_m is small compared with h_1.

Dumm [1954] uses the value $D = h_1 + h_m/2$ for the weighted mean depth of the flow medium. This value leads to satisfactory results if the drain completely penetrates the flow medium. If flow convergence near a partially penetrating drain needs to be accounted for, D may be evaluated by a method discussed by *Maasland* [1956], who uses the results of a study by *Hooghoudt* [1940]. *Hooghoudt* [1936] gives a simple correction to account for capillary fringe effects; this work has recently been reviewed by *van Schilfgaarde* and others [1957, p. 671]. *Ernst* [1954, 1956] gives some interesting methods for analyzing flow problems involving combinations of radial flow towards drains and lateral flow through various horizontal layers of different hydraulic conductivities.

For a condition such as is shown in Figure 1, where the hydraulic conductivity of the over-

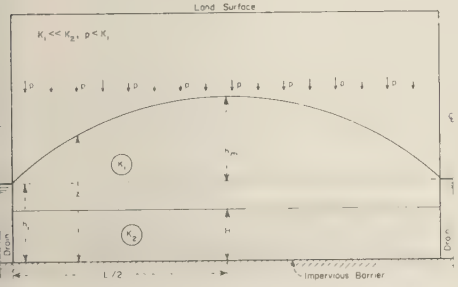

FIG. 2—Flow through a horizontal, highly permeable layer

lying material is relatively low (that is $K_1 \ll K_2$), we may take $D = H$ and $K = K_2$, where H is the thickness of the permeable stratum (with hydraulic conductivity K_2) through which the lateral flow occurs. In this case, (3) actually represents the piezometric rise in the aquifer. This rise is not equivalent to the water table in the overlying soil, particularly if $p \geq K_1$, where K_1 is the hydraulic conductivity of the overlying soil layer. The piezometric level in the aquifer will approximately coincide with the water table only if $p < K_1$; the smaller the ratio p/K_1, the better the approximation will be. The identification of the water table with the piezometric rise in the aquifer actually implies the assumption of negligible head loss in the overlying soil.

When, in a problem such as is shown in Figure 1, h_1 is small compared with h_m and $L \gg h_1 + h_m$, we may write

$$\frac{K}{2}\frac{\partial^2 z^2}{\partial x^2} = \frac{\epsilon}{2z}\frac{\partial z^2}{\partial t} - p \qquad (4)$$

By arbitrarily replacing the variable z in the factor $(\epsilon/2z)$ by the constant D, and dividing by $K/2$, we obtain from (4) the following linearized equation

$$\frac{\partial^2 z^2}{\partial x^2} = \frac{1}{k}\frac{\partial z^2}{\partial t} - P_w \qquad (5)$$

The subscript w of P_w is used to indicate that this equation is derived for a water table condition.

A detailed discussion of the derivation of (5) is given by *Werner* [1953, 1957]. *Maasland* [1958] reviews the derivation of (4). Note that our P_w differs from that of Werner by the factor ϵ; the factor p as used in (1) and (4) represents the amount of surface-applied recharge per unit area and per unit time.

For steady-state flow ($\partial z^2/\partial t = 0$), results derived from (4) have been subjected to extensive checks, some of which are reviewed by *Maasland* [1956]. *Engelund* [1951, p. 19] shows by methods of conformal mapping that, for steady-state flow towards flat drains embedded in a horizontal layer, the water table has an elliptic shape. The shape of the water table so derived is, for all practical purposes, identical to the one given by

$$z^2 = h_1^2 + (P_w/2)(L - x)x \qquad (6)$$

This is the steady-state formula obtained from (4) or (5) by elementary integration for $z = h_1$ at $x = 0$ and L. *Maasland* [1957] shows that, for Engelund's problem, the identity referred to above also holds for anisotropic soil. *Hooghoudt* [1936] and *Donnan* [1947] have made model studies to check the validity of (6). Others [for example, *van Deemter*, 1950; *Ernst*, 1954] report having used numerical methods for this purpose. All have found that (6) compares favorably with their results.

Equation (6) shows the water table to be elliptic, while (1) leads to a water table of parabolic shape (Eq. 3). For intermediate values of h and h_1, the difference between (3) and (6) becomes so small as to be negligible.

It is noted that (2) and (5) are analogous, linear, second-order differential equations. Although we will in the following analysis restrict ourselves mainly to solutions derived from (2), it will be clear that only minor modifications are needed to make these solutions applicable to (5). It only requires that z be replaced by z^2, h_1 by h_1^2, and P_c by P_w. This statement does not apply to (12) or to the developments derived therefrom. In that case, the transformations indicated must be made in (11) prior to the derivation of (12) from that equation.

In problems involving nonsteady-state flow, the weighted mean depth (D) of the profile through which the flow occurs may change appreciably as time proceeds, and it may be necessary to choose successive values for D to account for such variation.

Lateral flow through a layer of constant

depth D is assumed in the derivation of (2). While the predominance of lateral flow also is implied in (4), the depth of the flow medium (the saturated thickness) remains a variable. However, the nonlinear differential equation (4) is subsequently linearized to obtain (5) by putting $z = D$ in the factor $(\epsilon/2z)$. So, although allowance is initially made for the variation of the depth of the flow medium with the x-coordinate and is accounted for in the steady-state formula (6), the assumption of a flow medium of constant depth D is again introduced in (5) for the time-dependent factor so as to make the nonsteady-state problem amenable to a general mathematical treatment. A judicious choice of D is necessary in all applications of the developments derived from either differential equation; a further discussion of the implications of the assumptions can best be given on the basis of examples of the use of the formulas. We will therefore proceed with the analysis and delay further discussion until after its completion. The author plans to publish a subsequent paper on the application of the analytical results to field problems.

Basic nonsteady-state formulas—Let a constant rate of recharge of the ground water (p) commence at $t = 0$. The water table is then given by the formula [*Werner*, 1953, 1957]

$$z = h_1 + (P_e/2)\left\{x(L - x) - (8L^2/\pi^3) \cdot \sum_{n=0}^{\infty} (2n + 1)^{-3} \cdot \sin (2n + 1)\pi(x/L) \exp - \mu t\right\} \quad (7)$$

in which

$$\mu = k(2n + 1)^2(\pi/L)^2 \quad (8)$$

The presence in μ of the factor $(2n + 1)^2$ makes a subscript n to μ desirable; the subscript has been omitted because μ occurs so frequently in the further analysis.

Equation (7) is the solution of (2) subject to the following initial and boundary conditions

$$z = h_1 \quad \text{at} \quad x = 0 \quad \text{and} \quad L, \quad \text{for all } t$$

$$z = h_1 \quad \text{at} \quad t = 0 \quad \text{for} \quad 0 \leq x \leq L$$

$$P_e \begin{cases} = 0 & \text{for} \quad t < 0 \\ = P_e & \text{for} \quad t \geq 0 \end{cases}$$

It is noted that $x(L - x)$ has been developed into a Fourier sine-series, that is

$$x(L - x) = (8L^2/\pi^3) \sum_{n=0}^{\infty} (2n + 1)^{-3} \cdot \sin (2n + 1)\pi(x/L) \quad (9)$$

If, instead, we start at $t = 0$ with a steady-state condition whereby the water table is in equilibrium with a constant rate of recharge (Eq. 3) and if p becomes instantaneously zero at that time, we find from (2) the result [*Jacob*, 1943]

$$z = h_1 + (P_e/2)(8L^2/\pi^3) \sum_{n=0}^{\infty} (2n + 1)^{-3} \cdot \sin (2n + 1)\pi(x/L) \exp - \mu t \quad (10)$$

This is the solution of (2) subject to the following initial and boundary conditions:

$$z = h_1 \quad \text{at} \quad x = 0 \quad \text{and} \quad L, \quad \text{for all } t$$

$$z = h_1 + (P_e/2)(L - x)x \quad \text{at} \quad t = 0$$

$$P_e = 0 \quad \text{for} \quad t > 0$$

When the water table has *not* reached static equilibrium with the recharge p (which presumably started at $t = 0$) at time t_1, the time at which it is suddenly stopped, we find that for $t \geq t_1$ the water table is given by

$$z = h_1 + (P_e/2)(8L^2/\pi^3) \sum_{n=0}^{\infty} (2n + 1)^{-3} \cdot \sin (2n + 1)\pi(x/L) \cdot [\exp - \mu(t - t_1) - \exp - \mu t] \quad (11)$$

This is the solution of (2) when

$$z = h_1 \quad \text{at} \quad x = 0 \quad \text{and} \quad L, \quad \text{for all } t$$

$$z = h_1 \quad \text{at} \quad t = 0, \quad \text{for} \quad 0 \leq x \leq L$$

$$P_e \begin{cases} = 0 & \text{for} \quad t < 0 \quad \text{and} \quad t \geq t_1 \\ = P_e & \text{for} \quad 0 \leq t < t_1 \end{cases}$$

There exists a special relationship between (11) and Glover's formula (*Dumm*, 1954, Eq. 2)

s evidenced by the following derivation. Let
$= q/t_1$, where q is the total amount of recharge
vater added to the ground water per unit
rea during the time t_1. If we use this notation,
he factor $(q/KD)/t_1$ may be substituted for
$?_e$ in (11). By applying l'Hopital's rule of
imits for $t_1 \to 0$, we find from the slightly
nodified equation (11) the result

$$= h_1 + (q/\epsilon)(4/\pi) \sum_{n=0}^{\infty} (2n + 1)^{-1} \cdot \sin (2n + 1)\pi(x/L) \exp - \mu t \tag{12}$$

vhich is the formula used by Glover to calculate
he decline of the water table level following
in instantaneous recharge q. Using the terminol-
ogy of operational mathematics, it may be
tated that (7), (10), and (11) describe the
ehavior of the water table in response to a
step function' while (12) describes the effect
of an 'impulse.'

The above formulas may be used to evaluate
he effect of a series of intermittent recharges
vhich will be considered in the subsequent
nalysis.

Intermittent constant recharge—Assume that the
constant rate of recharge p commences at
$= 0$, suddenly stops at $t = t_1$, resumes at
$= T > t_1$, stops at $t = T + t_1$, resumes at

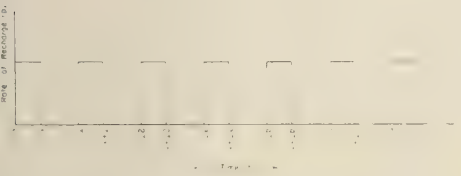

Fig. 3—Intermittent constant recharge rates at regular intervals

$t = 2T$, etc. (Fig. 3). As solutions of (2) are
additive, we may write from (7) and (11) the
result

$$z = h_1 + (P_e/2)\Big\{x(L - x)\alpha(t) - (8L^2/\pi^3) \sum_{n=0}^{\infty} (2n + 1)^{-3} \cdot \sin (2n + 1)\pi(x/L)(Q - R)\Big\} \tag{13}$$

in which

$$Q = \exp - \mu t + \exp - \mu(t - T) \cdots + \exp - \mu[t - (r - 2)T] + \exp - \mu[t - (r - 1)T] \tag{14}$$

and

$$R = \exp - \mu(t - t_1) + \exp - \mu(t - t_1 - T) \cdots + \exp - \mu[t - t_1 - (r - 2)T] + \beta(t) \exp - \mu[t - t_1 - (r - 1)T] \tag{15}$$

where

T = duration of the period (for example, time interval between successive irrigations. The zero point need not coincide with the time of the irrigation application. There will be some lag.)

t_1 = interval of recharge within the period T

r = number of periods considered

$$\alpha(t)\begin{cases} = 1 & (r - 1)T \le t < (r - 1)T + t_1 \\ = 0 & (r - 1)T + t_1 \le t < rT \end{cases}$$

$$\beta(t)\begin{cases} = 0 & (r - 1)T \le t < (r - 1)T + t_1 \\ = 1 & (r - 1)T + t_1 \le t < rT \end{cases} \tag{16}$$

Both Q and R are geometric progressions. Q consists of r terms, and R consists of $(r - 1)$ terms in the rth period for $t < (r - 1)T + t_1$ but has r terms in the interval between $(r - 1)T + t_1$ and rT. It thus follows for every finite t, that each term of the infinite series of (13) consists of two finite geometric progressions which may be summed separately. Excluding the last term from the summations, we find for Q and R the results:

$$Q = \exp - \mu t\left[\frac{1 - \exp (r - 1)\mu T}{1 - \exp \mu T}\right] + \exp - \mu[t - (r - 1)T] \tag{17}$$

and

$$R = \exp - \mu(t - t_1) \cdot \left[\frac{1 - \exp (r - 1)\mu T}{1 - \exp \mu T}\right] + \beta(t) \cdot \exp - \mu[t - t_1 - (r - 1)T] \tag{18}$$

It is finally found that:

$$\begin{aligned} Q - R &= (\exp \mu t_1 - 1) \\ &\cdot\left\{\frac{\exp - \mu[t - (r-1)T]}{1 - \exp \mu T}\right\} \\ &+ \exp - \mu[t - (r-1)T] - \beta(t) \\ &\cdot \exp - \mu[t - t_1 - (r-1)T] \\ &+ (1 - \exp \mu t_1)\left[\frac{\exp - \mu t}{1 - \exp \mu T}\right] \end{aligned} \tag{19}$$

Let us now define $\tau = t - (r-1)T$, so that τ ranges from 0 to T as t ranges from $(r-1)T$ to rT. This transformation is not a trivial one. It simplifies considerably the interpretation of the final results, because the first part of (19) is now a periodic function. If this substitution is made in the first three terms of (19), $(Q - R)$ assumes the form

$$\begin{aligned} Q - R = &\left(1 - \frac{\exp \mu t_1 - 1}{\exp \mu T - 1}\right) \\ &\cdot \exp - \mu\tau - \beta(t) \\ &\cdot \exp - \mu(\tau - t_1) \\ &+ \left(\frac{\exp \mu t_1 - 1}{\exp \mu T - 1}\right) \exp - \mu t \end{aligned} \tag{20}$$

Expressing $\alpha(t)$ of (13) and $\beta(t)$ of (20) also in terms of τ, we find from inspection of (16) that

$$\alpha(\tau)\begin{cases} = 1 & 0 \leq \tau < t_1 \\ = 0 & t_1 \leq \tau < T \end{cases} \qquad \beta(\tau)\begin{cases} = 0 & 0 \leq \tau < t_1 \\ = 1 & t_1 \leq \tau < T \end{cases} \tag{21}$$

The first two factors of (20) constitute a periodic function of period T, and the third factor is a transient function. Equations (13) and (20) may be combined, and the total expression thus obtained may be separated into its periodic and transient components. Let us write

$$z = h_1 + h_p - h_t \tag{22}$$

in which

h_p = the water table level calculated from the periodic part (expressed in τ)

h_t = the level calculated from the transient part (expressed in t, that is, the time since the beginning of the intermittent recharge)

It follows that

$$\begin{aligned} h_p = (P_e/2)\Bigg\{ &x(L - x)\alpha(\tau) \\ &- (8L^2/\pi^3) \sum_{n=0}^{\infty} (2_n + 1)^{-3} \\ &\cdot \sin (2n + 1)\pi(x/L) \\ &\cdot\left[\left(1 - \frac{\exp \mu t_1 - 1}{\exp \mu T - 1}\right) \exp - \mu\tau \right. \\ &\left. - \beta(\tau) \exp - \mu(\tau - t_1)\right]\Bigg\} \end{aligned} \tag{23}$$

and

$$\begin{aligned} h_t = (P_e/2)(8L^2/\pi^3) &\sum_{n=0}^{\infty} (2n + 1)^{-3} \\ &\cdot \sin (2n + 1)\pi(x/L) \\ &\cdot\left(\frac{\exp \mu t_1 - 1}{\exp \mu T - 1}\right) \exp - \mu t \end{aligned} \tag{24}$$

If $t_1 \rightarrow T$, then $(\exp \mu t_1 - 1)/(\exp \mu T - 1) \rightarrow 1$ and obviously $\beta(\tau) = 0$, so that the infinite series of the periodic function vanishes. If $\alpha(\tau) = 1$, it follows that for this condition (22) is identical to (7), as it should be.

The transient (Eq. 24) is a monotonic decreasing function consisting of a rapidly converging infinite series; as time increases, it becomes indefinitely small.

The periodic part gives the fluctuation of the water table when the water table and the intermittent recharge have reached dynamic equilibrium; that is, after the transient part has become negligibly small. The periodic function permits calculation of the maximum and minimum levels of the water table for the equilibrium condition. In addition, the rise and decline of the water table within the period T may be determined.

The number of periods required to reach equilibrium may be calculated from the transient part. Prior to equilibrium, the water table level at any time is obtained by subtracting the transient from the periodic part. Because of the nature of the differential equation (2), the effec

additional recharges superimposed on the
ittermittent one may be accounted for by
troducing a third or more functions.

Intermittent instantaneous recharge—The effect
intermittent equal impulses on the water
ble may be evaluated from (12). Let an in-
antaneous recharge of amount q per unit area
:ur at $t = 0, T, 2T$, etc. It then follows that

$$= h_1 + (q/\epsilon)(4/\pi) \sum_{n=0}^{\infty} (2n + 1)^{-1} \cdot \sin (2n + 1)\pi(x/L) S \tag{25}$$

which

$$= \exp - \mu t + \exp - \mu(t - T) \cdots + \exp - \mu[t - (r - 2)T] + \exp - \mu[t - (r - 1)T]$$

r

$$= \exp - \mu t \left[\frac{\exp \mu(r - 1)T - 1}{\exp \mu T - 1} \right] + \exp - \mu[t - (r - 1)T] \tag{26}$$

Again, let $\tau = t - (r - 1)T$, so that (26) can
e written as:

$$= \frac{\exp - \mu\tau}{\exp \mu T - 1} + \exp - \mu\tau - \frac{\exp - \mu t}{\exp \mu T - 1} \tag{27}$$

eparation of the periodic and transient functions
as thus been achieved and we may write

$$z = h_1 + h_{pi} - h_{ti} \tag{28}$$

here

h_{pi} = the water table level for instantaneous recharge, calculated from the periodic part (expressed in τ).

h_{ti} = the level calculated for instantaneous recharge from the transient part

follows from (25) and (27) that

$$_{pi} = (q/\epsilon)(4/\pi) \sum_{n=0}^{\infty} (2n + 1)^{-1} \cdot \sin (2n + 1)\pi(x/L) \cdot \left(1 + \frac{1}{\exp \mu T - 1}\right) \exp - \mu\tau \tag{29}$$

and

$$h_{ti} = (q/\epsilon)(4/\pi) \sum_{n=0}^{\infty} (2n + 1)^{-1} \cdot \sin (2n + 1)\pi(x/L) \cdot \left(\frac{1}{\exp \mu T - 1}\right) \exp - \mu t \tag{30}$$

Equation (30) is a monotonic decreasing function similar to (24). Equation (29) is a periodic function which describes the decline of the water table within the period T after the water table and the intermittent instantaneous recharge have reached dynamic equilibrium.

For $\tau = t$, that is, for a declining water table following a single recharge, (28) reduces to (12), as it should. Equations (29) and (30) can be derived directly from (23) and (24) by employing the same method as is used for the derivation of (12) from (11).

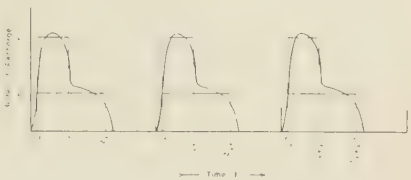

FIG. 4—Irregular recharge pattern substituted by two intervals of constant recharge

Irregular recharge patterns—The recharge pattern does not usually have the regularity assumed in the analysis and is largely dependent on the manner in which the soil profile discharges its excess water. Such irregular patterns may be studied by dividing them into a series of intervals of constant recharge. For example, the effect of the recharge pattern shown in Figure 4 may be evaluated by substituting for it two intervals of constant recharge within the period T: one with a rate of recharge $p_1 = p - p_2$ and recharge interval t_1, and another with a rate of recharge p_2 and recharge interval t_2. If the soil discharges a large part of its excess water in a short period of time, instantaneous recharge may be assumed for part of the recharge, while the remainder is accounted for by intervals of constant recharge. This would involve combinations of (23), (24), (29), and (30).

Should the pattern have a distinctly triangular or trapezoidal shape, developments derived from formula I.5.6 of *Werner* [1957] will prove useful. Such developments are not dealt with in this paper.

Water table levels of particular interest—It is of interest to know the maximum and minimum levels reached by the water table under conditions of intermittent recharge. Apart from these extreme levels it is equally, if not more, important to know how the water table rises and declines.

Considering first the relatively simple problem of instantaneous recharge, it is apparent that the water table rises over a height (q/ϵ) at the beginning of each period. This also follows from (29) by evaluating this formula for $\tau = 0$ and $\tau = T$ and subtracting the results so obtained, since we have the identity

$$(4/\pi) \sum_{n=0}^{\infty} (2n + 1)^{-1} \cdot \sin (2n + 1)\pi(x/L) = 1, \quad \text{for} \quad 0 < x < L.$$

For the condition of dynamic equilibrium (when the transient is negligibly small), the minimum water table (h_{pim}) for any x is calculated from (29) by putting $\tau = T$, that is

$$h_{pim} = (q/\epsilon)(4/\pi) \sum_{n=0}^{\infty} (2n + 1)^{-1} \cdot \sin (2n + 1)\pi(x/L)\left(\frac{1}{\exp \mu T - 1}\right) \tag{31}$$

The minimum equilibrium level midway between the drains (at $x = \frac{1}{2}L$) may be determined from (31) and is given by

$$h_{pil} = (q/\epsilon)(4/\pi) \sum_{n=0}^{\infty} (2n + 1)^{-1} (-1)^n \left(\frac{1}{\exp \mu T - 1}\right) \tag{32}$$

where

h_{pil} = minimum water table level midway between the drains for intermittent instantaneous recharge, calculated from the periodic function

and we also have

$h_{pih} = h_{pil} + (q/\epsilon)$; the maximum level midway between the drains

Equation (32) has special significance. Glover [see *Dumm*, 1954], who developed a drain spacing formula from (12), neglects all but the first term and writes

$$y = y_0(4/\pi) \exp - k(\pi/L)^2 t \tag{33}$$

However, instead of putting $y_0 = q/\epsilon$, as is required when (12) is used, Glover writes $y_0 = c + (q/\epsilon)$ and $y = c$. In the equation thus obtained, $c + (q/\epsilon)$ is apparently meant to signify the maximum water table under the assumed intermittent recharge conditions (see the example drain-spacing calculation included in Dumm's paper). That is, the effect of intermittent instantaneous recharge is being accounted for by an arbitrary change of (12) which is valid for one *single* recharge. No attempt is made to account for the accumulative effect of successive recharges in a consistent manner. Comparison of (29) with (33) shows that the latter formula is quite inadequate for an analysis of the fluctuation of the water table in response to a succession of instantaneous recharges even if the exclusion of all but the first term of the infinite series is permissible.

It is of interest to note that the value $c = h_{pi}$, assumed by Glover, may actually be calculated from (32). Whether dynamic equilibrium will be reached in the course of the irrigation season may be determined from (30). That formula enables us to determine the number of irrigations needed to approach h_{pil} to within any predetermined level. If drain spacings are calculated from (32) and if equilibrium is *not* approached during the irrigation season, the spacings so calculated may be adjusted to account for this effect.

The minimum water table for intermittent constant recharge (h_{pmin}) after equilibrium has been reached is calculated from (23) for $\tau = 0$ or T. According to (21), we have $\alpha(\tau) = 1$ and $\beta(\tau) = 0$ for $\tau = 0$, and $\alpha(\tau) = 0$ and $\beta(\tau) = 1$ for $\tau \to T$. Using (9), we obtain from (23) the result

$$h_{pmin} = (P_e/2)(8L^2/\pi^3) \sum_{n=0}^{\infty} (2n + 1)^{-3} \cdot \sin (2n + 1)\pi(x/L)\left(\frac{\exp \mu t_1 - 1}{\exp \mu T - 1}\right) \tag{34}$$

The maximum equilibrium water table occurs

t $\tau = t_1$, when $\alpha(\tau) = 0$ and $\beta(\tau) = 1$. It ollows that

$$h_{pmax} = (P_c/2)\left\{x(L - x) - (8L^2/\pi^3)\right.$$

$$\cdot \sum_{n=0}^{\infty} (2n + 1)^{-3} \sin (2n + 1)\pi(x/L) \quad (35)$$

$$\left. \cdot \left(1 - \frac{\exp \mu t_1 - 1}{\exp \mu T - 1}\right) \exp - \mu t_1 \right\}$$

If the amount of recharge water (q) is kept onstant, ($h_{pmax} - h_{pmin}$) will increase as t_1 ecreases, if all other factors remain invariant. For instantaneous recharge this difference is q/ϵ), as was pointed out earlier. The value of $_{pmin}$ and the transient (Eq. 24) are of consider- ble interest in various problems.

The minimum and maximum equilibrium vater table levels midway between the drains nay be determined from (34) and (35), namely

$$h_{pl} = (P_c/2)(8L^2/\pi^3)$$

$$\cdot \sum_{n=0}^{\infty} (2n + 1)^{-3}(-1)^n \left(\frac{\exp \mu t_1 - 1}{\exp \mu T - 1}\right) \quad (36)$$

nd

$$h_{ph} = (P_c/2)\left\{\tfrac{1}{4}L^2 - (8L^2/\pi^3)\right.$$

$$\cdot \sum_{n=0}^{\infty} (2n + 1)^{-3}(-1)^n \quad (37)$$

$$\left. \cdot \left(1 - \frac{\exp \mu t_1 - 1}{\exp \mu T - 1}\right) \exp - \mu t_1 \right\}$$

n which

h_{pl} = minimum water table level midway between the drains for intermittent constant recharge

h_{ph} = maximum water table level midway between the drains for intermittent constant recharge

It is observed that formula (29) is discontinu- ous for $\tau = 0$ and T; at these points it makes a ump of (q/ϵ). Equation (23) is discontinuous or $\tau = 0$, t_1, and T since the left-hand and right- and derivatives are not identical at these oints. However, the latter function is single- alued for all values of τ.

Interrupted intermittent recharge—If the intermittent recharge is discontinued after a certain number of recharges have been applied, the resultant declining water table may be determined as follows. Let $(r - 1)$ recharges be applied before they are stopped. The position of the water table at any time $t > rT$ may then be calculated from the formula

$$z = h_1 + h_t' - h_t \quad (38)$$

in which h_t is given, as usual, either by (24) for intermittent constant recharge or by (30) for intermittent instantaneous recharge; h_t' is also given by either (24) or (30) with a slight modification. In these formulas, the factor $\exp - \mu t$ is now to be replaced by $\exp - \mu(t - rT)$.

Equation (38) may be derived by introducing, for $t \geq rT$, negative intermittent recharges that are equal to and occur simultaneously with the 'positive' recharges. The result is that the effective recharge becomes zero and the periodic components cancel out.

Concluding remarks—The drain discharge per unit length of drain (Q_d) at any time may be calculated from

$$Q_d = K D(\partial z/\partial x)|_{x=0} \quad (39)$$

If inflow occurs from both sides of the drain ditch, the discharge will be twice that found from (39).

The factor $(\exp \mu t_1 - 1)/(\exp \mu T - 1)$ has been evaluated for some particular values of μt_1 and μT (Fig. 5) since it occurs in all problems of intermittent constant recharge.

It may be remarked that the assumption of predominance of lateral flow below the water table is fundamental to the applicability of the theory, or rather to the validity of either (2) or (5). In fact, head losses due to flow components in the vertical direction are virtually neglected. Flow convergence near a partially penetrating drain may be accounted for by such methods as used by *Ernst* [1954] or Moody [see *Maasland*, 1956], or, which is better in many problems, by reducing D as is done by *Maasland* [1956] for (33). Significant errors in the estimate of the height of the water table will occur in highly anisotropic soils if p is not small compared with K_v, K_v being the vertical hydraulic conductivity of the saturated soil.

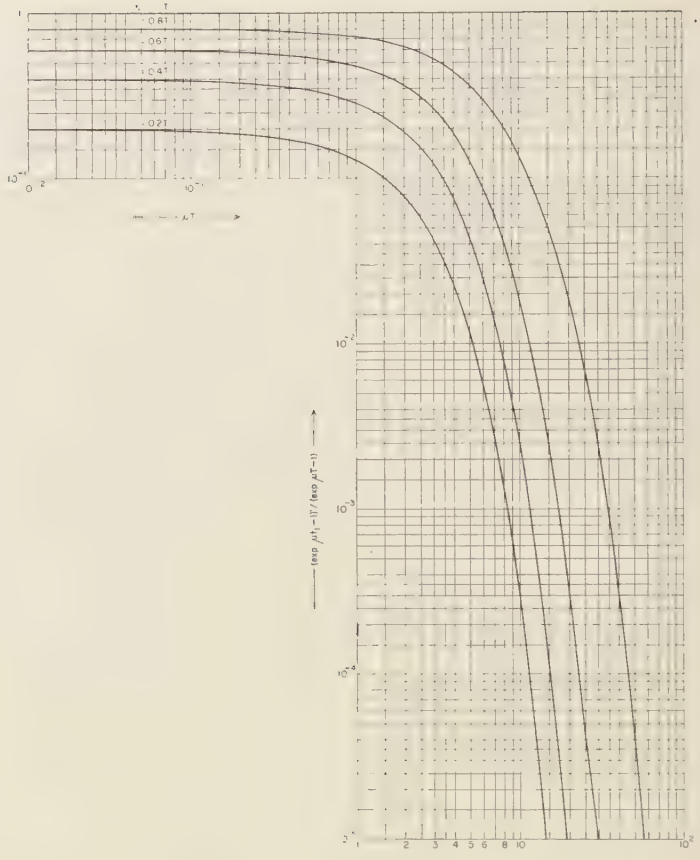

FIG. 5.—(exp $\mu t_1 - 1$)/(exp $\mu T - 1$) vs. μT for $t_1 = 0.2T$, $0.4T$, $0.6T$, and $0.8T$

It is obvious that a critical evaluation of the climatic and field conditions should precede application of the analytical results to practical problems. In the study of water-table fluctuations induced by excess irrigation applications, the method of irrigation enters into the problem as an additional factor and requires careful consideration.

Note—A recent paper by *Kraijenhoff* [1958] was brought to the attention of the author after the present study had been submitted for publication. He considers in detail the effect of a single surface-applied recharge on the groundwater storage and its depletion. Equation (11), which is arrived at here by using (7) and taking into account the initial and boundary condition for the particular problem, is obtained b Kraijenhoff from (12) by a process of integratior

REFERENCES

DONNAN, W. W., Model tests of a tile-spacin formula, *Soil Sci. Soc. Am. Proc.*, **11**, 131–13 1947.

DUMM, L. D., Drain spacing formula, *Agr. Eng* **35**, 726–730, 1954.

ENGELUND, F., Mathematical discussion of drainag problems, *Trans. Danish Acad. Tech. Sci.*, no. 64 pp., 1951.

ERNST, L. F., Het berekenen van stationnai grondwaterstromingen welke in een vertica vlak afgebeeld kunnen worden, Landbouwproe

sta. en Bodemkundig Inst. T.N.O., Groningen, Netherlands (mimeo.), no. 3, 55 pp., 1954.

Ernst, L. F., Calculation of the steady flow of ground water in vertical cross sections, *Neth. J. Agr. Sci.*, **4**, 126–131, 1956.

Hantush, M. S., and C. E. Jacob, Nonsteady Green's functions for an infinite strip of leaky aquifer, *Trans. Am. Geophys. Union*, **36**, 101–112, 1955.

Hooghoudt, S. B., Bijdragen tot de kennis van enige natuurkundige grootheden van de grond, *Verslag. Landbouwk. Onderzoek.*, **42**, 449–541, 1936.

Hooghoudt, S. B., Bijdragen tot de kennis van enige natuurkundige grootheden van de grond, *Verslag. Landbouwk. Onderzoek.*, **46**, 515–707, 1940.

Jacob, C. E., Correlation of ground-water levels and precipitation on Long Island, New York, *Trans. Am. Geophys. Union*, **24**, pt. 1, 564–573, 1943; **25**, pt. 2, 928–939, 1944.

Kraijenhoff van de Leur, D. A., A study of non-steady groundwater flow with special reference to a reservoir-coefficient, *Ingenieur, Utrecht*, **70**, 87–94, 1958.

Maasland, M., The relationship between permeability and the discharge, depth, and spacing of tile drains, *Groundwater and Drainage Series*, Water Cons. Irr. Comm., N.S.W., Australia, Bull. no. 1, 21–23, 1956.

Maasland, M., Soil anisotropy and land drainage, *Drainage of agricultural lands*, J. N. Luthin, ed., Agron. Monograph VII, Am. Soc. Agron., Madison, Wisc., 249–254, 1957.

Maasland, M., Discussion of "Some problems in non-artesian groundwater flow," *Trans. Am. Geophys. Union*, 39, 738–740, 1958.

van Deemter, J. J., Theoretische en numerieke behandeling van ontwatering-en infiltratie-problemen, *Verslag. Landbouwk. Onderzoek.*, no. 56.7, 67 pp., 1950.

van Schilfgaarde, J., D. Kirkham, and R. K. Frevert, Physical and mathematical theories of tile and ditch drainage and their usefulness in design, *Iowa State Coll. Agr. Exp. Sta. Bull. 436*, 667–704, 1956.

Werner, P. W., On non-artesian groundwater flow, *Geofis. Pura Appl.*, 25, 37–43, 1953.

Werner, P. W., Some problems in non-artesian ground-water flow, *Trans. Am. Geophys. Union*, 38, 511–518, 1957.

(Manuscript received March 28, 1958; revised May 8, 1958.)

The Analysis of Aquifer Test Data or Thermal Conductivity Measurements which Use a Line Source

J. C. JAEGER

Department of Geophysics
Australian National University
Canberra, Australia

Abstract—A simple numerical method for analyzing observations of drawdown in the neighborhood of a pumped well is described. It makes use of the ratio of the values of the drawdown at any two times and a graph computed from the theory. It has the advantage over existing procedures in that it is available for the analysis of isolated results and for small values of the time. The same method is applicable to the determination of thermal conductivity and practical examples of both cases are given.

One of the most satisfactory methods of measuring the thermal conductivity of powders consists of heating a long straight wire and measuring the temperature variation at a point some distance from it; similarly, the properties of an aquifer may be measured by pumping from a well and measuring the drawdown at a second well. In both cases the theory is that of the continuous line source in radial flow [*Carslaw* and *Jaeger*, 1959, p. 261] and a simple theoretical solution is available. In the hydrological case, reduction of the results is done [*Brown*, 1953] either by a process of curve fitting or by the use of the logarithmic asymptote of the theoretical solution: in conduction of heat, the latter method has always been employed: in both cases it implies that relatively long times must be used and it does not provide a very accurate value for the coefficient of storage or, in the thermal case, the diffusivity.

The method of reduction described below is available for all times, and the writer has found it particularly useful for measurements of thermal conductivity: it is set out here in hydrological terms in case it may also be useful in that context. The notation is that of *Brown* [1953].

The drawdown s at distance r from a well for which the discharge is Q (constant) for times $t > 0$ in an aquifer whose coefficients of transmissibility and storage are T and S, respectively, is given by [*Brown*, 1953, Eq. (1)]

$$s = \frac{Q}{4\pi T} W(u), \quad \text{where} \quad u = \frac{r^2 S}{4Tt} \tag{1}$$

and the 'well-function' $W(u)$ is just the tabulated exponential integral $-Ei(-u)$ so that

$$W(u) = -Ei(-u) = \int_u^\infty e^{-x} x^{-1}\, dx \tag{2}$$

and, for small values of u,

$$W(u) = -\ln Cu + u - \tfrac{1}{4}u^2 + \cdots \tag{3}$$

where $C = 1.7811$ is Euler's constant. It follows from (3) that if $u < 0.01$, $W(u) = -\ln Cu$ with an error of less than 1 per cent. The most useful tables of $-Ei(-u)$ for the present purpose are those of the *Works Projects Administration* [1940] but a short table is given by *Jahnke* and *Emde* [1933].

In practice, s is determined as a function of t for known values of Q and r and it is required to solve (1) for S and T. The method of reduction suggested is as follows: let t_0 be any convenient time and let N be any number (in practice N is conveniently taken to be 2); then if $s(t_0)$ and $s(Nt_0)$ are the values of the drawdown at times t_0 and Nt_0, it follows from (1) that

$$\frac{s(Nt_0)}{s(t_0)} = \frac{W(r^2 S/4TNt_0)}{W(r^2 S/4Tt_0)} \tag{4}$$

Here $s(Nt_0)/s(t_0)$ is known experimentally and so $(r^2S/4TNt_0)$ can be read from a table or graph of $W(u)/W(Nu)$. Figure 1 shows such graphs for the values 2, 3, and 4 of N, and Figure 2 gives the case $N = 2$ on a different scale. When $(r^2S/4TNt_0)$ has been found in this way, Q/T follows from (1) if the value of $s(Nt_0)$

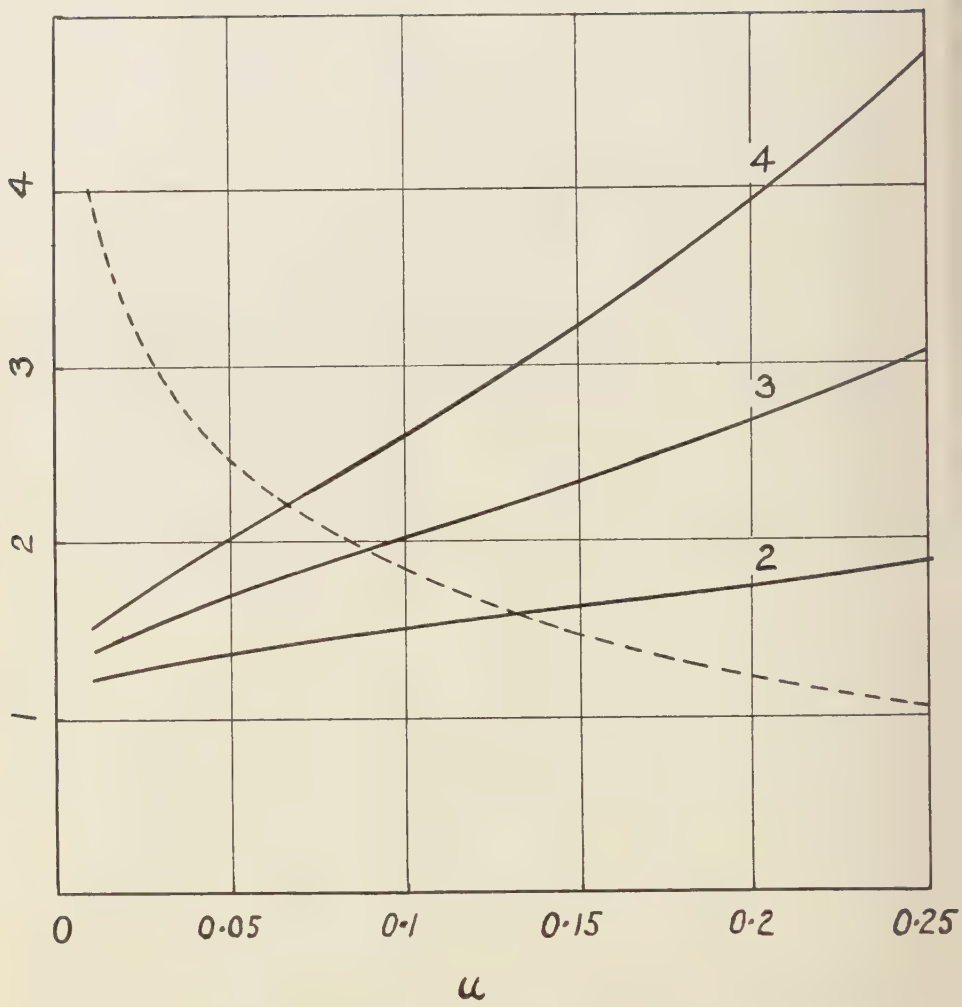

FIG. 1.—Values of $W(u)/W(Nu)$ as a function of u for $N = 2, 3, 4$; the numbers on the curves are the values of N. The dotted curve shows the value of $W(u)$.

and a table or graph of $W(u)$ are used. This graph is shown dotted in Figures 1 and 2.

As an example, some actual figures given by *Brown* [1953, Table 1] are considered. These are shown in Table 1 in which the figures in brackets have been found by graphical interpolation to enable integral values of N to be used in the present method.

As an example, taking $t_0 = 4$ min, $N = 4$, we have $s(16)/s(4) = 3.57$, and it follows from Figure 1 with $N = 4$ that $r^2S/4TNt_0 = 0.175$, also from the dotted curve in Figure 1 or a table of $W(u)$ we get $W(0.175) = 1.334$. In this example the values of Q and r are 500 gpm and 500 ft, respectively, so that, in the units used by *Brown* [1953] we have

$$T = \frac{60 \times 24 \times 500}{4\pi} \times \frac{1.334}{1.57}$$

$$= 48700 \text{ gpd/ft}$$

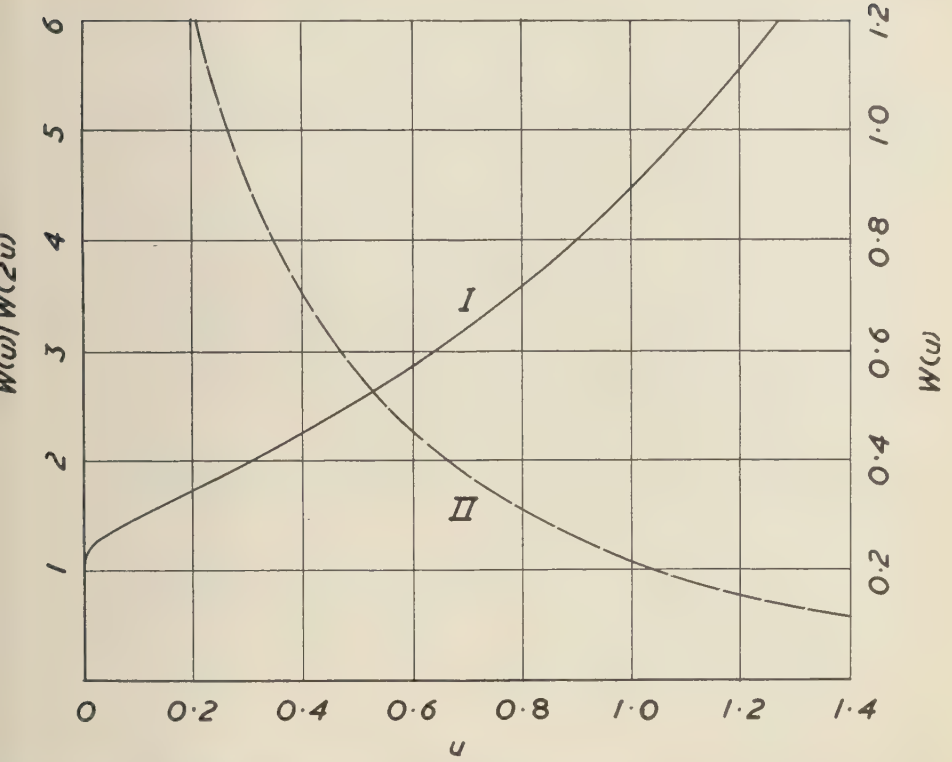

FIG. 2 -Curve I, left-hand scale, values of $W(u)/W(2u)$ as a function of u. Curve II, right-hand scale, values of $W(u)$.

and

$$S = \frac{48700 \times 16 \times 0.175}{1.87 \times (500)^2 \times 60 \times 24}$$

$$= 2.02 \times 10^{-4}$$

These may be compared with the values $T = 50{,}000$, $S = 2 \times 10^{-4}$ obtained by Brown by reducing the whole of the data of Table 1. It is interesting that the values obtained from measurements at so short a time agree so well with the average values. It is not suggested, of course, that observations should only be made for small values of the time (though in some cases this might be convenient) or that only two points be used. In the author's procedure for measuring thermal conductivity a convenient value of t_0 is chosen and observations are made at times t_0, $2t_0$, $4t_0$, $8t_0$, ... and each pair of these reduced separately. This gives a set of numbers whose standard deviation gives a measure of the accuracy of the measurement.

Values of S and T obtained by reducing six different pairs in this way are shown in

TABLE 1—*Reduction of drawndown test data*

t(min)	s(ft)	t_0	N	$T \times 10^{-4}$	$S \times 10^4$
0	0	...	...	...	...
4	0.44	4	4	4.9	2.0
13.75	(1.38)	13.75	4	4.9	2.1
15	1.50	...	...	...	...
16	(1.57)	...	...	...	...
55	2.83	55	3	4.8	2.2
165	(4.10)	...	...	...	...
180	(4.20)	180	2	5.2	1.7
185	4.22	...	...	...	...
360	4.96	360	2	5.0	2.0
720	5.75	720	2	4.8	2.2
1440	6.57	...	...	...	...

Table 1 and show clearly the spread inherent in the measured values of s and the experimental conditions. This procedure has the additional advantage that any trend in the results may often be attributed to a physical cause (limited size of the specimen or aquifer, variation of Q with time, etc.) which probably would not be observed if the points are reduced simply by drawing a linear asymptote.

For the larger values of the time for which only the logarithmic term in (3) is of importance, (4) gives immediately

$$\frac{Cr^2S}{4Tt_0} = \exp\left\{\frac{\ln N}{1 - s(Nt_0)/s(t_0)}\right\} \qquad (5)$$

In measurements of thermal conductivity, the temperature v at time t at distance r from an infinite line source which has been emitting heat at the constant rate Q per unit time per unit length for $t > 0$ is given as in (1) by

$$v = \frac{Q}{4\pi K} W\left(\frac{r^2}{4\kappa t}\right) \qquad (6)$$

where K and κ are, respectively, the thermal conductivity and diffusivity of the surrounding material which is supposed to be infinite and at a constant temperature (taken to be zero) at $t = 0$. The method of reduction is precisely the same as before. To illustrate it, Table 2

Table 2—*Reduction of thermal conductivity data*

t(sec)	v(°C)	$v(2t)/v(t)$	$r^2/8\kappa t$	r^2/κ	$1.08\ W(110/t)$
0	0	...	...	...	...
15	0.000	...	...	...	0.000
30	0.004	...	...	...	0.006
45	0.029	5.7	1.22	440	0.029
60	0.069	4.0	0.90	430	0.067
75	0.113	3.4	0.75	450	0.114
90	0.166	2.9	0.61	440	0.165
105	0.221	2.6	0.52	440	0.219
120	0.273	...	...	...	0.273
150	0.380	...	...	...	0.379
180	0.480	...	...	...	0.480
210	0.574	...	...	...	0.574

shows some results for the temperature v as a function of the time t at a distance $r = 1$ cm from a heater wire of resistance 0.278 ohm/cm carrying a current of 0.35 amp in a dry sand of density 1.48 gm/cm³.

The third column of Table 2 gives the ratio $v(2t)/v(t)$ and the fourth column the corresponding values of $r^2/8\kappa t$ read from Curve I of Figure 2. The fifth column gives the values of r^2/κ which should all be the same and are seen to be in reasonable agreement, their mean being 440. Using this mean value, the values of v in Table 2 should, by (6), be proportional to $W(110/t)$, and choosing a constant of proportionality of 1.08, we obtain the figures in the last column of Table 2 which in no case depart from the experimental values by more than 0.002°C. By (6) this constant of proportionality is $Q/4\pi K$; so finally

$$K = \frac{Q}{4\pi \times 1.08}$$

$$= \frac{0.278 \times (0.35)^2}{4\pi \times 1.08 \times 4.2} = 0.00060$$

This determination of K does not involve the distance r from the heater to the point at which the temperature is measured and which may not be known accurately. If the value of r is known, the value of r^2/κ obtained as above gives κ without involving Q or K; thus putting $r = 1$ in the example above gives $\kappa = 0.00227$. These values for K and κ lead to the reasonable value $K/\kappa = 0.26$ for the volumetric heat capacity which provides a useful check on the consistency of the method.

Finally it may be remarked that this general method of using the ratio of the values of the drawdown or temperature at a sequence of times in conjunction with a theoretical curve is not confined to the case of a line source but is applicable to many other situations.

References

Brown, R. H., Selected procedures for analyzing aquifer test data, *J. Am. Water Works Assoc.*, 45, 844–866, 1953.

Carslaw, H. S., and J. C. Jaeger, *Conduction of heat in solids*, Clarendon Press, Oxford, 2nd ed., 510 pp., 1959.

Jahnke, E., and F. Emde, *Tables of functions*, 2nd ed., Teubner, Leipzig, 330 pp., 1933.

Works Projects Administration, *Tables of sine, cosine and exponential integrals*, vol. 1, 444 pp., 1940; vol. 2, 225 pp., 1940.

(Manuscript received January 13, 1959; revised February 25, 1959.)

Some Implications on Mantle and Crustal Structure from G Waves and Love Waves *

Frank Press

Seismological Laboratory
California Institute of Technology
Pasadena, California

Abstract—G-wave velocities for continental and oceanic paths do not differ by more than about 2 per cent. Since the G-wave velocity is controlled by the low velocity zone in the mantle, this zone is present beneath continents and oceans. This suggests that the composition and distribution of temperature are the same for depths greater than about 50 km under continents and oceans. The low velocity zone may be the source of the primary basaltic magma and could account for the long-period nature of S waves. It may also represent a zone of decoupling for relative movements between crust and mantle.

Love waves with long propagation paths recorded with long period seismographs are used to infer that the mean value of continental crustal thickness lies in the range of 32 to 37 km.

G-wave results—Measurements which lead to a comparison of the outer mantle beneath continents and oceans are of fundamental importance in geophysics. Upon these measurements depend the answers to such questions as the source of silicic materials which form the continental masses, the mechanism of heat genesis and flow beneath continents and oceans, and the nature of the Mohorovicic discontinuity.

Elastic wave velocities provide the most direct measurement for comparing sub-continental and sub-oceanic mantle. Compressional wave velocities as determined in explosion seismological studies of crustal structure could be used. Although a large number of observations have been made at continental and oceanic stations, the results have been so variable as to preclude a definitive statement on the existence of differences between sub-continental and sub-oceanic mantle. Moreover these observations represent point by point determinations so that a larger number of observations than is now available may be needed before statistically valid sampling of upper mantle velocity has been achieved.

In this study we make use of earthquake-generated G waves with long continental and oceanic propagation paths. G waves offer the advantage that their velocities depend primarily on the properties of the outer mantle averaged horizontally over continental dimensions. They are less susceptible to the local heterogeneity, which probably accounts for the velocity variations found by explosion seismological methods.

The G wave was first discussed by Gutenberg and named after him by Byerly. It is a horizontally polarized shear wave with predominant periods in the range of 50 to 180 sec. G is transient in character and is followed by a train of dispersed Love waves when the propagation path is continental (Fig. 1, A and B). For oceanic paths

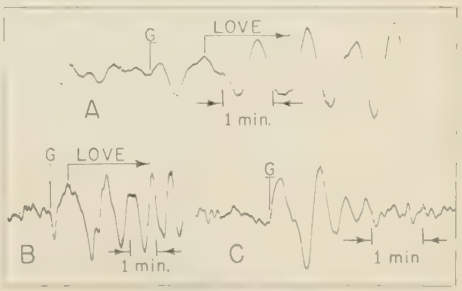

Fig. 1—G waves and Love waves; (A) October 28, 1958, continental path; (B) December 4, 1957, continental path; (C) November 1, 1958, oceanic path (no Love waves)

* Contribution No. 919, Division of Geological Sciences, California Institute of Technology.

where the crust is thin, the Love wave train has brief duration or may be absent, a consequence of the negligible dispersion for periods longer than 20 sec (Fig. 1C).

The velocity of G waves [*Benioff* and others, 1954; *Sato*, 1958] has been reported as 4.4 km/sec for mixed continental and oceanic paths, a value significantly below the upper mantle shear wave velocity of 4.7 km/sec determined from explosions. This difference may be accounted for by postulating a mechanism of G-wave propagation which is controlled by the vertical velocity distribution in the upper mantle. That G waves, like mantle Rayleigh waves, show little absorption in crossing continental margins is further evidence for the association of G waves with the properties of the upper mantle.

The availability of new seismographs [*Benioff* and *Press*, 1958; *Press* and others, 1958] with good response in the period range of 30 to 200 sec made the study feasible at this time.

The new instruments record G waves from earthquakes with magnitudes as small as 6, so that an adequate number of velocity determinations can be made for purely oceanic paths. The improved long-period response insures that the beginning of G and not a later cycle of the continental Love wave train has been used in the velocity determination.

Tables 1 and 2 show the data for oceanic and continental paths respectively. Continental paths to the Pasadena seismograph station include large segments of Asia and North America connected at the Bering Strait. The long propagation path reduces errors due to uncertainties in epicenter location and partially compensates for the smaller number of continental observations. The results give mean G-wave velocities of 4.41 km/sec for seventeen Pacific Ocean paths and 4.41 km/sec for five mixed Asian–North American paths. The estimated standard error of the difference in these mean values is 0.05 km/sec, and it may be concluded that oceanic and continental G-wave velocities probably do not differ by more than about 2 per cent. This agreement is consistent with the observation that G waves for mixed continental and oceanic paths travel with the same velocity.

The shear wave velocity distribution in the upper mantle to a depth of several hundred kilometers must be consistent with the G-wave velocity data. A given G velocity does not imply a unique shear wave velocity–depth relationship, but places restrictions on it. These restrictions

TABLE 1—*G waves for oceanic paths*

Date	Lat. (degrees)	Long. (degrees)	Origin time (UT) h m s	Magnitude	Distance (km)	Travel time (sec)	Velocity (km/sec)
1957							
Jan. 28	15½S	173 W	08 16 19	6½	7,978	1806	4.417
June 10	13½N	143½E	03 13 11	6¾–7	9,936	2259	4.398
June 19	24 S	175½W	01 29 48	6¼–6½	8,825	1988	4.439
June 19	16½S	176½E	08 01 30	6½	8,883	1974	4.500
June 22	1½S	137 E	23 50 23	7¼	11,453	2568	4.460
July 24	20 S	169 E	11 02 30	6½	9,742	2132	4.569
Nov. 20	54 N	165 W	12 40 23	6¼–6½	4,244	970	4.375
Dec. 13	52½N	170 W	20 26 22	...	4,548	1021	4.454
Dec. 17	12 S	167 E	13 50 05	7¾	9,379	2113	4.439
1958							
Jan. 24	56½N	163 E	05 53 58	6½	6,259	1436	4.359
Feb. 1	1½N	79 W	20 45 45	6¾	5,436	1285	4.230
Mar. 9	34 S	178½W	10 22 25	6½–6¾	9,811	2184	4.492
Mar. 20	51 N	173 W	01 38 04	...	4,744	1067	4.446
Apr. 13	53 N	161 E	12 29 07	...	6,476	1471	4.402
May 9	1½N	94½W	00 44 12	6	4,367	1017	4.294
July 12	5 S	106½W	00 48 30	6	4,498	1075	4.184
Nov. 1	17½S	168 E	12 16 36	6 –6¼	9,667	2154	4.488

TABLE 2—*G waves for continental paths*

Date	Lat. (degrees)	Long. (degrees)	Origin time (UT) h m s	Magnitude	Distance (km)	Travel time (sec)	Velocity (km/sec)
1951							
Nov. 18	31 N	90½E	09 35 43	7½	12,194	2743	4.445
1952							
Aug. 17	30½N	91½E	16 02 05	7¼–7½	12,208	2853	4.279
1957							
Dec. 4	45½N	99½E	03 37 45	7¾–8	10,411	2398	4.341
1958							
Jun. 23	49 N	102 E	05 10 03	...	9,978	2215	4.505
Oct. 28	30½N	85 E	10 46 27	...	12,465	2793	4.463

are made more severe when explosion data are also utilized.

The G-wave velocity of 4.41 km/sec together with the explosion-determined upper mantle shear velocity of 4.7 km/sec require the existence of a low velocity zone in the upper mantle [*Press* and *Ewing*, 1956; *Landisman* and *Sato*, 1958]. This was postulated by *Gutenberg* [1953] who showed that shear wave velocity increases above and below this zone at depths of 100 to 200 km. The G-wave velocity data indicate that this zone is present under continents and oceans. A recent study based on mantle Rayleigh waves also supports this conclusion (*Takeuchi* and others, in press). Therefore, according to the simplest hypothesis, the parameters which most affect shear wave velocity are probably distributed in the upper mantle in essentially the same way at depths greater than about 50 km under continents and oceans. Among these parameters are temperature, pressure, and composition. This last conclusion must be tempered with the remark that the shear wave dependence on composition may be sufficiently insensitive to mantle materials to vitiate any comparison.

The present study indicates that the low velocity zone in the mantle is a world-wide phenomenon. It is not unreasonable to ascribe the low velocity to a state near the melting point. Petrologic data seem to require the existence of a primary basaltic magma. The distribution of basaltic rocks in time and space and the geometry of the intrusions and flows are concordant with a source having world-wide distribution and occurring at depths as great as 150 km. The inference that the source of the primary basaltic magma coincides with the low velocity zone in the mantle is not inconsistent with these very limited data. If such is the case, it would also account for the long-period nature of S waves by a process of selective absorption [*Press* and *Ewing*, 1956]. The low velocity zone, if it is near the melting point, would represent a layer having imperfect elasticity for shear waves, one which would therefore act as a low pass filter for S. To hypothesize still further, this zone may be the place where the mantle is effectively decoupled from the crust for tectonic processes and differential movements between crust and mantle.

Love-wave results—Love waves with long continental paths recorded with long period seismographs yield dispersion curves of higher precision than are ordinarily obtainable. The long path minimizes effects of errors in epicenter location, and the long period instruments respond to the initial waves in the train which would otherwise be overlooked.

Data for paths which include long segments of Asia and North America are presented in Table 2 and Figure 2. Also included in Figure 2 for comparison are data for a path from Nevada to New York [*Ewing* and others, 1957].

For any given period the group velocities for the six earthquakes differ by less than 0.15 km/sec. This corresponds to an uncertainty in crustal thickness of about five kilometers which is near the limit of the precision of group velocity methods for studying the continental crust. The experimental data in Figure 2 may be considered as representative of Love-wave

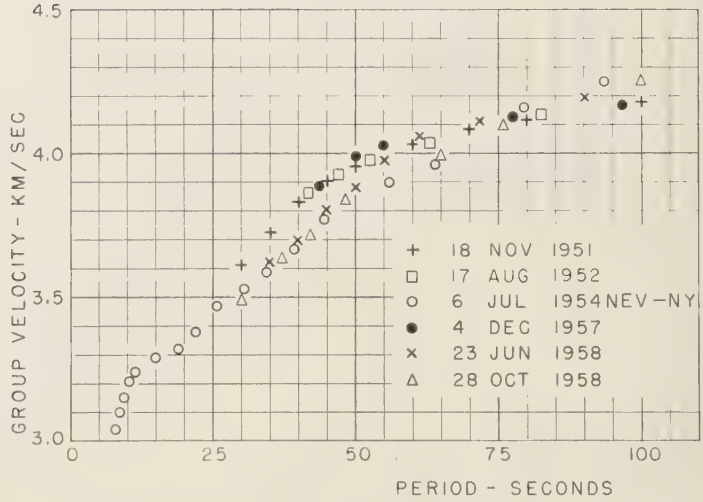

FIG. 2—Experimental group velocity curve for Love-wave propagation across a long Asian–North American path

dispersion for continents. The average elevation for these Asian–North American paths is about 3200 ft, which is close to the value of 2900 ft for the mean elevation of the continents. The usual methods of interpreting these data [*Ewing* and others, 1957, pp. 213–216] indicate that the mean continental crustal thickness lies in the range of 32 to 37 km. The low velocities for periods of less than 25 sec have been interpreted as an effect of sediments and non-least time propagation paths.

Acknowledgments—The author wishes to thank Ralph Gilman for his help in computations and reduction of seismograms. This work was supported by a grant from the National Science Foundation as part of the Interdisciplinary Research Program of the International Geophysical Year.

REFERENCES

BENIOFF, H., B. GUTENBERG, AND C. F. RICHTER, Progress report of the Seismological Laboratory, *Trans. Am. Geophys. Union*, **36**, 713–718, 1954.

BENIOFF, H., AND F. PRESS, Progress report on long period seismographs, *Geophys. J. Roy. Astron. Soc.*, **1**, 208–215, 1958.

EWING, M., W. S. JARDETZKY, AND F. PRESS, *Elastic waves in layered media*, McGraw-Hill Book Co., 380 pp., 1957.

GUTENBERG, B., Wave velocities at depths between 50 and 600 kilometers, *Bull. Seis. Soc. Am.*, **43**, 223–232, 1953.

LANDISMAN, M., AND Y. SATÔ, Shear wave velocities in the upper mantle, *Abstr. Trans. Am. Geophys. Union*, **39**, 522–523, 1958.

PRESS, F., AND M. EWING, A mechanism for G-wave propagation, *Abstr. Trans. Am. Geophys. Union*, **37**, 355–356, 1956.

PRESS, F., M. EWING, AND F. LEHNER, A long period seismograph system, *Trans. Am. Geophys. Union*, **39**, 106–108, 1958.

SATÔ, Y., Attenuation, dispersion, and the wave guide of the G wave, *Bull. Seis. Soc. Am.*, **48**, 231–251, 1958.

TAKEUCHI, H., F. PRESS, AND N. KOBAYASHI, Rayleigh wave evidence for the low velocity zone in the mantle, *Bull. Seis. Soc. Am.*, in press.

(Manuscript received February 9, 1959.)

Pressure Effects on Thermoluminescence of Limestone Relative to Geologic Age

Ernest E. Angino

Department of Geology, University of Kansas
Lawrence, Kansas

Abstract—Thermoluninescence as modified by pressure has been studied, and a relationship between pressure effects and geologic age has been observed. Experimental evidence indicates that the amount of pressure and the length of time that it is applied cause a marked variation in the ratio of thermoluminescence of pressed to unpressed samples. Geologically young samples showed a greater variability in the induced time-pressure effects than did geologically older samples.

The ratio of thermoluminescence of pressed to unpressed samples plotted against the time the pressure was applied showed a systematic variation from low values through a pronounced maximum and back to intermediate values. The amplitude of this curve shows an inverse relationship to the geologic age of the sample for limestones younger than Mesozoic.

Introduction and Theory

Certain minerals possess the ability to store energy in the form of metastable electrons. An electron, displaced by some external source of energy such as natural alpha radiation, can be moved from its normal position and 'trapped' by some type of imperfection in the crystal lattice structure. Any excess energy possessed by the electron becomes 'frozen' in the trap, and when released by the application of heat, the excess energy is dissipated in the form of heat and light. The light thus produced is termed thermoluminescence.

A given specimen exhibits thermoluminescence only once. Unless the specimen is subsequently exposed to some kind of high-energy radiation, a second heating will not produce light.

A quantitative method of measuring thermoluminescence was devised by *Daniels* and *Saunders* [1950]. An amplifier and photomultiplier were used to convert and amplify a weak light signal, thermoluminescence, into a measurable electric current. This current was then fed into a recorder and plotted as light intensity. The development of a reliable means of measuring thermoluminescence gave to the geologist a new tool for use in correlation and age determination studies. *Zeller* [1954] was the first to use thermoluminescence as an indicator of geologic age. *Zeller* and others [1957] showed that there was an apparent relationship between the geologic age of a sample and the ratio of pressed (Tl_p) to unpressed (Tl_u) thermoluminescence.

There are three types of thermoluminescence which are classified according to the process which is thought to cause the electron displacements: radiation-induced, pressure-induced, and crystallization-induced thermoluminescence. The method described in this paper is based on pressure-induced thermoluminescence.

All carbonates contain some impurity ions in the crystal lattice, and impurities, especially radioactive impurities, are known to have a controlling effect upon the radiation-induced thermoluminescence of a given sample. It is generally believed that impurities, by trapping electrons and storing energy, are responsible for individual glow curve peaks.

The actual mechanisms causing pressure-induced thermoluminescence are not known. It has been suggested [*Zeller* and others, 1955] that high pressures applied to an aggregate of crystals generate high electrostatic voltages in local areas by point contact and friction effects. These voltages are greater than those necessary to release electrons in the crystal lattice, and quite possibly some electrons may be released in this manner. In the pressure experiments of *Zeller* and others [1957], the samples under study were subjected to 6895 bars for five minutes.

In every case it was found that pressure increased the thermoluminescence of the 350°C peak of the younger samples, including laboratory precipitates. Lower Tertiary samples exhibited a smaller increase in natural thermoluminescense after pressure than did upper Tertiary samples.

Figure 1, a block diagram of the system, shows the equipment which was used to obtain the thermoluminescence of the samples.

Procedure

Thirty-five samples (essentially all $CaCO_3$), ranging from Cretaceous to Recent in age, were assembled from selected formations of known age. Every sample was carefully examined to assure that insofar as possible it was homogeneous, free of vugs and calcite veinlets, unweathered, and not recrystallized. Each sample was then ground to pass through a 100-mesh screen, and a natural and 'pressed' glow curve was run. The pressed samples were subjected to 7720 bars for two minutes. A pressure of 7720 bars was chosen because it is the highest pressure obtainable with the equipment, and it far exceeds any value to which the sample could have been subjected naturally by loading.

Results

After all curves were run, the area under the glow curves between 260° and 350°C was measured by planimetry, and the ratios of the areas of pressed to unpressed samples were determined.

Analysis of a plot of the ratios versus geologic time showed no simple relationship between the ratios and geologic time. As the spread of values within each geologic period was very large, the causes of the large spread were investigated.

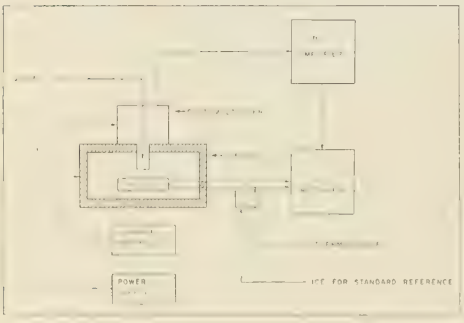

Fig. 1—Block diagram of equipment

Calcite-aragonite effects—Calcite and aragonite are known to have different thermoluminescence characteristics, and the metastable aragonite is fairly common in many of the Tertiary limestones. Accordingly, an investigation was made to determine whether this could be a factor in causing the observed spread in the values.

Gross mixtures, ranging from 100 per cent calcite to 100 per cent aragonite, were prepared from laboratory precipitates, and the thermoluminescence of pressed and unpressed samples was determined. It was found that aragonite greatly inhibits thermoluminescence, both before and after pressing. A high percentage of aragonite would have given a falsely low ratio. Consequently, in subsequent experiments, if the aragonite content exceeded 5 per cent, the sample was discarded.

Effects of grain size—A sample (Jewfish Creek, AB–7) of Pleistocene age was sieved, and pressed and unpressed glow curves were run for eight fractions (ranging from 60 to 300 mesh). The results showed that the ratio of pressed to unpressed thermoluminescence generally increased with increasing fineness of sample. To obtain an average ratio for the sample, all the −100 mesh material was retained. As the scattering effects of the +100 mesh fraction were great enough to cause concern, they were eliminated from the sample.

Time effects—In order to test the influence of the time of pressure application, two samples (of Pleistocene and Oligocene age) were subjected to 7720 bars for increasing intervals of time (1, 2, 5, 10, 15, and 30 minutes). After the samples were pressed, the ratios were determined in the usual manner and plotted against time. These samples showed curves of similar general form resembling a heavily damped sine function. The amplitude of the curves showed a relationship to geologic age.

To determine whether other samples would have similar curves with respect to time, seven more samples, ranging from Cretaceous to Recent in age, were selected at random from

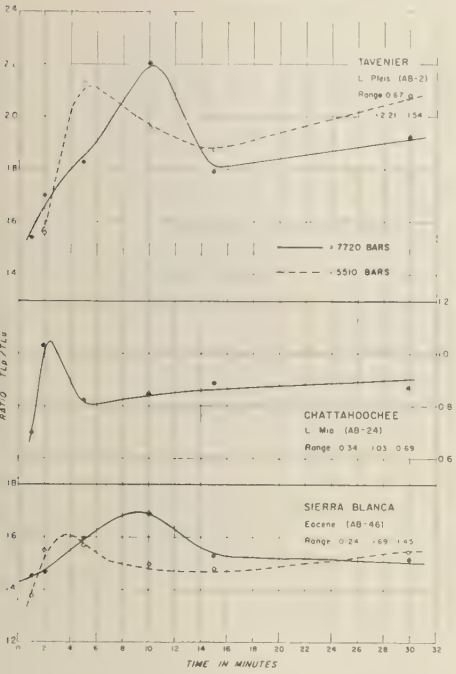

FIG. 2—Curves of three Tertiary samples showing systematic decrease in amplitude with increasing geologic time

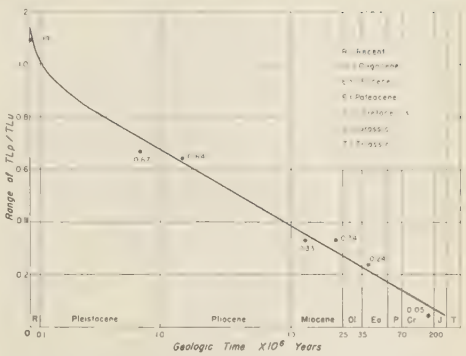

FIG. 3—Experimental age curve showing systematic decrease in range of Tl_p/Tl_u with increasing geologic time

the samples already run and subjected to similar treatment.

Figure 2 shows the curves of three of these samples arranged chronologically. All the curves are plotted on the same scale. Careful examination of these curves reveals that they are all similar and that for the same time increments both the 7720 and the 5510 bar curves have similar characteristics. They are skewed to the left, and they all have peak ratios in the 2- to 10-minute range. Some show a slight rise at 30 minutes. (Note that pressure decreased the thermoluminescnece of the Chattahoochee sample.) However, the most striking fact shown by these curves is that the amplitude decreased with increasing geologic time. The amplitude is the calculated difference (range) between the highest and lowest Tl_p/Tl_u of a sample. It might be argued that the experimental points are not spaced closely enough to be sure that the true maxima of the curves have actually been found; however, work on other samples (the curves of which are not shown) indicates that the values obtained at intermediate points would not deviate radically from the curves as drawn. Figure 3, a semi-logarithmic plot modified to show recent time, is a graph of the amplitude of the time-pressure curves plotted against the geologic age of the sample.

The observed effects are actually what should be expected, as the younger samples have had less time to be affected by pressure and annealing processes which would tend to produce a more stable lattice. Consequently, they should show the greatest change with pressure and increasing time. Samples older than Cretaceous behave similarly and approach a range of ratio value of 0.05 regardless of time and pressure. In order to date Mesozoic and Paleozoic samples, other methods must be employed.

The results plotted have been rechecked twice and were found to be reproducible to within 10 per cent.

If the effect of pressure upon the calcite crystal lattice is found to be sufficiently consistent in its relation to the geologic age of the sample, it may be possible to develop a workable method for geologic age determination in Tertiary and Quaternary limestones. However, certain specific sources of error must be considered in any evaluation of results.

Discussion

Sources of error—The apparatus used sets definite working limits on the thermoluminescence

measurements. The furnace control unit must produce a linear temperature rise, or reproducibility of results is difficult to attain. If more than one furnace is to be used, care must be taken that all furnaces have similar heating characteristics; otherwise, the heating-rate curve may not be reproducible. For this reason, a given sample (pressed or unpressed) was always run on the same furnace to assure similar characteristics and comparability.

Heterogeneous composition (both mineralogic and chemical) is a possible source of error. This can be a serious problem when the glow curves of different substances are not similar, especially since the wavelength of the light which they emit is likely to be different. For example, the photomultiplier is more sensitive to the spectrum emitted by calcite than dolomite, but the dolomite can store more energy and may partially mask the calcite.

In the pressed samples the condition of the pellet is critical. The pellet used must be perfect and must rest flat on the furnace surface. If the pellet does not rest flat, a thermal gradient is developed across the air gap between the pellet and the surface of the furnace. In this case the temperature of the pellet at a given instant is not that of the furnace but actually is lower by an indefinite amount.

Theoretical interpretations—The actual mechanisms causing the so-called time-pressure effects are not known. Work is continuing on this phase of the problem.

The causes of the inhibiting effect of aragonite are also uncertain. Point charge effects and their resulting force fields may be a possible explanation for this phenomenon [*Angino*, 1958]. The aragonite, because of its needle-like crystal shape, may concentrate electric charges at the points of each needle crystal; likewise most of the calcite charge may be concentrated at the eight rhomb apices. By this concentration of charge, the electrostatic force field in each local area may be warped; and the stresses and strains set up in the area may trap electrons. Local electrostatic fields may be set up which possess sufficient energy to prevent the drainage of traps by temperatures as high as 400°C. If enough such areas are formed, then conceivably the total thermoluminescence observed can be less for the mixtures than for the pure samples.

Grain size and pressure affect the thermoluminescence observed; however, their effects appear to be minor with respect to those of time. Further work on the effects of grain size and pressure is in progress.

Conclusions

In view of the above data, a simple means of determining the relative geologic age of carbonate samples of Tertiary age might be developed if further tests substantiate these results. For example, assume that an unknown sample was subjected to the treatment outlined and that an amplitude value of 0.52 was obtained. Its apparent age, according to the age curve (Fig. 3), would be Pliocene.

Refined techniques and improved theory and instrumentation will undoubtedly alter the limits within the age curve as presented here; however, there does appear to be a systematic decrease in the amplitude of Tl_p/Tl_u curves with increasing Tertiary age.

Pressure and grain size have some influence on the amplitude; however, it appears to be relatively minor when compared with that of time.

If the exact mechanism operating in the calcite-aragonite mixture to inhibit thermoluminescence is determined, a correction factor for aragonite can be applied to samples high in aragonite.

It should be kept in mind, however, that this study is still in its preliminary stages. Further work on the pressure phases of this problem is in progress, and it is hoped that a reasonable theoretical explanation of the apparent relationship between amplitude and geologic time will be obtained.

In our work we continually encounter unexpected phenomena which we cannot explain on the basis of accepted concepts of solid-state physics. These problems should be examined by solid-state physicists, and their inquiries and suggestions will be welcomed.

Acknowledgments—I wish to express my sincere thanks to E. J. Zeller of the Department of Geology, University of Kansas, who suggested this study and made many helpful suggestions and criticisms. Financial assistance under contract AT(11-1)83, Project 5, from the Atomic Energy Commission is gratefully acknowledged.

References

Angino, E. E., Pressure-induced thermoluminescence as a geologic age determination method, Unpublished master's thesis, Dept. of Geology, Univ. of Kansas, 1958.

Daniels, F., and D. F. Saunders, The thermoluminescence of rocks, *Science*, 111, p. 462, 1950.

Zeller, E. J., Thermoluminescence as a radiation damage method of geologic age determination, *19th International Geologic Congress*, Algiers, 1952, part 12, pp. 365–373, 1954.

Zeller, E. J., J. L. Wray, and F. Daniels, Thermoluminescence induced by pressure and crystallization, *J. Chem. Phys.*, 23, p. 2187, 1955.

Zeller, E. J., J. L. Wray, and F. Daniels, Factors in age determination of carbonate sediments by thermoluminescence, *Bull. Am. Asso. Petrol. Geologists*, 40, 140–152, 1957.

(Manuscript received February 3, 1959.)

A Note on the System Fe_2O_3-H_2O*

ROBERT F. SCHMALZ**

Department of Geology
Harvard University
Cambridge, Massachusetts

Abstract—Hydrothermal investigation of a portion of the system Fe_2O_3-H_2O has served to locate approximately the hematite-goethite phase boundary. Calculations derived from the experimental data provide the following estimates of the thermodynamic properties of goethite at 25°C: $\Delta H_f = -132$ Kcal/mol; $S° = +18.1$ cal/mol-degree; $\Delta S_f = -51.0$ cal/mol-degree; $\Delta G_f = -117$ Kcal/mol. Goethite is shown to be the stable ferric oxide phase under sub-aerial weathering conditions where relative humidity exceeds 60 per cent. Goethite is also shown to be stable in all normal marine environments, though hematite may become stable in contact with saline liquors of an evaporite basin.

Introduction—An investigation of the system Fe_2O_3-H_2O was undertaken in an attempt to define the fields of stability of hematite and goethite, and to determine the thermodynamic properties of goethite. Unfortunately, it was necessary to defer the study after completing only two isobars (at 800 and 900 bars) and roughing in a third (970 bars). Together with the data of *Posnjak* and *Merwin* [1922], however, the results of the present study provide a reasonable approximation of the boundary between the stability fields of hematite and goethite and permit the calculation of approximate values for the thermodynamic properties of goethite.

Experimental procedure—The experimental apparatus (Fig. 1) included a high-pressure kerosene pump, isolated from the aqueous portion of the system by a 1 : 1 separation cylinder. A low-pressure pump and reservoir allowed the introduction of distilled water into the system. Stainless-steel rod-bombs designed and built for this investigation (Fig. 2) were coupled to the pressure system by capillary tubing and appropriate needle valves. A pressure reservoir with a volume about 500 times that of a charged rod-bomb was included in the system to minimize the pressure effect of minor leaks. Pressures were measured by a dead-weight calibrated Heise gauge, scaled from 0 to 1000 bars in one-bar divisions. The bombs were sealed in nichrome-wound furnaces controlled by thyratron regulators of the type described by *Bancroft* [1942]. Temperatures were measured by copper-constantan thermocouples calibrated at five melting and boiling points within the temperature range of the experiments; their potential was measured on a Leeds and Northrup type K potentiometer. The cold junction was maintained at 0°C in an ice bath prepared entirely from distilled water, and all junctions of dissimilar metals in the thermoelectric system were similarly thermostated. Thermal gradients within the bombs were corrected for by making melting-point determinations in the bombs with external thermocouples in place.

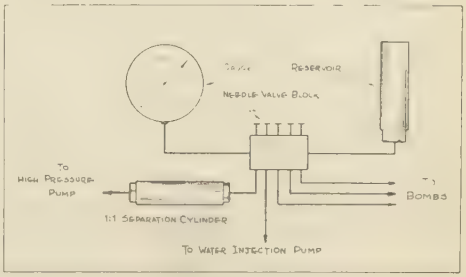

FIG. 1—Schematic diagram of experimental apparatus used in the present investigation (see text)

* Paper No. 174 published under the auspices of the Committee on Experimental Geology and Geophysics and the Division of Geological Science at Harvard University.

** Present address: Department of Geology, The Pennsylvania State University, University Park, Pennsylvania.

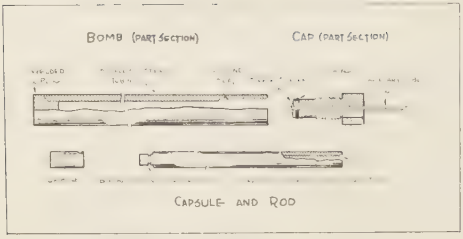

FIG. 2—Sketch, not to scale, of the cold-seal bomb designed for the present study by F. Birch, Dunbar Laboratory, Harvard University

The starting material used in the study was ferric hydroxide paste prepared by precipitation from ferric chloride solution with ammonium hydroxide. The precipitate was disaggregated and washed with distilled water until the wash water gave a negative test for chloride ion with silver nitrate solution (0.1 M). The material was amorphous to x-rays.

Charges were placed in open, stainless steel capsules (Fig. 2). The volume of water in the bomb was such as to fix the free energy of oxygen in the system well within the stability fields of hematite and goethite. No oxidation of bomb, rod, or capsule was observed in any of the runs.

The runs were of eight hours' duration. Replicate runs of up to 30 days' duration were found to give identical results. Pressures and temperatures were measured every thirty minutes during eight-hour runs. Runs which showed variation in pressure greater than ±1 bar or variation in temperature greater than ±0.5°C were rejected.

All reaction products were identified by x-ray diffraction.

Experimental results—Pressure and temperature data for the runs at 800, 900, and 970 bars are tabulated below (see Table 1) and plotted in Figure 3. Included also is the 130°C (approximate) equilibrium temperature determined by *Posnjak* and *Merwin* [1922]. Although Posnjak and Merwin did not measure the pressure on their runs, the pressure in their reaction cell may be estimated* as 4 bars at 130°C.

All of the experimentally determined points in the system lie at pressures well in excess of the vapor pressure of pure water. In a system in which all phases are condensed, a transition curve may be approximated as a straight line. In the present system, the straight line determined by Posnjak and Merwin's point at 130°C and the bracketing runs at 900 bars is compatible with all of the available data. Accordingly this line (Fig. 3) is taken as the hematite-goethite transition curve. It must be emphasized that this boundary was located by the formation of either of the bounding phases as the product of the reaction of a third phase. Although several runs confirm the location of the boundary by the transition goethite to hematite, the reverse tran

TABLE 1—*Temperature and pressure data for runs in the system* Fe_2O_3-H_2O

Run	Pressure (bars)	Temperature (°C)	Product[a]
34	801	138.5	G
38	802	151.0	G
36	803	159.0	G
35	801	160.5	G
39	800	163.5	G
37	802	164.0	G
33	802	167.0	H
40	802	169.5	H
42	804	174.5	H
28	906	154.0	G
29	906	166.0	G
41	907	170.0	G
31	908	171.0	H
30	905	173.0	H
43	907	175.0	H
44	906	178.5	H
24	968	152.5	G
23	966	166.0	G
22	974	170.5	G
21	967	179.0	H
Posnjak and *Merwin* [1922]	4 (approx.)	130.0 ± 5	G + H

[a] Goethite–G; Hematite–H. Starting material in all runs tabulated was ferric hydroxide paste.

* Glass tubes were half filled with solution sealed, and raised to temperature. The pressure in the cell at reaction temperature will equal approximately, the sum of the vapor pressure of pure water at that temperature, plus the increase in air pressure due to heating at constant volume plus the increase in air pressure due to expansion of the liquid phase. These values are, approximately 2.66 bars, 0.38 bar, and 0.07 bar, respectively. Total pressure in the cell at 130°C, including the atmospheric pressure in the cell at the time of sealing is accordingly 4 bars.

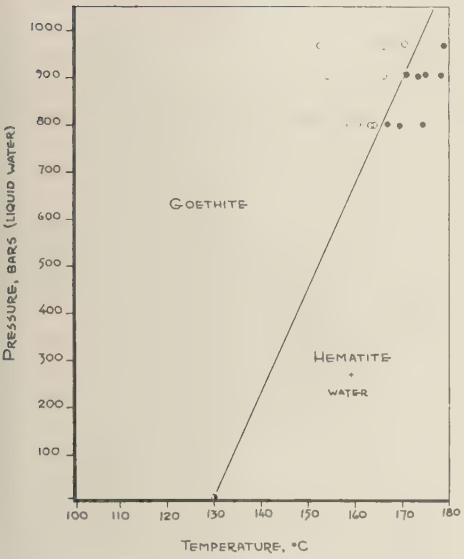

FIG. 3—The hematite-goethite phase boundary as approximately located in the present investigation; open circles represent bomb runs in which goethite was produced; filled circles, hematite; the half-filled circle at 130°C represents the results reported by *Posnjak* and *Merwin* [1922]; slope of the boundary is 22.3 bars/degree

sition, hematite to goethite, could not be effected. (The refractory character of hematite makes reversal of the reaction almost impossible in a pure system. Runs located well within the goethite field maintained at 2000 bars for periods up to 30 days showed no reaction.) Since the phase boundary has not been determined by reversing the phase transition, its location must be considered approximate. If this approximation departs significantly from the actual transition curve, it probably lies at too high a temperature, and the derived values for the thermodynamic properties of goethite (below) would be in error. Allowing an uncertainty in the actual equilibrium temperature as great as 30°C occasions an error of only 1 per cent in the tabulated values, however, and this uncertainty is not significant. The slope of the approximate phase boundary is 22.3 bars/degree.

Thermodynamic properties of goethite—The thermal expansion of the solid phases, which may be assumed to compensate for one another, may be neglected but the expansion of water must be taken into account. Then the volume change of the reaction

$$\text{hematite} + \text{water} = 2\ \text{goethite}$$

at 130°C and one bar is −6.8 cc/mol (hematite). For the purpose of the present approximation, the change in the equilibrium temperature occasioned by extrapolating the equilibrium curve to one bar may be neglected.

From the relation

$$dP/dT = \Delta S'/\Delta V'$$

it is possible to derive the entropy change of the reaction at 130°C

$$\Delta S' = -151.6 \text{ cc-atm.}$$

$$= -3.7 \text{ cal/degree-mol (hematite).}$$

To evaluate the thermodynamic properties of goethite at 25°C we assume that hematite, goethite, and water are in equilibrium at P' and T' (in this case one bar and 130°C respectively), and that ΔC_p for the reaction is a constant. Then at $P = P'$ and $T \neq T'$

$$\Delta H = T'\,\Delta S' + \Delta C_p(T - T')$$

$$= T'\,\Delta V'(dP/dT)' + \Delta C_p(T - T') \qquad (1)$$

$$\Delta S = \Delta S' - \Delta C_p \ln (T'/T)$$

$$= \Delta V'(dP/dT)' - \Delta C_p \ln (T'/T) \qquad (2)$$

and

$$\Delta G = (T' - T)[\Delta V'(dP/dT)' - \Delta C_p] + \Delta C_p T \ln (T'/T) \qquad (3)$$

The value of $\Delta S'$ has been calculated above from the experimental data. If we assume that the heat capacities of hematite and goethite are in the same simple proportion as those of corundum and diaspore, the heat capacity of goethite may be estimated as

$$C_p \cong 18.7 \text{ cal/degree-mol (goethite).}$$

The heat capacity values for water and hematite are given by *Rossini* [1952]. From these data the heat capacity change for the reaction may be estimated as

$$\Delta C_p \cong -5.6 \text{ cal/degree-mol (hematite).}$$

The energy changes for the reaction at 25°C may now be calculated from the relations (1), (2), and (3)

$$\Delta H = -904 \text{ cal/mol (hematite)}$$

$$\Delta S^\circ = \Delta S_f = -2.0 \text{ cal/mol-degree (hematite)}$$

$$\Delta G = -304 \text{ cal/mol (hematite).}$$

Rossini's data for hematite and water at 25°C now permit the calculation of values for the thermodynamic properties of goethite.

$$\Delta H_f = -132.0 \text{ Kcal/mol}$$

$$S^\circ = +18.1 \text{ cal/mol-degree}$$

$$\Delta S_f = -51.0 \text{ cal/mol-degree}$$

$$\Delta G_f = -117.0 \text{ Kcal/mol.}$$

The major sources of uncertainty in these values derive from the approximation of the heat capacity of goethite and the uncertainty in the slope of the postulated phase boundary. The estimated heat capacity is quite certainly accurate to ± 1 cal/mol. The uncertainty in the slope of the phase boundary, largely attributable to the $\pm 5°$ uncertainty in Posnjak and Merwin's work, causes an uncertainty of ± 0.5 cal/mol-degree in the entropy change for the reaction. If we take these uncertainties into account, we may conclude that the values obtained for the thermodynamic properties of goethite have uncertainties of the order of ± 1 Kcal/mol (ΔH_f and ΔG_f) and ± 0.5 cal/degree-mol (S° and ΔS_f).

Conclusions—If we assume pure solid phases, then equilibrium in the reaction at any temperature will be determined by the free energy of water. In the absence of the liquid phase, the free energy of water in the system will be controlled by the vapor pressure of water. In the presence of the liquid phase, the free energy of water may be reduced by dissolved salts. Both factors may be conveniently treated in terms of the ratio of water vapor pressure present in the system to the vapor pressure of water in equilibrium with pure liquid water at the temperature of the system. If this ratio is represented by η, the reduction in the free energy of water occasioned by either dissolved salts or an undersaturated vapor phase (due to the absence of liquid water) may be derived from the relation

$$\Delta G = -RT \ln (\eta) \qquad (4)$$

If, at any point within the stability field of goethite, the free energy of water is reduced by an amount just equal to the change in free energy of the reaction

$$\text{hematite} + \text{water} = 2 \text{ goethite},$$

the reaction will be in equilibrium. Thus, a combination of (3) and (4) gives an expression which defines an equilibrium state at any temperature T in terms of the ratio η

$$\begin{aligned} -RT' \ln (\eta) &= (T' - T) \\ &\quad \cdot [\Delta V'(dP/dT)' - \Delta C_p] \\ &\quad + \Delta C_p T \ln (T'/T) \end{aligned} \qquad (5)$$

From (5) the equilibrium relative humidity in the system may be calculated at any temperature. The hematite-goethite phase boundary is plotted below (Fig. 4) as a function of relative humidity and temperature. At 25°C, the reaction will come to equilibrium at relative humidity of 60 per cent; at lower relative humidities, hematite will be the stable phase, at higher, goethite. Under conditions of sub-aerial weathering, rela-

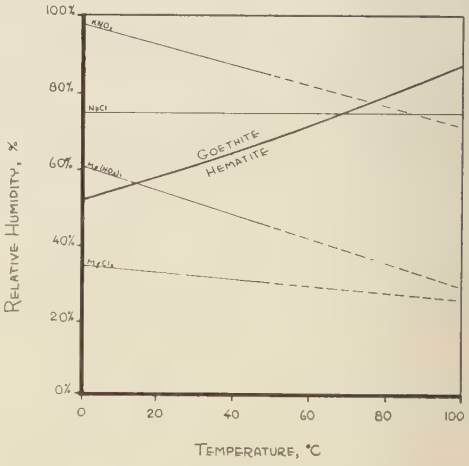

FIG. 4—The hematite-goethite phase boundary plotted as a function of relative humidity (100η) against temperature, with equilibrium water-vapor-pressure over saturated solutions of several mineral salts; salt data from *Wexler* and *Hasegawa* [1954]

ive humidities less than 60 per cent are commonly observed, and consequently hematite might be expected to appear frequently as the weathering product of ferruginous rocks.

The same reduction in the free energy of water might be accomplished by the presence of dissolved salts, although the magnitude of the necessary reduction is rather large. In Figure 4, the relative humidity in equilibrium with saturated aqueous solutions of several mineral salts is plotted against temperature [data from *Wexler and Hasegawa*, 1954]. At 25°C, saturated solutions of KNO_3 (niter), KCl (sylvite), or NaCl (halite) would not have sufficiently low free energy to stabilize hematite, but $Mg(NO_3)_2 \cdot 6H_2O$ (nitromagnesite) or $MgCl_2 \cdot 6H_2O$ (bischofite), and probably $CaCl_2$ (hydrophilite), in saturated solution would be more than adequate to dehydrate goethite. Thus, although hematite would not be expected to form in the presence of saturated solutions of sodium chloride, the residual liquors in an evaporite basin might be sufficiently concentrated to make hematite the stable phase. Field confirmation of this conclusion is available. Hydrated ferric oxides form on iron and steel tools in salt mines; similarly, iron and steel objects exposed to sea water form hydrated oxides even in the intertidal or spray zones where the brines may become highly saturated by evaporation. Hematite is frequently observed, however, as a pigmenting agent in the late members of evaporite sequences. Petrographic studies of iron-bearing evaporite sequences should prove of interest as further confirmation of this proposal.

Even at tempreatures up to 70°C, saturated solutions of halite, sylvite, or niter would appear to be inadequate to stabilize hematite relative to goethite, and goethite should be stable in the presence of sea water at temperatures up to the boiling point.

The foregoing calculations suggest that naturally occurring red ferruginous pigments in sedimentary deposits must have been formed as sub-aerial weathering products, introduced into the sediment as detritus. Exceptions to this interpretation would include hematite in the late members of iron-rich evaporite sequences and ferruginous sediments which show evidence that agencies other than inorganic precipitation (organic agents might include bacteria or algae) were actively involved in the iron deposition.

Acknowledgments—The writer is indebted to F. Birch of Harvard University for his support of the investigation. J. B. Thompson, Jr. and R. M. Garrels of Harvard University and E. Zen of the University of North Carolina critically reviewed the manuscript. To all of these, the writer expresses his thanks. The writer is also indebted to J. B. Thompson, Jr. for the formulation of the equations for the energy changes of the reaction (1, 2, 3, and 4) employed in the text.

References

Bancroft, D., Two bridge-controlled thyratron thermostats, *Rev. Sci. Instr.*, **13**, 24–27, 1942.

Posnjak, F. D., and H. E. Merwin, The system Fe_2O_3—SO_3—H_2O, *J. Am. Chem. Soc.*, **44**, 1965–1994, 1922.

Rossini, F. D., D. D. Wagman, W. H. Evans, S. Levine, and I. Jaffe, Selected values of chemical thermodynamic properties, *Natl. Bur. Standards, U. S., Circ. 500*, 1268 pp., 1952.

Wexler, A., and S. Hasegawa, Relative humidity-temperature relationships of some saturated salt solutions in the temperature range 0° to 50°C, *J. Research, Natl. Bur. Standards*, **53**, 19–26, 1954.

(Manuscript received January 15, 1959.)

Letters to the Editor

Volcanic Eruption in Belgian Congo

E. Berg

Institut pour la Recherche Scientifique en Afrique Centrale
Lwiro, Bukavu, Belgian Congo

On August 7, 1958 at about 2240 UT a brief eruption occurred on the northern side of Nyamuragira in the active area of eastern Belgian Congo. A swarm of small earthquakes of maximum magnitude 2.6 preceded the eruption by some three hours. The volcanic activity stopped quickly, but small earthquakes continued to the beginning of the main eruption at 0245 UT on August 10 at a place called Kitsimbanyi (1°20′S 29°10′E, altitude about 1700 m) some 13 km north of Nyamuragira and 14 km from the Rumangabo seismographic station which is jointly operated by the Institut pour la Recherche Scientifique en Afrique Centrale (I.R.S.A.C.) and the National Parks of the Belgian Congo.

The variation of maximum trace amplitudes of the sinusoidal earth tremors at Rumangabo revealed periods of 20 to 25 days, corresponding to the eruptive activity. (The tremors are of 0.7 sec period with maximum amplitude of 65 mm on the Benioff vertical short period seismograph.)

When it stopped on November 21 the lava outflow measured about 20 km. The maximum outflows from the very spectacular cinder cone were reported (from the Albert National Park) to be of about 50 m^3/sec.

This is the northernmost eruption of this active area and is one of the most important eruptions which has occurred in at least the last half century.

(Received January 28, 1959.)

GEOGRAPHICAL VARIATIONS IN GEOMAGNETIC MICROPULSATIONS

H. J. DUFFUS, J. A. SHAND, C. S. WRIGHT, P. W. NASMYTH

Pacific Naval Laboratory, H. M. C. Dockyard, Esquimalt, B. C.

AND

J. A. JACOBS

Department of Geophysics, University of British Columbia Vancouver, B. C.

In attempting to discover the origin and characteristic properties of geomagnetic micropulsations [*Obayashi* and *Jacobs*, 1958; *Duffus and Shand*, 1958] it has been common practice to compare the data from quite distant magnetic observatories without having any clear idea of how great a variation was to be found between points only a few miles apart. The comparison of data taken simultaneously at two stations approximately 25 miles apart will be reported in this letter. *Significant differences consistently occur.* These will have to be reconciled before any detailed comparison can safely be made between the records of widely separated observatories. At the same time, the general similarity of records suggests that the origin of the normal daytime micropulsations (Pc's) must be either a point source more than 25 miles away or an extended source coherent over that distance.

Simultaneous observations of geomagnetic micropulsations were made with identical equipment at two stations on Vancouver Island, British Columbia, some 25 miles apart. The base station is situated by the sea at Albert Head (approximately 48°23′N, 123°29′W) near Victoria, where observations have been made for a number of years. The other station was a mobile field station (the equipment being housed in a truck) which was set up inland at Bear Creek, about 12 miles from the sea.

The detecting equipment for Z, the rate of change of the vertical component of the magnetic field, consisted of an air-core induction coil, 20 ft in diameter. The two components for the horizontal field (X north; Y east) were observed with two mu-metal-cored coils. The signals from all three coils were fed to dc chopper amplifiers driving Esterline-Angus pen recorders. Each amplifier incorporated an integrating circuit of one minute time constant.

The records were analyzed by visual inspection; any part of the record with three or more equally spaced corresponding axis crossings was treated as an oscillation. No analysis of phase relationships has been attempted.

In general, good similarity was found between the records from the two stations in each of the three components.

The only exceptions to the good correlation between disturbances recorded at the two stations were (a) on two occasions a ripple appeared in the Z component at the base station only; and (b) on three occasions large, long-period ($>$ 10 min) excursions occurred on the records of all three components at the field station only. It is probable that both of these phenomena were of instrumental origin.

The ratio of the amplitude of corresponding components at the two stations has been computed and plotted as a function of the period. The results are reproduced in Figures 1, 2, and 3. The two sets of points correspond to different periods of observations—one during three consecutive magnetically disturbed days in May 1958, and the other during four consecutive quiet days about a month later. It can be seen that the ratios are insensitive to the degree of magnetic activity. Although there is considerable scatter in the points in all three diagrams, certain inferences may be drawn.

For periods of less than about two minutes,

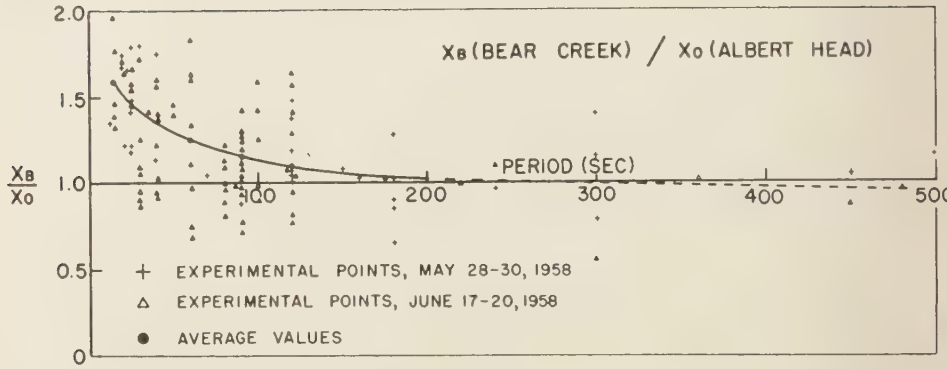

FIG. 1—Amplitude ratio of micropulsations of X components as a function of period

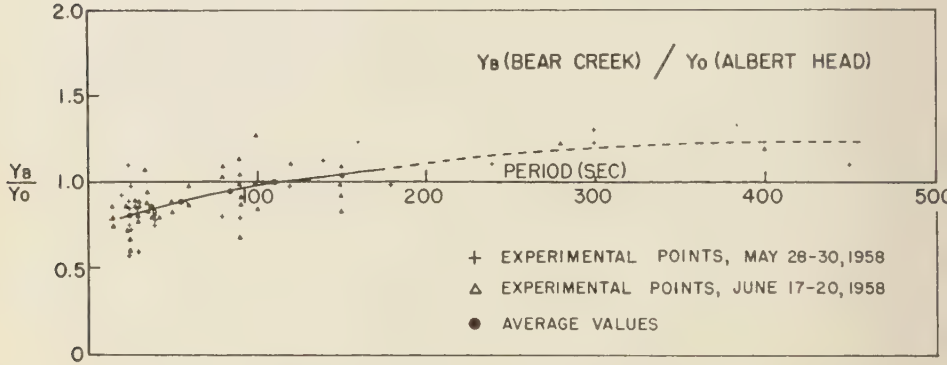

FIG. 2—Amplitude ratio of micropulsations of Y components as a function of period

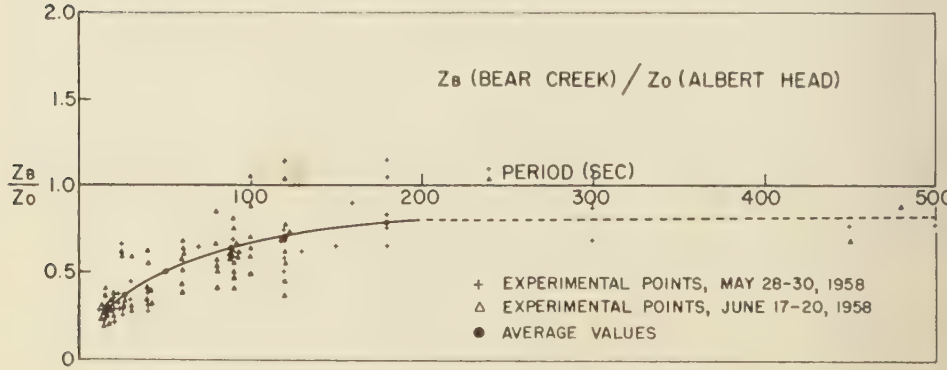

FIG. 3—Amplitude ratio of micropulsations of Z components as a function of period

$X_B > X_0$. The increase is about 25 per cent at periods of the order of one minute and 50 per cent at periods of the order of 30 seconds. There appears to be little difference between the values of X at the two stations for periods greater than about two minutes. It is not easy to draw a mean curve through the data; there is some evidence that the ratio X_B/X_0 may have a local minimum of 1.0 at about 80 sec and may reach a local maximum of 1.2 at about 120 sec. For periods of less than 15 sec, the ratio X_B/X_0 shows a marked increase. There were more than ten occasions (not shown in Figure 1) when the ratio reached values between two and three.

Y shows better agreement between the two stations than either X or Z, although at any one station it behaves differently from X and Z. The over-all trend is that $Y_B < Y_0$ for periods less than about two minutes and $Y_B > Y_0$ for longer periods. The variation is approximately linear, and over the range of periods investigated it does not exceed about 20 per cent.

The ratio of the Z components is the most interesting. Z_B/Z_0 is always < 1. Even at periods of the order of 10 minutes, this ratio is only about 0.8. For periods of the order of 20 sec, $Z_B/Z_0 < 0.3$, and there is every indication that at shorter periods this ratio decreases even more rapidly.

It is extremely important to reconcile the differences between the records of two such closely situated stations; otherwise, comparisons between stations in widely separated parts of the earth become meaningless. It is probable that the sea, with its high electrical conductivity, influences the results at Albert Head [compare *Cagniard*, 1956]. An attempt is being made to interpret the cause of the fluctuations by a theoretical study of hydromagnetic waves in the upper atmosphere [*Obayashi* and *Jacobs*, 1958].

This investigation has been extended by setting up the field station some 250 miles away in the interior of British Columbia and subsequently some 550 miles away in southern Alberta. It is also hoped that it may be possible at some future date to run three or four stations simultaneously. By obtaining the magnetic vector (at a particular frequency) at each station, it may prove possible to recognize the external part of the disturbance and hence assess that of internal origin.

This work is supported by the Defense Research Board of Canada and was carried out at the Pacific Naval Laboratory.

References

Cagniard, L., Electricité Tellurique, *Handbuch der Physik*, Geophysik 1, pp. 407–469, Springer-Verlag, 1956

Duffus, H. J., and J. A. Shand, Some observations of geomagnetic micropulsations, *Can. J. Phys.* **36**, 508–526, 1958.

Obayashi, T., and Jacobs, J. A., Geomagnetic pulsations and the earth's outer atmosphere, *Geophys. J. Roy. Astron. Soc.*, **1**, 53–63, 1958.

(Received December 29, 1958.)

Abstracts of the Papers Presented at the Pacific Northwest Regional Meeting,

Portland, Oregon, November 13-14, 1958

FRANKLIN I. BADGLEY (Department of Meteorology, University of Washington, Seattle, Wash.) *Review of the meteorology program of the IGY*—Special weather observing stations for the IGY have been located in the Arctic, the Antarctic, and along a longitudinal strip between 70°W and 80°W stretching from pole to pole.

The micrometeorology of snow and ice surfaces is being studied in both polar regions and on glaciers in temperate latitudes.

Rocket studies of the upper atmosphere and artificial satellite observations from outside the atmosphere may prove to be of more ultimate value to meteorologists than the conventional studies close to earth.

Preliminary IGY results already published show: (1) The atmospheric circulation over Antarctica is dominated by a low aloft which is asymmetrical with respect to the continent and which varies with the seasons. (2) Micrometeorological processes over snow and ice surfaces are dominated by radiative exchange of energy; turbulent fluxes play a minor role. (3) The Arctic Basin is the site of much more cyclonic activity than United States references indicate.

KONRAD K. BUETTNER (Department of Meteorology, University of Washington, Seattle, Wash.) *The surface of the moon*—Plans for the future landing of manned or unmanned space vehicles on the moon depend on its surface characteristics. From the observations of the surface temperatures during the lunar day and lunar eclipses, and also from the temperatures derived from radio emissions of the moon, it can be concluded that the lunar surface is covered by a layer of very loose dust which is about three feet thick. This dust layer seems to cover the plains as well as the mountain slopes. The low heat conductivity and density of this air-free dust causes the excessive surface temperature changes. The crumbling of the originally rocky surface is thought to be caused by the destruction of crystal bonds by cosmic-ray primaries.

LAWRENCE A. DEAN (Bonneville Power Administration, Portland, Ore.) *The use of long-range streamflow forecasts in the control of the Columbia River power system*—Forecasts of streamflow provide a workable scheme for the most efficient withdrawal of storage to meet power loads. The amount of storage that may be released without endangering future contractual commitments during the period when energy from natural flow must be supplemented with energy from reservoir storage is guided by streamflow forecasts made each week for from one to six months in advance. A relationship between antecedent streamflow levels and subsequent flows is employed to prepare forecasts which represent given probabilities of occurrence, and a Bendix G-15 digital computer is used to determine the system's power output from the set of streamflows. The power system presently consists of four storage reservoirs with usable contents of 10.4 million acre-feet and 12 hydroelectric plants with an installed peaking capacity of 619 million kilowatts.

DONALD W. KUEHL (U. S. Weather Bureau River Forecast Center, Portland, Ore.) *Use of electronic computers in water supply forecasting*—The basic seasonal precipitation-volume runoff relationship used by the U. S. Weather Bureau in water supply forecasting, plus the auxiliary data processing, was adapted to an IBM 650 digital computer by the River Center, Portland, Oregon. Programs have been written to forecast water year and residual runoff, to interpolate missing precipitation amounts, to compare forecasts for adjacent basins for consistency, and to prepare forecast listing for reproduction. Advantages of machine processing are: (1) reduction of time lag in release of forecasts, (2) elimination of computational errors, (3) reduction of cost of forecast operation, (4) relieving professional hydrologists of routine computation, (5) permitting use of more complex relationships, and (6) permitting more frequent forecast computation.

EDWARD R. LACHAPELLE (Department of Meteorology and Climatology, University of Washington, Seattle, Washington) *Annual mass and energy exchange on the Blue Glacier, Mount Olympus*—The field work of the IGY station on the Blue Glacier, Mount Olympus, is briefly described, together with techniques of study and methods of instrumentation. In discussion of the annual mass budget, the residual accumulation, net ablation, net mass balance, snow cover melt rate, and net ice ablation rate are all presented as functions of time. Total mass transfer and values of specific accumulation, ablation, and net balance are discussed. The total melt rate for the entire glacier, representing runoff from the glacier proper, is also presented as a function of time. The 1958 mass budget shows a deficit of 7.1×10^6 cubic meters of water, with a corresponding energy gain of 5.8×10^{14} gram calories. This basic relationship between the mass and energy budgets is analyzed, and the various contributions to energy gain and loss are summarized. Particular details are given for the parameters of surface energy exchange affecting ice melt during the middle of the ablation season. During the 1958 melt season the primary source of heat was solar radiation, with a substantial contribution from eddy conduction, and a smaller but definite yield from condensation of water vapor.

Mark F. Meier (U. S. Geological Survey, Tacoma, Wash.) *IGY glacier research in the United States*—Glaciers in the United States are being studied in connection with the International Geophysical Year program. These studies are directed toward certain fundamental difficulties involved in the proper interpretation of results from detailed glacier studies around the world, and toward completing our share of a world-wide census of glaciers and their present and past behavior. Fundamental investigations include: (1) study of the mass budget and the mass and energy processes of Blue Glacier (reported elsewhere), (2) study of the surface and englacial velocity field of the Lower Blue Glacier tongue to obtain new data on the flow law of ice and the mechanism of flow response to the mass budget, and (3) an integrated study of the hydrology, mass budget, and flow dynamics of South Cascade Glacier. Yearly surveys of selected glaciers are being made by cooperators in Glacier, Yosemite, Olympic, and Mount Ranier National Parks, in the Northern Cascade Mountains, and in several other areas. Preliminary results from the surveys of glaciers in the state of Washington suggest that although equilibrium or resurgent glacier conditions were general in the decade 1947–1957, the subsequent year was characterized by substantially negative mass budgets.

Egbert S. Wengert (Department of Political Science, University of Oregon, Eugene, Ore.) *The politics of IGY*—The IGY constitutes a case study or a type of a complex scheme of collaboration, really an administrative system to put scientific intellectual capital to use, to harness scattered energies of men and women all over the world, to pose old problems more precisely, to outline their solutions, and in the course of these efforts, to mark out for the future the problems to which attention will need to be given. In all of this there is significant political meaning: how IGY arranges, disposes, controls, and distributes resources (for example, institutions, concepts and ideas, tools, raw materials, human hopes, wants, and wishes) illustrates conflicts and cooperation among people, the struggle for power, the search for the public interest as they seek to govern themselves.

As a case study IGY raises into sharp relief the issues that are posed for scientists everywhere in the midst of the struggle between the Soviet Union and the United States. This greatest of all scientific research programs transcends the limits of national science, yet its most dramatic and highly publicized aspects—ventures into space—have become essentially competitions in the cold war.

IGY forecasts changes in some basic future conditions of human life. On our globe the imminent control of climate opens up a new frontier. Like the frontiers of our own history, this new frontier will no doubt encapsulate the processes of politics associated with the struggle for the control of basic resources. A second new frontier, analogous to the discoveries of the New World of the fifteenth and sixteenth centuries, demands that we determine how social and political good health may be achieved in using the world of space. IGY demands that political scientists move to clarify the nature of possible mutual interests particularly to enable the U. S. and the U.S.S.R. to build the new relations needed for a space age.

The politics of IGY is essentially the politics of modern science in general. Our scientific age calls for more trained specialists. The progress of modern science requires public support. The scientific community has to turn to government to help mobilize the resources of men and materials it needs. So the mold of modern science comes to be shaped in the political process.

We know the risks of stultification under heavy-handed administration. We are less sensitive to the dangers that we face as communication among the specialists of science threatens to break down. Increasingly, too, scientists and members of the community at large, including its decision-makers, find communication grown difficult or even impossible. As communities of specialists become isolated, criticism may be frustrated; closed monopolistic elites may develop narrow guild spirit; the very idea of science may be killed. We are not producing the kind of generalizing mind, particularly among our administrators, to steer a course to enable specialists to relate themselves creatively to each other. We are not producing administrators who can avoid the anarchy of logrolling among specialists without regimentation that threatens the progress of specialized science we depend on. The politics of IGY does not point the way out of these dilemmas.

Information for Contributors
to the *Journal of Geophysical Research*

Manuscripts—Send manuscripts to J. A. Peoples, Jr., Department of Geology, University of Kansas, Lawrence, Kansas. Manuscripts, including proof copies of figures, should be submitted in triplicate to expedite review and publication. Manuscripts should be in English, typewritten on heavy paper on one side of page only, double spaced (including abstracts and references), with generous margins.

Ample space should be allowed for mathematical expressions, which should be typed or very plainly written by hand. Particular attention should be given to legibility of subscripts and superscripts and to differentiation between capital and lower case letters. Unusual symbols and cumbersome notations should be avoided. Fractional exponents should be used in preference to root signs, and the solidus (/) should be used for fractions wherever its use will save vertical space.

Authors are urged to have their papers critically reviewed by their associates for scientific validity, manner of presentation, and use of English before submitting them for publication.

Abstracts—An abstract must accompany each manuscript. It should be a concise but comprehensive condensation of the essential parts of the paper, suitable for separate publication, and adequate for the preparation of general indexes to geophysical literature.

References and footnotes—References should be indicated in the text by the insertion in brackets of the author's name and the year of publication, thus: [*Trelease*, 1951]. If the author's name is part of the text, only the year is bracketed. If there are two or more references citing different papers published in the same year by the same author, distinguish them by the letters a, b, c after the year. At the end of the paper, list all references alphabetically by the authors' names. Include in each entry the following: name of senior author, followed by his initials; names of junior authors, each preceded by his initials; title of paper (or book); title of publication or journal; volume number; inclusive page numbers; year of publication. Abbreviations of journals follow the style used in *Chemical Abstracts*. If in doubt, give the full title of the publication or journal. When a book is cited, add the publisher's name, the city of publication, and the total number of pages. Reference to specific pages may be made in the text if appropriate Acknowledge unpublished reports and private communications in the text, not as references. Avoid footnotes to the text; use parenthetic sentences instead of footnotes if possible.

Tables and figures—Material suitable to tabular form should be arranged as a table and may be typewritten on a separate page. Tables must be numbered according to their sequence in the text, and each table should have a title. Column headings should be short and self-explanatory; more complete explanation may be given in footnotes to the table. Authors should avoid repeating in the text material which is given in tables or figures.

Figures should be prepared with the column width of this Journal in mind (a scale of two to four times that of the published figure is usually adequate). Lettering and symbols should be large enough to stand reduction and remain legible. Captions should be typed on a separate page, not lettered in the figures. Necessary legends or lettering in the figures should be executed to meet competent drafting standards, not typewritten. If the author cannot arrange for suitable lettering, he may send the drawings with the lettering lightly penciled in or shown on a proof copy, and the lettering will be done at the editorial office.

Line drawings should be in India ink on white paper or tracing cloth. Coordinate paper should be avoided, but, if used, it must be blue-lined and the coordinate lines which are to show must be inked.

Photographs are acceptable only if they have good intensity and contrast. They should be unmounted, glossy prints.

Figures should be identified by numbering lightly in pencil, and 'top' of each figure should be indicated.

Acknowledgments—Acknowledgments should be made only for significant contributions by the author's professional associates. A brief closing statement will usually suffice.

References

American Chemical Society, *List of periodicals abstracted by Chemical Abstracts*, Chemical Abstracts Service, Ohio State Univ., Columbus, 314 pp., 1956.

American Institute of Physics, *Style Manual*, American Institute of Physics, New York, 28 pp., 1951.

American Mathematical Society, A manual for authors of mathematical papers, *Bull. Am. Math. Soc.*, 49, no. 3, pt. 2, 1–16, 1943.

Emberger, M. R., and M. R. Hall, *Scientific writing*, Harcourt, Brace and Co., New York, 468 pp., 1955.

Taft, K. B., J. F. McDermott, and D. O. Jensen, *The technique of composition*, 3rd ed., Farrar and Rinehart, New York, 628 pp., 1941.

Trelease, S. F., *The Scientific paper—how to prepare it, how to write it*, Williams and Wilkins Co., Baltimore, 175 pp., 1951.

U. S. Geological Survey, *Suggestions to authors of the reports of the United States Geological Survey*, 5th ed., U. S. Govt. Printing Office, Washington, 255 pp., 1958.

William Byrd Press, *Mathematics in type*, Richmond, 58 pp., 1954.

(Journal of Geophysical Research, Vol. 64, No. 5, May 1959)

Contents

PAGE

Investigation of the Equatorial Electrojet by Rocket Magnetometer
Laurence J. Cahill, Jr. 489

Solar Activity and Transient Decreases in Cosmic-Ray Intensity.....*D. Venkatesan* 505

Daily and Annual Courses of Natural Atmospheric Radioactivity
Marvin H. Wilkening 521

Green Coronal Line Intensity and Geomagnetism.....*C. Warwick* 527

Formation of Thermal Microstructure in a Narrow Embayment during Flushing
Jack T. Shaw and G. R. Garrison 533

Comparison of Several Methods for Rainfall Frequency Analysis
F. A. Huff and J. C. Neill 541

Water Table Fluctuations Induced by Intermittent Recharge....*Marinus Maasland* 549

The Analysis of Aquifer Test Data or Thermal Conductivity Measurements which Use a Line Source.....*J. C. Jaeger* 561

Some Implications on Mantle and Crustal Structure from G Waves and Love Waves
Frank Press 56[illegible]

Pressure Effects on Thermoluminescence of Limestone Relative to Geologic Age
Ernest E. Angino 56[illegible]

A Note on the System Fe_2O_3–H_2O.....*Robert F. Schmalz* 57[illegible]

Letters to the Editor:

Volcanic Eruption in Belgian Congo.....*E. Berg* 58[illegible]

Geographical Variations in Geomagnetic Micropulsations
H. J. Duffus, J. A. Shand, C. S. Wright, P. W. Nasmyth and J. A. Jacobs 58[illegible]

Abstracts of the Papers Presented at the Pacific Northwest Regional Meeting, Portland, Oregon, November 13–14, 1958..... 58[illegible]